SU(N) gauge theories in 3+1 dimensions: glueball spectrum, string tensions and topology

Andreas Athenodorou[a,b] **and Michael Teper**[c,d]

[a] *Dipartimento di Fisica, Università di Pisa and INFN, Sezione di Pisa,*
  Largo Pontecorvo 3, 56127 Pisa, Italy

[b] *Computation-based Science and Technology Research Center, The Cyprus Institute,*
  20 Kavafi Str., Nicosia 2121, Cyprus

[c] *Rudolf Peierls Centre for Theoretical Physics, University of Oxford,*
  Parks Road, Oxford OX1 3PU, U.K.

[d] *All Souls College, University of Oxford, High Street, Oxford OX1 4AL, U.K.*

  E-mail: a.athenodorou@cyi.ac.cy, mike.teper@physics.ox.ac.uk

ABSTRACT: We calculate the low-lying glueball spectrum, several string tensions and some properties of topology and the running coupling for $SU(N)$ lattice gauge theories in $3 + 1$ dimensions. We do so for $2 \leq N \leq 12$, using lattice simulations with the Wilson plaquette action, and for glueball states in all the representations of the cubic rotation group, for both values of parity and charge conjugation. We extrapolate these results to the continuum limit of each theory and then to $N = \infty$. For a number of these states we are able to identify their continuum spins with very little ambiguity. We calculate the fundamental string tension and $k = 2$ string tension and investigate the N dependence of the ratio. Using the string tension as the scale, we calculate the running of a lattice coupling and confirm that $g^2(a) \propto 1/N$ for constant physics as $N \to \infty$. We fit our calculated values of $a\sqrt{\sigma}$ with the 3-loop β-function, and extract a value for $\Lambda_{\overline{MS}}$, in units of the string tension, for all our values of N, including $SU(3)$. We use these fits to provide analytic formulae for estimating the string tension at a given lattice coupling. We calculate the topological charge Q for $N \leq 6$ where it fluctuates sufficiently for a plausible estimate of the continuum topological susceptibility. We also calculate the renormalisation of the lattice topological charge, $Z_Q(\beta)$, for all our $SU(N)$ gauge theories, using a standard definition of the charge, and we provide interpolating formulae, which may be useful in estimating the renormalisation of the lattice θ parameter. We provide quantitative results for how the topological charge 'freezes' with decreasing lattice spacing and with increasing N. Although we are able to show that within our typical errors our glueball and string tension results are insensitive to the freezing of Q at larger N and β, we choose to perform our calculations with a typical distribution of Q imposed upon the fields so as to further reduce any potential systematic errors.

Contents

1 Introduction

In this paper we calculate various physical properties of SU(N) gauge theories in $3+1$ dimensions. We do so by performing calculations in the corresponding lattice gauge theories over a sufficient range of lattice spacings, a, and with enough precision that we can obtain plausible continuum extrapolations. We also wish to be able to extrapolate to the theoretically interesting $N = \infty$ limit and to compare this to the physically interesting SU(3) theory. To do so we have performed our calculations for $N = 2, 3, 4, 5, 6, 8, 10, 12$ gauge theories.

Our main aim is to provide a calculation of the low-lying 'glueball' mass spectrum for all quantum numbers and all N. This means calculating the lowest states in all the irreducible representations, R, of the rotation group of a cubic lattice, and for both values of parity P and charge conjugation parity C. We also calculate the confining string tension, σ, so as to provide a useful scale for the glueball masses. In addition we calculate a number of other interesting quantities. However these are side-products of our glueball calculations rather than being dedicated calculations of these quantities. The first is the $k = 2$ string tension, $\sigma_{k=2}$ and the nature of its approach to $N = \infty$. The second is an estimate of the scale parameter $\Lambda_{\overline{MS}}$ for all our SU(N) gauge theories. Thirdly, in order to monitor the topological 'freezing' as a becomes small at fixed N, or N becomes large at fixed a, we calculate the interval (in units of our Monte Carlo steps) between changes in the topological charge, as well as the renormalisation of that charge, and also the topological susceptibility.

Our calculations of the glueball spectrum are intended to make necessary improvements to previous work. We recall that the pioneering glueball calculations in [1, 2] were restricted to obtaining the continuum masses of the lightest and first excited $J^{PC} = 0^{++}$ glueballs and the lightest 2^{++} glueball, in units of the string tension, with the continuum spin assignments being based on plausible assumptions. This sufficed to provide the first fully non-perturbative demonstration that the basic physical quantities of the SU(3) gauge theory are 'close to' those of SU(∞), as had long been hoped, but it did not provide the kind of detailed $N = \infty$ glueball spectrum that would be useful in testing theoretical approaches. Such a detailed spectrum was subsequently provided in [3] where the lightest masses in all the irreducible representations of the rotation group of the cubic lattice were calculated for $N \in [2, 8]$ and extrapolated to $N = \infty$. In addition a serious effort was made in that work to identify those states that might be multi-glueball 'scattering' states or finite volume artifacts (based on conjugate pairs of winding flux tubes), rather than being the single glueballs that one would obtain in an infinite volume. The important drawback of this calculation is that it was made at a fixed value of the lattice spacing a ('fixed' in units of the deconfinement temperature), corresponding to a value of $\beta \simeq 5.895$ in SU(3). This corresponds to a coarse lattice discretisation, typically between the two largest lattice spacings used in our present work. This has two important adverse consequences. The first is that it leaves uncertain the values of the masses in the desired continuum limit. (Although the calculations in [3] and earlier SU(3) calculations left room for being optimistic about the limited size of any lattice corrections.) The second problem is that since the lattice

masses aM are large when a is large, as in that paper, it makes the extraction of heavier glueball masses much more ambiguous and the statistical errors much larger than they would be at smaller values of a. A corollary is that it renders continuum spin assignments more ambiguous, except for the very lightest glueballs, since the spin assignment depends on observing near-degeneracies amongst states in appropriate irreducible representations of the lattice rotation group, and for this it is clearly essential to achieve an adequate precision in the various mass estimates. In addition to this earlier work, there recently appeared a potentially more relevant paper [4] when our work was largely completed. This paper provides a pioneering calculation of the masses of the lightest glueballs in all the irreducible representations, of a number of continuum $\mathrm{Sp}(2N)$ gauge theories with an extrapolation to $N = \infty$. In principle this extrapolation is equally relevant to the $N \to \infty$ limit of $\mathrm{SU}(N)$ gauge theories, as pointed out in [4], since the $\mathrm{Sp}(2N)$ and $\mathrm{SU}(N)$ gauge theories share a common (perturbative) planar limit. In practice, however, the usefulness for $\mathrm{SU}(N \to \infty)$ turns out to be very limited. Firstly, $\mathrm{Sp}(2N)$ has no $C = -$ sector, so there are no predictions for half the $\mathrm{SU}(N \to \infty)$ spectrum. Secondly the limited range of N in [4], coupled with the fact that in $\mathrm{Sp}(2N)$ the leading correction to $N = \infty$ is $O(1/N)$ renders the large-N extrapolations less convincing and much less precise when compared to $\mathrm{SU}(N)$ where the leading correction is $O(1/N^2)$. The net result is that the errors on the $\mathrm{SU}(N \to \infty)$ glueball masses obtained in [4], are larger by a factor of ~ 5–20 compared to the values obtained in this paper, and the mass estimates are mainly for just the ground states in each channel. This means that the evidence for the assignment of a continuum spin J only appears plausible for the $J^P = 0^+, 0^-, 2^+, 2^-$ ground states. Of course, none of these comments detract from the success of [4] in their primary aim of elucidating the mass spectrum of $\mathrm{Sp}(2N)$ gauge theories.

In this paper we provide a calculation of the masses of the ground states and some excited states in all the irreducible representations R of the rotation group of our cubic lattice with an extrapolation of these masses (in units of the string tension) to the continuum limit. To make this extrapolation more reliable and more precise we extend the range of our calculations to much smaller lattice spacings than earlier work. This enables us to extract the masses of the heavier ground states and most of the first few excited states much more reliably than earlier calculations. As an important by-product, all this will allow us to make a significant number of continuum spin assignments after the extrapolation to the continuum limit. We recall that the assignment of a continuum spin typically depends on observing near-degeneracies amongst both ground and excited states in the various irreducible representations of the lattice rotation group, and this requires both precision in the mass estimates and small enough lattice spacings for the masses of the heavier excited states to be plausibly estimated. We also extend the range of our calculations to larger values of N. This is not only to make the extrapolation to $N = \infty$ somewhat more reliable and precise but also, and perhaps more importantly, to help in excluding from our $N \to \infty$ glueball spectrum any multiglueball scattering states and finite volume states, since these states will decouple from our single trace operators as $N \uparrow$.

This kind of calculation is of course standard in the case of $\mathrm{SU}(3)$, see for example [5–11], and what we have attempted to do is to bring the $\mathrm{SU}(N)$ calculations towards a similar level

of sophistication. The computational cost of performing calculations at larger N means that further improvement to our work is still desirable. (It would also be very interesting to see the existing calculations at very large N using space-time reduction [12] extended to calculations of the glueball spectrum, just as they have been in $2 + 1$ dimensions [13].) Nonetheless we are able in this paper to provide the first calculation of the masses of the ground states in all the R^{PC} channels of the continuum $\mathrm{SU}(N \to \infty)$ gauge theory, as well as some excited states in most channels.

The plan of the paper is as follows. In the next section we introduce our lattice setup and describe how we calculate energies from correlators. We discuss some of the main systematic errors affecting these calculations and how we deal with them, with a particular focus on the rapid loss of tunneling between sectors of differing topology as $N \uparrow$. In section 3 we describe in detail our calculation of the confining string tension, σ, which we will later use as the physical scale in which to express our glueball masses. As a side product we also calculate the string tension, $\sigma_{k=2}$, of the lightest flux tubes carrying $k = 2$ units of fundamental flux. In section 3.4 we study the approach of the ratio $\sigma_{k=2}/\sigma$ to the $N = \infty$ limit so as to address the old controversy concerning the power of $1/N$ of the leading correction. In section 4 we show how our precise calculation of the fundamental string tension, $a^2\sigma$, as a function of the lattice coupling enables us to confirm the expected scaling of g^2 with N, and motivates (lattice improved) perturbative fits that allow us, in section 4.2, to estimate a value for $\Lambda_{\overline{MS}}$ as a function of N. We also provide, in section 4.3, some analytic interpolation/extrapolation formulae for the variation of the string tension with the coupling, which may be of use in other calculations. We then turn, in section 5, to our main calculation in this paper, which is that of the low-lying glueball spectrum. We calculate the masses on the lattice, extrapolate to the continuum limit, and then extrapolate to $N = \infty$. Although these states are classified according to the representations of the rotation group of our cubic lattice, we are able to identify the continuum spins in many cases, as described in section 5.7. In doing all this we need to address the problem of the extra states that winding modes introduce into the glueball spectrum and also the possible presence of multi-glueball 'scattering' states. We complete section 5 with a brief comparison of our results with those of some earlier calculations. We then return, in section 6, to some of the properties of the topological fluctuations in our lattice fields. After illustrating in section 6.1 how our cooling algorithm reproduces the topological charge of a lattice field, we calculate in section 6.2 the rate of topological freezing with increasing N and with decreasing $a(\beta)$ and compare our results to the simplest theoretical expectations. In section 6.3 we provide our results for the topological susceptibility in the continuum limit of $\mathrm{SU}(N \leq 6)$ gauge theories and in the $N \to \infty$ limit. Then, in section 6.4, we calculate the multiplicative renormalisation of our lattice topological charge for each $\mathrm{SU}(N)$ group and provide interpolating formulae which may be useful in calculations with a θ parameter in the lattice action. Section 7 summarises our main results.

Finally we remark that in parallel with the present calculations most of our $\mathrm{SU}(3)$ calculations, which are of particular physical interest, have recently been published separately [11].

2 Calculating on a lattice

2.1 Lattice setup

We work on hypercubic lattices of size $L_s^3 L_t$ with lattice spacing a and with periodic boundary conditions on the fields. The Euclidean time extent, aL_t, is always chosen large enough that we are in the confining phase of the theory, at a temperature that is well below the deconfining phase transition [14]. Our fields are SU(N) matrices, U_l, assigned to the links l of the lattice. The Euclidean path integral is

$$Z = \int \mathcal{D}U \exp\{-\beta S[U]\}, \tag{2.1}$$

where $\mathcal{D}U$ is the Haar measure and we use the standard plaquette action,

$$\beta S = \beta \sum_p \left\{ 1 - \frac{1}{N} \mathrm{ReTr} U_p \right\} ; \quad \beta = \frac{2N}{g_L^2}. \tag{2.2}$$

Here U_p is the ordered product of link matrices around the plaquette p. We write $\beta = 2N/g_L^2$ since in this way we recover the usual continuum action when we take the continuum limit of the lattice theory and replace $g_L^2 \to g^2$. The subscript L reminds us that this coupling is defined in a specific coupling scheme corresponding to the lattice and the plaquette action. Since g_L^2 is the bare coupling corresponding to a short distance cut-off a, it provides a definition of the running coupling $g_L^2(a) = g_L^2$ on the length scale a. Since the theory is asymptotically free $g_L^2(a) \to 0$ as $a \to 0$ and hence $\beta \to \infty$ as $a \to 0$ and so we can decrease the cut-off a and so approach the desired continuum limit of the theory by increasing β. Our calculations of this lattice path integral are carried out via a standard Monte Carlo using a mixture of Cabibbo-Marinari heat bath and over-relaxation sweeps through the lattice. We typically perform $\sim 2 \times 10^6$ sweeps at each value of β at each lattice size, and we typically calculate correlators every ~ 25 sweeps and the topological charge every 50 or 100 sweeps. Naturally we choose values of β that place us on the weak coupling branch of the lattice theory. We discuss the 'bulk' transition that separates weak coupling from strong coupling, and becomes a first order transition for $N \geq 5$ [15], in section 5.4. There are of course other possible choices for the action, and we briefly comment upon our choice in section 5.9, where we compare our results to those of other recent calculations.

We simulate SU(N) lattice gauge theories for $N = 2, 3, 4, 5, 6, 8, 10, 12$ over a range of values of β so as to be able to plausibly obtain, by extrapolation, the glueball spectra and string tensions of the corresponding continuum gauge theories. A summary of the basic parameters of our calculations is given in tables 1–8. For each of our SU(N) calculations we show the values of β, the lattice sizes, the average plaquette, the string tension, $a^2\sigma$, and the mass gap, am_G. In the header of each table we show the approximate spatial size in units of the string tension. Since finite volume corrections are expected to decrease with increasing N we decrease the lattice volume as we increase N. This expectation needs to be confirmed by explicit calculations which we shall provide in section 5.2.

2.2 Energies and correlators

We calculate energies from correlation functions in the standard way. Suppose we wish to calculate glueball masses in some representation R^{PC}. If one picks an operator $\phi(t)$ with quantum numbers R^{PC} and momentum $p = 0$ then the correlator will provide us with the energies E_i of states with those quantum numbers

$$C(t) = \langle \phi^\dagger(t)\phi(0) \rangle = \sum_{n=0} |c_n|^2 \exp\{-E_n t\} \xrightarrow{t \to \infty} |c_0|^2 \exp\{-E_0 t\}, \qquad (2.3)$$

where $E_n \leq E_{n+1}$ and E_0 is the lightest state with R^{PC} quantum numbers — which will often be the lightest glueball in that sector. (If ϕ has vacuum quantum numbers then one uses the vacuum subtracted operator.) Since on the lattice time is measured in lattice units, $t = an_t$, what we obtain is the value, aE_0, of the mass in lattice units. If we calculate two masses, aM and $a\mu$, in this way then the lattice spacing drops out of the ratio and if we calculate the ratio for several values of $a(\beta)$ we can extrapolate to the continuum limit in the standard way, using

$$\frac{aM(a)}{a\mu(a)} = \frac{M(a)}{\mu(a)} \simeq \frac{M(0)}{\mu(0)} + ca^2\mu^2 \qquad (2.4)$$

once $a(\beta)$ is small enough. (This standard tree level extrapolation could be improved with perturbative corrections [16] and with higher order power corrections but our calculations are not so extensive and precise as to motivate such modifications.)

The starting point for an operator ϕ is the trace of a closed loop on the lattice. For an operator that projects onto glueballs the loop should be contractible. A non-contractible loop that closes across the periodic spatial boundary will project onto a confining flux tube that winds around that spatial torus. For the contractible glueball loop one takes a suitable linear combination of rotations of that loop for it to be in the desired representation R of the lattice rotation group and together with the parity inverse this allows us to form an operator with parity P. The real and imaginary parts of the original loop will correspond to $C = +$ and $C = -$ respectively. Summing this linear combination over all spatial sites at time t gives us the operator with $p = 0$.

The statistical errors on $C(t)$ are roughly independent of t while its value decreases exponentially with t, so if we are to estimate aE_0 from $C(t)$ in eq. (2.3) we need to be able to do this at small t. (The fluctuations of $\phi^\dagger(t)\phi(0)$ involve the higher order correlator $(\phi^\dagger(t)\phi(0))^2$ which typically has a vacuum channel and this is independent of t.) For this to be possible we need the operator ϕ to have a large overlap onto the state $|n = 0\rangle$ that corresponds to E_0, i.e. that $|c_0|^2/\sum_n |c_n|^2 \sim 1$. One can achieve this using iteratively 'blocked' link matrices and loops [17, 18] as described in detail in, for example, [2]. To monitor the approach of $C(t)$ to the asymptotic exponential decay in eq. (2.3) it is useful to define an effective energy

$$\frac{C(an_t)}{C(a(n_t - 1))} = \exp\{-aE_{\text{eff}}(n_t)\}. \qquad (2.5)$$

(In practice we use a cosh modification of this definition to take into account the periodicity in the temporal direction.) If, within errors, $aE_{\text{eff}}(n_t) = \text{const}$ for $n_t \geq \tilde{n}_t$ then we can

use $aE_{\mathrm{eff}}(\tilde{n}_t)$ as an estimate for aE_0, or we can do a simple exponential fit to $C(t)$ for $n_t \geq \tilde{n}_t - 1$ to estimate aE_0.

To calculate not just the ground state energy but also some usefully precise excited state energies from $C(t)$ in eq. (2.3) would require a precision that is at present unachievable. Instead the standard strategy is to use a variational calculation. One chooses some basis of n_0 operators $\{\phi_i(t) : i = 1, \ldots, n_0\}$, calculates the cross-correlators $C_{ij}(t) = \langle \phi_i^\dagger(t) \phi_j(0) \rangle$ and finds the linear combination, $\Phi = \Phi_0$, that maximises $C(t) = \langle \Phi^\dagger(t) \Phi(0) \rangle$ for some suitable small $t = t_0$. This is then our best estimate of the wave-functional of the ground state $|n = 0\rangle$. We then extract aE_0 from the asymptotic exponential decay of $C(t) = \langle \Phi_0^\dagger(t) \Phi_0(0) \rangle$. To calculate the first excited energy aE_1 we consider the subspace of $\{\phi_i : i = 1, \ldots, n_0\}$ that is orthogonal to Φ_0 and repeat the above steps. This gives our best estimate Φ_1 for $|n = 1\rangle$ and we estimate aE_1 from the asymptotic exponential decay of the correlator of $\Phi_1(t)$. Similarly by considering the subspace of the operator vector space that is orthogonal to Φ_0 and Φ_1 we can obtain estimates for the next excited state and so on. As with any variational calculation, the accuracy of such estimates will depend on having a large enough basis of operators.

2.3 Systematic errors

In addition to the statistical errors in the calculation of energies and masses, which can be estimated quite reliably, there are systematic errors that are harder to control. We will now briefly point to some of these, leaving a more detailed discussion till later on.

Since the error to signal ratio on $C(n_t)$ increases at least as fast as $\propto \exp\{+aE_0 n_t\}$, the range of n_t which is useful rapidly decreases when the energy aE_0 increases, and an obvious systematic error is that we begin our fit of the asymptotic exponential decay at too small a value of $t = an_t$. Given the positivity properties of our correlators, this means that as the true value of E_0 increases, so does our overestimate of its value. For any particular state this problem will become less severe as we decrease a, and this provides some check on this error.

The correlator of an excited state, using our best variational choice of operator, may contain small contributions from lighter excitations since our basis is far from complete. So at large enough n_t these will dominate the correlator and the effective mass will drop below that of the mass of the state of interest. This does not appear to be a severe problem for us because the pattern of our statistical errors, which grow rapidly with n_t, prevents us from obtaining values at large n_t. In any case we attempt to identify at most an intermediate effective mass plateau from which we extract the desired mass.

If a state has too small an overlap onto our basis of operators then, given the exponential growth with t of the statistical error on the effective energy, the state will be, at best, assigned a mass that is much too high and so it will typically not appear in its correct order in the mass spectrum. If so this means that there will be a missing state in our calculated glueball spectrum and this will not be helpful if, for example, one wishes to check theoretical models of the spectrum against the lattice spectrum. To reduce the possibility of this occurring one needs to use a large basis of operators, just as in any variational calculation.

The states we are primarily interested in are single particle glueball states rather than multi-glueball scattering states. (In our finite spatial volume multiglueball states are interacting at all times but for simplicity we refer to them as scattering states.) We use single trace operators which should ensure that at large N our correlators receive no multi-glueball contributions but this is not necessarily the case at smaller N. This is of course related to the fact that at smaller N heavier glueball states may have substantial decay widths. Later in the paper we will provide an exploratory analysis of this issue by combining single and double trace operators.

The spectrum in a finite spatial volume will differ from the spectrum in an infinite volume. One type of correction to a glueball propagator comes, for example, from a virtual glueball loop where one line of the two in the loop encircles the spatial torus. Such corrections are exponentially small in, typically, $M_G L$ where M_G is the mass gap (the lightest scalar glueball) and L is the spatial size [19]. These corrections will be very small in our calculations. For the intermediate volumes on which we work a much more relevant finite volume correction comes from a confining flux tube that winds once around one of the spatial tori. Such a flux tube is often referred to as a torelon. By itself a torelon has zero overlap onto local particle states. However a state composed of two torelons, where one is conjugated, will in general have a nonzero overlap. Such a 'ditorelon' will not only shift the energies of the usual particle glueballs but will introduce extra states into the glueball spectrum. These extra states can be identified through their volume dependence and in some other ways as we shall see later on.

In addition to the usual gradual loss of ergodicity as the lattice spacing decreases, the tunnelling between sectors of differing topological charge Q suffers a much more rapid supression not only as $a \to 0$ at fixed N but also as N increases at fixed a. This affects a significant part of our calculations and we discuss next how we deal with it in practice.

2.4 Topological freezing

We begin by briefly summarising the reason that one loses ergodicity in the topology of lattice gauge fields much faster than in other typical quantities as $a \to 0$ at fixed N and as $N \to \infty$ at fixed a, when using a local Monte Carlo algorithm,. We then describe where this impacts on our particular calculations and why this inpact should be minor on theoretical grounds. We provide explicit calculations to confirm this expectation and, finally, we describe the additional procedure that we follow to minimise any remaining systematic errors. It is important to note that all these arguments are for pure gauge theories and would have to be reconsidered in the presence of light fermions as in QCD.

In a periodic four-volume a continuum gauge field of topological charge Q cannot be smoothly deformed into a gauge field of charge $Q' \neq Q$. So in a sequence of lattice fields that have been generated using a Monte Carlo algorithm that is local any change in the value of Q should be increasingly suppressed as we approach the continuum limit. This statement can be made quantitative as we do below. But before that we note that there is a separate suppression that occurs at any fixed small value of a when we increase N. To smoothly deform a lattice field from, say, $Q = 1$ to $Q = 0$ in a finite volume with periodic gauge potentials, the core of an original extended instanton must gradually

shrink until it disappears within a hypercube, leaving a simple gauge singularity centered on that hypercube. Before it does so it will be a small instanton (assuming a is small) which we can describe using standard semiclassical methods. So its effective action will be $S_I(\rho) \sim 8\pi^2/g^2(\rho)$ where ρ is the size of the core and provides the relevant scale, and the probability of it existing in a field will be $\propto \exp\{-S_I(\rho)\} \sim \exp\{-8\pi^2/g^2(\rho)\}$ per unit volume up to a $1/\rho^4$ volume factor and some less important factors [20, 21]. Now at large N the 't Hooft coupling $\lambda = g^2 N$ needs to be kept constant for a smooth limit [22, 23]. In terms of the running coupling this means $\lambda(l) = g^2(l)N$ is independent of N up to corrections that are powers of $1/N$, where l is measured in some physical units, e.g. the mass gap. So the weight of a small instanton vanishes as $\propto \exp\{-8\pi^2 N/\lambda(\rho)\}$, i.e. it vanishes exponentially with N [25, 26]. Since the process of going 'smoothly' from a field with $Q = 1$ to a field with $Q = 0$ necessarily involves at an intermediate stage of the process the presence of fields containing such small instantons, we immediately infer that the change in topology must be at least exponentially suppressed with increasing N once a is small. Such a strong suppression has indeed been observed in earlier lattice calculations [1, 27]. Returning to the $a \to 0$ limit at fixed N we note that one can use the one-loop expression for $g^2(\rho)$ and this leads to a suppression of the tunnelling between topological sectors that is the appropriate power of ρ and hence of a, once $\rho \sim O(a)$.

In our calculations we normally start a Monte Carlo sequence with the trivial $Q = 0$ gauge field $U_l = I, \forall l$, and 'thermalise' with some tens of thousands of sweeps to reach the 'equilibriated' lattice gauge fields which we can begin to use for our calculations. As described above, for larger N and smaller a the topological tunnelling can become sufficiently rare that the fields remain at $Q = 0$ even after our attempted equilibration. In practice this proves not to be an issue for any of our SU(2), SU(3), SU(4) and SU(5) calculations. For SU(6) it becomes a problem for the smallest values of a and for SU($N \geq 8$) it is a problem for all but our largest values of a. That is to say, within our statistics and our range of a topological freezing is largely an issue to do with $N \uparrow$ rather than with $a \downarrow$. This distinction is important since the currently accepted theoretical picture [28] tells us that we are sitting in a vacuum with periodicity in the θ parameter of $2\pi N$ rather than 2π. (It is other interlaced θ-vacua that provide the expected 2π periodicity.) This implies that higher moments in Q disappear as inverse powers of N, and so does the correlation between the topological charge and gluonic operators. Lattice calculations [29] have confirmed this expectation. This tells us that at large enough N the loss of ergodicity should not affect physical quantities such as glueball masses.

Of course we do not know in advance what value of N is 'large enough' and so it is useful to perform an explicit check of how such freezing affects the physics we are interested in. For this we choose to work in SU(8) at $\beta = 45.50$ where changes in topology are extremely rare, but which is close to the value $N = 6$ where we begin to encounter a serious loss of topological ergodicity in our calculations. We begin with a comparison of two sets of about 2×10^6 fields on a $14^3 20$ lattice, with glueball and flux tube 'measurements' taken every 25'th update. One set of fields has $Q = 0$ throughout while the other has what one expects to be the correct distribution of Q imposed through about 40 different starting configurations as described above. We calculate glueball and flux tube correlators in exactly

the same way in both ensembles of fields and perform the usual variational calculation for each representation R^{PC}. Note that here we include all the states that we obtain and make no attempt to identify any of the finite volume ditorelon states alluded to in section 2.3. In most, but not all, cases the effective energy plateau in the effective energies, $aE_{\text{eff}}(t)$, defined in eq. (2.5) begin at $t = 2a$. So we show in table 9 the values of $aE_{\text{eff}}(t = 2a)$ that we obtain in each of the two sets of fields, for the ground states and some of the lowest lying excited states. We see that the two sets of values are remarkably consistent within errors, with only a small handful of heavier states differing by slightly more than 2σ. In addition to the glueball effective energies we also show those for the lightest two states of a flux tube that winds around the spatial torus. We do so for the flux in the fundamental representation ($k = 1$) and for the flux in the ($k = 2$) = ($k = 1$) $\otimes$ ($k = 1$) representation. Here too we see consistency within statistical errors. In addition to this study on the $14^3 20$ lattice we perform a similar one on a smaller $12^3 20$ lattices at the same β. This is the lattice size, in physical units, that is used in our calculations later on in this paper, and we recall that in general the local effects of constraining the topological charge should increase with decreasing volume (see e.g. [30]). Again we have consistency within errors for almost all the states. The conclusion of these explicit calculations is that within our typical statistical errors the physical quantities we calculate in this paper are not affected by constraining the total topological charge to $Q = 0$.

Although both the theory and our above explicit checks suggest that the loss of topological ergodicity in our calculations will have very little effect on our measured glueball spectrum, we implement the following additional procedure that is designed to reduce any remaining biases. Suppose we are confronted with topological freezing on a lattice of size $L_s^3 L_t$ at some value of β in some SU(N) theory. Now instead of starting with a $Q = 0$ field with $U_l = I, \forall l$, we produce a set of sequences in parallel which start with fields that have various values of Q. We choose the ensemble of these starting fields to roughly reproduce the expected distribution. What is 'expected' we infer from what we observe at the lower values of N where there is no topological freezing and also from the values obtained at the same value of N but at the larger values of $a(\beta)$ (if any) where the freezing has not yet set in. This is a plausible strategy since we find that in those cases where the distribution of Q can be determined there is little variation in the distribution of Q with either N or a on an equal physical volume. To produce such a starting field with some Q we generate a sequence of SU(3) fields on the same size lattice as our SU(N) one and we pick out a field with the desired charge Q. We 'cool' this field to produce a field with minimal fluctuations apart from the net topological charge. (See section 6 for details.) We then embed this lattice field of 3×3 complex matrices into a suitable corner of our set of $N \times N$ unit matrices, so as to produce a set of SU(N) matrices with charge Q. If we have topological freezing then this starting distribution of Q will be maintained in our set of Monte Carlo sequences. This method has some disadvantages but also some advantages. One advantage is that the lack of topological tunneling is a better representation of the continuum theory: we are sampling disconnected sectors. After all, the field configurations near the point of topological tunnelling have no continuum correspondence and are a lattice artifact. The major disadvantage is that we necessarily have a rather limited set of parallel sequences

(typically 20 or 40) and hence values of Q, and so only the most probable values of Q are properly represented. Lattice fields with values of Q that have a low probability simply do not appear. That is to say we are missing the tail of the Q distribution, and so any physics that depends on higher moments of Q will be something we cannot address here. However theory tells us that the correlation between such higher moments of Q and our gluonic operators will be suppressed as a correpondingly higher power of N, so any bias should be a small fraction of what, as we have seen above, will be at most a very small shift to the glueball masses.

In conclusion, our explicit calculations, the theoretical arguments, and our additional procedure of imposing upon our fields something quite close to the expected distribution of Q makes us confident that within our typical statistical errors any systematic error from the freezing of topology is negligible in our glueball calculations.

3 String tensions

Let us label the sites of the hypercubic lattice by the integers n_x, n_y, n_z, n_t. To project onto a fundamental ($k=1$) flux tube the simplest operator we can use is $\mathrm{Tr}(l_f)$ where l_f is the product of link matrices along a minimal path encircling the spatial torus. This is just the usual spatial Polyakov loop. For example, if the spatial lattice size is L then the Polyakov loop in the x direction is

$$l_f(n_y, n_z, n_t) = \prod_{n_x=1}^{n_x=L} U_x(n_x, n_y, n_z, n_t). \tag{3.1}$$

We also use such Polyakov loops composed of blocked links and we translate the operator along the x direction. Clearly the parities of such states are positive. This loop is translationally invariant along the flux tube direction and so the momentum along the flux tube is zero; $p_\parallel = 0$. It is rotationally invariant around its axis, so $J = 0$. Because of the usual centre symmetry (see below) the $C = +$ and $C = -$ flux tubes are degenerate. We then sum $l_f(n_y, n_z, n_t)$ over n_y and n_z so that the transverse momentum $p_\perp = 0$. Thus the lightest state onto which this final operator projects should be the ground state of the winding flux tube that carries fundamental flux. To project onto a $k = 2$ flux tube we do the same using linear combinations of the operators $\mathrm{Tr}(l_f l_f)$ and $\mathrm{Tr}(l_f)\mathrm{Tr}(l_f)$. For $k = 3$ we use linear combinations of $\mathrm{Tr}(l_f l_f l_f)$, $\mathrm{Tr}(l_f l_f)\mathrm{Tr}(l_f)$ and $\mathrm{Tr}(l_f)\mathrm{Tr}(l_f)\mathrm{Tr}(l_f)$, and so on for higher k. The defining property of a k-string that winds around the spatial torus in say the x direction is that under a transformation of the link matrices $U_x(n_x, n_y, n_z, n_t) \to \exp\{i2\pi/N\}U_x(n_x, n_y, n_z, n_t)$ for all n_y, n_z, n_t and at some fixed value of n_x, it will acquire a factor $\exp\{i2k\pi/N\}$. Since this transformation is a symmetry of the theory (the action and measure are unchanged) and at low temperatures the symmetry is not spontaneously broken, any two operators for which this factor of $\exp\{i2k\pi/N\}$ differ will have zero mutual overlap. So we have separate sectors of flux tubes labelled by k with the fundamental $k = 1$ strings existing for $N \geq 2$, the $k = 2$ strings for $N \geq 4$, the $k = 3$ strings for $N \geq 6$, and so on. We note that our basis of operators for a k-string could easily be extended by multiplying the operators by factors such as $\mathrm{Tr}(l_f)\mathrm{Tr}(l_f^\dagger)$, but while this might be useful to

improve the overlap onto massive excitations it would be very surprising if it improved the overlap onto the ground state which is what we are interested in here.

3.1 Finite volume corrections

As described above, we calculate the ground state energy of a flux tube that winds once around a spatial torus. If the lattice has size $l^3 l_t$, this flux tube has length l and we generically denote the energy by $E_k(l)$, where $k = 1$ corresponds to a flux tube carrying fundamental flux and k to a k-string (carrying k units of fundamental flux). The string tension σ_k is the energy per unit length of a very long flux tube

$$\sigma_k = \lim_{l \to \infty} \frac{E_k(l)}{l}. \tag{3.2}$$

In practice our tori are finite and so we expect that there will be corrections to the leading linear dependence of $E_k(l)$. In our calculations we will normally estimate the asymptotic string tension σ_k using the 'Nambu-Goto' formula

$$E_k(l) = \sigma_k l \left(1 - \frac{2\pi}{3\sigma_k l^2} \right)^{\frac{1}{2}}. \tag{3.3}$$

When expanded in powers of $1/\sigma_k l^2$ this formula generates all the known universal terms [31–34] and, at least for fundamental flux, proves to accurately describe numerical calculations for the range of l relevant to our calculations [35]. However, strictly speaking, these results hold for flux tubes that are effectively in an infinite transverse volume, while in our case, in order to maintain the rotational symmetry needed for our glueball calculations, the transverse size is $l \times l$ and so decreases when we decrease l. We therefore need to perform some explicit checks, i.e. to check whether eq. (3.3) encodes all the finite-l corrections that are visible within our typical statistical errors.

We see from eq. (3.3) that the relevant scale is l in units of the string tension, i.e. $l\sqrt{\sigma}$. These scales are listed in the headers of tables 1–8 and they vary from $l\sqrt{\sigma} \sim 4$ for lower N to $l\sqrt{\sigma} \sim 2.6$ for our highest values of N. As far as glueball masses are concerned the theoretical justification for this decrease in the volume is that we expect finite volume corrections to decrease as N grows and the practical reason is that the expense of the $SU(N)$ matrix product calculations grows as $\propto N^3$. In order to check whether there are significant corrections to eq. (3.3) at the values of l we use, we calculate σ on larger (sometimes smaller) lattices at selected values of β. These calculations are summarised in table 10. For $N = 8, 10, 12$ the scale $l\sqrt{\sigma} \sim 2.6$ corresponds to $l = 12$ in the table, and we see that the value of $a\sqrt{\sigma}$ is the same for the longer $l = 14$ flux tube, suggesting that there are no significant finite l corrections to eq. (3.3) for these values of N. The same conclusion holds for the other groups in table 10. All this provides evidence that the fundamental string tensions quoted in tables 1–8 do not suffer significant finite volume errors, at least within our typical statistical errors.

The energies of $k \geq 2$ flux tubes are larger and therefore so are the statistical and systematic errors in estimating them. Since the energies grow with k, we have only attempted a finite volume study for $k = 2$ flux tubes. This is presented in table 11. The message

here is more nuanced than for $k = 1$: while any finite l corrections to eq. (3.3) appear to be insignificant when $l\sqrt{\sigma} \gtrsim 3$, and hence for our $N \leq 6$ string tension calculations, there is strong evidence that there is a correction of $\simeq 1.9(5)\%$ to the values obtained with $l\sqrt{\sigma} \sim 2.6$, which are the values we emply for $N \geq 8$. This is something we will need to consider when we estimate the errors on our $k = 2$ string tensions. Presumably the $k = 3$ and $k = 4$ string tensions show corrections at least as large, but we do not have any finite l study of these.

3.2   Fundamental ($k = 1$) string tensions

We calculate the ground state energies of the fundamental flux tube for the lattices, couplings and gauge groups listed in tables 1–8. We then use eq. (3.3) to extract our estimates of the infinite volume string tensions. The energies are obtained by identifying effective energy plateaux as described in section 2.2. As an example we show in figure 1 the effective energies that lead to the SU(8) string tension estimates in table 6. As one increases β and hence decreases a, the energy in lattice units decreases so that we can obtain precise effective energies over a larger range of n_t which in turn makes it easier to identify a plateau and so estimate the corresponding value of $E_{\text{eff}}(n_t \rightarrow \infty)$. Although we attempt to show in figure 1 the error bands on our estimates of the corresponding flux tube energies, these are almost invisible because the errors are too small on the scale used in the plot. We therefore replot, in figure 2, the effective energies for $\beta = 47.75$, which is the calculation that is the closest to the desired continuum limit, with a sufficient rescaling to expose the errors on the effective masses. On the plot we show the best estimate for the energy obtained from a fit to the correlation function, together with the energies corresponding to ± 1 standard deviations.

For the corresponding SU(3) plots we refer the reader to figure 1 of [11]. The fact that the SU(3) lattices are (much) larger than the SU(8) ones at similar values of $a\sqrt{\sigma}$ means that the flux tubes are more massive, so the correlators decrease faster with n_t and the extraction of $E_{\text{eff}}(n_t \rightarrow \infty)$ is less compelling — despite the fact that the calculations extend closer to the continuum limit in the case of SU(3). These SU(3) plots are typical of our $N \leq 4$ calculations, where the lattices are chosen to be particularly large, while the SU(8) plot is typical of $N \geq 8$ where the spatial volumes used are smaller.

In the case of SU(2) and SU(3) we have also calculated the string tension on smaller volumes which are still large enough for the flux tube calculations even if too small for reliable glueball calculations. This enables us to extend the calculations to smaller values of $a\sqrt{\sigma}$ at modest computational cost. The purpose of these calculations is to feed into our analysis of the running coupling later on in this paper. We list the results of the calculations in tables 12, 13.

3.3 $k = 2$ string tensions

One expects that as $N \rightarrow \infty$ the $k = 2$ flux tube will become two non-interacting $k = 1$ flux tubes and we will have $\sigma_{k=2} \rightarrow 2\sigma_{k=1}$. However, as earlier calculations have shown [27, 35, 36], at lower values of N one finds that $\sigma_{k=2}$ is substantially less than $2\sigma_{k=1}$, so that one can think of it as behaving like a bound state of two fundamental flux tubes. This suggests that at lower values of N the $k = 2$ flux tube can be treated as a single 'string'

with finite volume corrections well described by eq. (3.3). As we increase N the $k = 2$ flux tube should increasingly look like two fundamental flux tubes that are loosely bound with the binding energy vanishing as $N \to \infty$. Here one might expect each of these two flux tubes to have finite volume corrections given by eq. (3.3) so that the overall finite volume behaviour of the energy of a $k = 2$ flux tube becomes significantly different:

$$E_{k=2}(l) \stackrel{\text{small } N}{=} \sigma_{k=2} l \left(1 - \frac{2\pi}{3\sigma_{k=2} l^2} \right)^{\frac{1}{2}} \stackrel{N \to \infty}{\longrightarrow} \sigma_{k=2} l \left(1 - \frac{4\pi}{3\sigma_{k=2} l^2} \right)^{\frac{1}{2}} \tag{3.4}$$

with $\sigma_{k=2} = 2\sigma_{k=1}$. One can expect a smooth transition between these two behaviours which clearly creates ambiguities in extracting the string tension $a^2 \sigma_{k=2}$ from the flux tube energy $a E_{k=2}(l)$.

Assuming for now that we can treat the $k = 2$ flux tube as a single string with finite volume corrections as given by eq. (3.3) we calculate $\sigma_{k=2}$ on our various ensembles of lattice fields. Using the previously calculated values of $\sigma_f \equiv \sigma_{k=1}$ we form the dimensionless ratio $\sigma_{k=2}/\sigma_f$ which we then extrapolate to the continuum limit using eq. (2.4). We show the extrapolations in figure 3. For $N \leq 6$ these appear to be under good control, but for larger N that is less clear. One would expect the slope of the extrapolation to vary smoothly with N, and that is certainly what one sees for $N = 4, 5, 6$. But then there is a violent break in the behaviour between $N = 6$ and $N = 8$ and wild oscillations when comparing the $N = 8, 10, 12$ slopes. It may be that this is due to our use of smaller spatial volumes for $N \geq 8$. In any case, we calculate the continuum limits from these fits and the results for our various gauge groups are presented in the second column of table 14. As remarked earlier, there is good evidence from table 11 that for the smaller lattices that we have used for $N \geq 8$ we should apply an additional finite volume correction of $\simeq 1.9(5)\%$. Doing this leads to the values in the third column of table 14, which are the values we consider to be more reliable. There is a caveat here: at our largest values of N the values of $\sigma_{k=2}/\sigma_f$ are quite close to the asymptotic value of two, and so we might expect that we are in the range of N where the stronger finite volume behaviour displayed in eq. (3.4) is setting in. To settle this question would require a dedicated calculation that is beyond the scope of this paper.

We have also obtained continuum extrapolations of the $k = 3$ and $k = 4$ string tensions. These have been obtained from the corresponding flux tube energies using eq. (3.3) and this undoubtedly underestimates the finite volume corrections. Indeed as $N \to \infty$ we expect $\sigma_k \to k\sigma_f$ as the k-string becomes k non-interacting fundamental strings, and then we expect a version of eq. (3.4),

$$E_k(l) \stackrel{N \to \infty}{\longrightarrow} k\sigma_f l \left(1 + \frac{2\pi}{3\sigma_f l^2} \right)^{\frac{1}{2}} = \sigma_k l \left(1 + \frac{2k\pi}{3\sigma_k l^2} \right)^{\frac{1}{2}}. \tag{3.5}$$

Given this uncertainty and the increasing ambiguity with increasing k of extracting an effective energy plateau (because of their increasing energies), we do not discuss these values any further here.

3.4 $N \to \infty$ extrapolations

An interesting question about the ratio $\sigma_{k=2}/\sigma_f$ concerns its dependence on N. On general grounds we expect the leading correction to the asymptotic value to be $O(1/N^2)$. However there are old ideas under the label of 'Casimir Scaling', that the (string) tension of a flux tube should be proportional to the smallest quadratic Casimir of the representations that contribute to that flux, as though the flux tube joining two sources behaved, in this respect, just like one gluon exchange. For the k flux tube the relevant representation is the totally antisymmetric one and this predicts

$$\frac{\sigma_k}{\sigma_f} \stackrel{CS}{=} \frac{k(N-k)}{N-1} \stackrel{N \to \infty}{=} k - \frac{k(k-1)}{N} - \frac{k(k-1)}{N^2} + O\left(\frac{1}{N^3}\right) \tag{3.6}$$

so that the leading correction is $O(1/N)$ rather than $O(1/N^2)$. Previous lattice calculations have often favoured Casimir scaling as a good approximation [39] so it is interesting to test this idea against our $k = 2$ values listed in table 14. In figure 4 we plot our continuum values of $\sigma_{k=2}/\sigma_f$ against $1/N^2$. In addition we know that $\sigma_{k=2}/\sigma_f = 2$ at $N = \infty$ so we impose this as a constraint in our fits. In figure 4 we show our best fit in powers of $1/N^2$

$$\frac{\sigma_{k=2}}{\sigma_f} = 2.0 - \frac{1.28(19)}{N} - \frac{4.78(90)}{N^2} \tag{3.7}$$

with a χ^2 per degree of freedom of ~ 0.5 and an alternative best fit in powers of $1/N^2$

$$\frac{\sigma_{k=2}}{\sigma_f} = 2.0 - \frac{14.43(60)}{N^2} + \frac{73.8(12.1)}{N^4} \tag{3.8}$$

with a χ^2 per degree of freedom of ~ 2.2. The former fit is clearly better, but the latter cannot be entirely excluded. On the other hand while the fit in powers of $1/N$ is very good, the coefficients are very different from those obtained if we expand the Casimir scaling prediction, as in eq. (3.6). One may speculate that for the range of N where the $k = 2$ flux tube is a bound state the N dependence of the string tension is best described in powers of $1/N$ while once N is large enough that it has become a weakly interacting pair of fundamental flux tubes, the dependance will be best described in powers of $1/N^2$. At which N this transition occurs will depend on the length l of the flux tube. If we use the formula in eq. (3.3) for the fundamental and $k = 2$ flux tubes and if we assume that $\sigma_{k=2} = 2\sigma - O(1/N)$, then one finds that the lightest state will be the weakly interacting pair of fundamental flux tubes for $l \leq l_c$ where $l_c\sqrt{\sigma} \propto N^{\frac{1}{2}}$. (This essentially reflects a competition between the leading linear terms and the $O(1/l)$ Luscher corrections.) That is to say, for any fixed length l, the (very) asymptotic leading correction is $O(1/N^2)$ as expected by the usual large-N counting. However one has to be careful in which order one takes the $l \to \infty$ and $N \to \infty$ limits.

4 Running coupling

A question of theoretical interest is whether our calculations show that we should keep the 't Hooft coupling g^2N fixed as $N \to \infty$ in order to have a smooth large-N limit. A question

of phenomenological interest is whether we can estimate the scale Λ of our SU(N) gauge theories, from the calculated running of the gauge coupling, and in particular whether we can do so for SU(3). Finally something that is often useful in lattice calculations is to have an interpolation function for $a(\beta)$. These are the three issues we address in this section. A summary of the technical background to the perturbative calculations has been placed in appendix A.

4.1 Scaling with N

Since the lattice coupling g_L^2 defined in eq. (2.2) provides a definition of the running coupling on the scale a, and our above calculation of the (fundamental) string tension at various β enables us to express a in physical units, i.e. as $a\sqrt{\sigma}$, we can use these calculations to address some questions about the properties of the running coupling in SU(N) gauge theories. Before doing so we recall that this lattice coupling, corresponding to the particular coupling scheme defined by the lattice and the plaquette action, is well-known to be a 'poor' definition of a running coupling in the sense that higher order corrections will typically be very large. This is indicated, for example, by the relationship between the scale parameters Λ_L and $\Lambda_{\overline{MS}}$ in this scheme and the standard $\overline{MS}$ scheme [37, 38]:

$$\frac{\Lambda_{\overline{MS}}}{\Lambda_L} = 38.853 \exp\left\{-\frac{3\pi^2}{11N^2}\right\}. \tag{4.1}$$

This is a long-standing issue that has led to the formulation of a number of improved couplings. (For a review see [40].) Here we shall use the 'mean-field' improved coupling of Parisi [41],

$$\frac{1}{g_I^2} = \frac{1}{g_L^2}\langle\frac{1}{N}\mathrm{Tr}U_p\rangle, \tag{4.2}$$

which has a nice physical motivation as the effective coupling experienced by a background field (in a simple approximation). Denoting the corresponding scale by Λ_I, one finds

$$\frac{\Lambda_{\overline{MS}}}{\Lambda_I} = \frac{\Lambda_L}{\Lambda_I}\frac{\Lambda_{\overline{MS}}}{\Lambda_L} = \exp\left\{-\frac{w_1}{2b_0}\right\} \times 38.853\exp\left\{-\frac{3\pi^2}{11N^2}\right\} \simeq 2.633 \tag{4.3}$$

using eq. (4.1) and eqs. (A.12), (A.17), with the value of Λ_L/Λ_I being obtained using eq. (A.7) for each Λ, with g_I^2 and g_L^2 related by eqs. (A.16), (A.17), and then taking $g^2 \to 0$. This already suggests that g_I^2 has the potential to be more-or-less as good as $g_{\overline{MS}}^2$. One can also show [42] that this coupling tracks quite accurately the Schrodinger-functional coupling [43, 44] over a very wide range of scales. (See [42] for a detailed discussion.) So from now on, in this section, we shall use $g_I^2(a)$ as our lattice running coupling.

The main question we address concerns the N dependence of $g_I^2(a)$. The usual large N counting tells us that we expect to approach constant physics as $N \to \infty$ if we keep g^2N fixed. For the running coupling this means that if we plot $g_I^2(a)N$ against the calculated values of $a\sqrt{\sigma}$ in our SU(N) gauge theories, they should approach a common envelope as $N \to \infty$. The interesting question is whether the approach is slow or fast, indicating that our values of N are 'far from' or 'near to' $N = \infty$ respectively. In figure 5 we plot our calculated values of the running 't Hooft coupling $g_I^2(a)N$ against $a\sqrt{\sigma}$ for all our values of N. The

results are quite remarkable: even SU(2) is very close to SU(∞) in this respect, and it is only when the lattice spacing becomes large that appreciable differences appear. It is also interesting to see what happens if one uses the poor $g_L^2(a)$ coupling instead of $g_I^2(a)$, and one finds that while the convergence to a large N limit is still evident, the corrections at lower N are substantial indicating that, not surprisingly, higher order non-planar contributions are important using this coupling scheme. Finally we comment that these conclusions are not unexpected or novel: similar analyses have appeared in for example [1, 42], albeit usually with less accuracy and over more limited ranges of N and $a\sqrt{\sigma}$.

4.2 Perturbative running and $\Lambda_{\overline{\mathrm{MS}}}$

The second question we address is whether the running coupling dependence displayed in figure 5 can be described by the usual perturbative β-function for at least some N once a is small. If so we can extract a value of Λ_I for each such N and a corresponding value of $\Lambda_{\overline{MS}}$ using eq. (4.3). Our analysis will broadly follow that of [42] and we refer the reader to that paper for background and context; here we merely outline the calculation, with more details in appendix A. To fix our notation we begin with the standard β-function for the lattice bare coupling g_I^2:

$$\beta(g_I) = -\frac{\partial g_I^2}{\partial \log a^2} = -b_0 g_I^4 - b_1 g_I^6 - b_2^I g_I^8 + \ldots + O(a^2), \tag{4.4}$$

where the scheme independent coefficients b_0, b_1 and the scheme dependent b_2^I are given in eq. (A.12) and eq. (A.18) of appendix A. As shown in appendix A this motivates the following 3-loop expression for a:

$$a\sqrt{\sigma}(a) \overset{\mathrm{3loop}}{=} \frac{\sqrt{\sigma}(0)}{\Lambda_I} \left(1 + c_\sigma a^2 \sigma\right) \left(b_0 g_I^2(a)\right)^{-\frac{b_1}{2b_0^2}} e^{-\frac{1}{2b_0 g_I^2(a)}} e^{-\frac{1}{2}\int_0^{g_I^2(a)} dg^2 \left(\frac{b_0 b_2^I - b_1^2 - b_1 b_2^I g^2}{b_0^3 + b_0^2 b_1 g^2 + b_0^2 b_2^I g^4}\right)}. \tag{4.5}$$

Here the first factor on the right after the coefficient is a non-perturbative tree-level lattice spacing correction. The motivation is that we could just as well use some physical mass, $\mu(a)$, as a scale in place of $\sqrt{\sigma}(a)$ and since $\mu(a)/\sqrt{\sigma}(a) = \mu(a=0)/\sqrt{\sigma}(a=0)(1+O(a^2))$ it must be the case that we have, in general, a factor $(1 + O(a^2))$ multiplying the perturbative expression [42, 45]. Here we choose to use σ as our scale for a^2: using some other μ^2 would only change the $O(a^4)$ term and we will assume that a is small enough that we can neglect any $O(a^4)$ terms. We evaluate numerically the integral in the exponential for any given value of $g_I(a)$: for such a smooth integrand any simple technique will be able to give accurate results. We now describe the result of fitting this function to our values of $a\sqrt{\sigma}$, as listed in tables 12, 13 for SU(2) and SU(3) and in tables 3–8 for SU(4) to SU(12). In performing these fits one can either use the measured values of $a^2\sigma$ in the $(1 + c_\sigma a^2\sigma)$ lattice correction factor, or the value calculated from the formula itself. In the latter case eq. (4.5) becomes a quadratic equation for $a\sqrt{\sigma}$. Not surprisingly, for the range of $g_I^2(a)$ where eq. (4.5) provides a good fit to our calculated string tensions, the difference between the two methods is insignificant, and we choose here to use the measured value in the correction term.

The results of our fits using eq. (4.5) are shown in table 15. For each value of N we fit our lattice values of $a\sqrt{\sigma}$ discarding the largest values until we obtain a reasonably acceptable fit. The range of lattice spacings for the fits is listed for each N, together with the χ^2 per degree of freedom, χ^2/n_{df}. In the few cases labelled by $*$ in table 15 the fits are very poor with $\chi^2/n_{df} \geq 3$, and so we quadruple the stated error in those cases in the hope that this encodes the increased uncertainty. Referring to tables 1–8 we see that the number of values used within a given fit varies from 6 in SU(3) to 4 in SU(10) and SU(12). Since we have 2 parameters in our fit, 4 points is a very small number for a fit. Moreover, for SU(10) and SU(12) the lattice spacings do not extend to values as small as for lower N. Hence one should treat the resulting fits with extra caution.

In table 15 we also list the fitted values of the perturbative scale parameter, Λ_I, in units of the continuum string tension. We then convert this to the corresponding $\Lambda_{\overline{MS}}$ scale in the widely used $\overline{MS}$ coupling scheme, using the N-independent relation $\Lambda_{\overline{MS}}/\Lambda_I \simeq 2.633$ from eq. (4.3) and the results are listed in the last column of table 15, again in units of the string tension. The quoted errors on our values of Λ_I are very small, but they are purely statistical and their smallness reflects the very small errors on the string tensions that are fitted. The systematic errors involved in, for example, the truncation of the beta-function may be much larger. To get some measure of this error we also perform an extra fit using the exact 2-loop running,

$$a\sqrt{\sigma}(a) \stackrel{2\text{loop}}{=} c_I \left(1 + c_{\sigma,I} a^2\sigma\right) e^{-\frac{1}{2b_0 g_I^2}} \left(\frac{b_1}{b_0^2} + \frac{1}{b_0 g_I^2}\right)^{\frac{b_1}{2b_0^2}}. \tag{4.6}$$

The resulting 2-loop values of Λ_I are also listed in table 15. We see that $\Lambda_I^{2\text{loop}}$ is typically about 10% smaller than the $\Lambda_I^{3\text{loop}}$. We have decided to use half of this difference as a measure of the error associated with dropping 4-loop and higher coefficients from the 3-loop calculation. This is added as a second error, within square brackets, to the resulting 3-loop values for $\Lambda_{\overline{MS}}$ that are listed in the last right-hand column of table 15. Unlike the statistical errors, this error will affect the results for all values of N in the same direction.

In figure 6 we display the values that we obtain from our 3-loop fits for $\Lambda_{\overline{MS}}/\sqrt{\sigma}$ as a function of N. (We use only the statistical errors in these fits.) It is clear that the variation with N is very weak. If we fit all our values for $N \leq 12$ we find the fit,

$$\frac{\Lambda_{\overline{MS}}}{\sqrt{\sigma}} = 0.5055(7)[250] + \frac{0.306(12)}{N^2}, \quad \chi^2/n_{df} = 2.70, \qquad N \in [2, 12], \tag{4.7}$$

which is displayed in figure 6. Although the χ^2/n_{df} is not good, the calculated values appear to be scattered around the fit in a random pattern. Other possible fits include

$$\frac{\Lambda_{\overline{MS}}}{\sqrt{\sigma}} = 0.5067(11)[250] + \frac{0.258(12)}{N^2}, \quad \chi^2/n_{df} = 1.65, \qquad N \in [4, 12],$$

$$\frac{\Lambda_{\overline{MS}}}{\sqrt{\sigma}} = 0.5060(8)[250] + \frac{0.303(13)}{N^2}, \quad \chi^2/n_{df} = 3.81, \qquad N \in [2, 8],$$

$$\frac{\Lambda_{\overline{MS}}}{\sqrt{\sigma}} = 0.5093(16)[250] + \frac{0.206(38)}{N^2}, \quad \chi^2/n_{df} = 0.44, \qquad N \in [4, 8]. \tag{4.8}$$

In all the above fits we have included within square brackets an estimate of $\sim 5\%$ for the systematic error associated with the truncation of the perturbative expansion. We note that this systematic error is much larger than the differences between the various fits above, and is the dominant source of uncertainty.

To finish we turn briefly to the case of SU(3) where the value of $\Lambda_{\overline{MS}}$ has phenomenological interest. Here we can attempt to transform our value into MeV units as follows. We begin with its value in units of the string tension, as listed in table 15, and we then transform this into a value in terms of the Sommer length scale r_0 [46] using a recent calculation [11] that gives $r_0\sqrt{\sigma} = 1.160(6)$. A recent review [47] of calculations in lattice QCD with light quarks concludes that $r_0 = 0.472(5)\text{fm} = 1/418(5)\text{MeV}^{-1}$. The usual expectation is that the value of r_0 is not very sensitive to the inclusion of light quarks, so we use this MeV value in the pure gauge theory. (This is of course the arguable step.) Doing so we arrive at

$$\left.\frac{\Lambda_{\overline{MS}}}{\sqrt{\sigma}}\right|_{\text{SU3}} = 0.5424(13)[185] \Longrightarrow r_0\Lambda_{\overline{MS}} = 0.629(4)[22] \Longrightarrow \Lambda_{\overline{MS}} \overset{\text{SU3}}{=} 263(4)[9]\text{MeV}, \quad (4.9)$$

where the first error is statistical and the second is systematic. This value is consistent with the values recently obtained in the dedicated calculations [48, 49] that use very different methods, and our value has a similar accuracy. This adds confidence that our calculations of $\Lambda_{\overline{MS}}$ for the other SU(N) groups are also reliable.

4.3 Interpolating and extrapolating functions for $a(\beta)$

It can often be useful to know the value of $a(\beta)$, in physical units, at some value of β. This can be provided, for example, by the value of $a\sqrt{\sigma}$. However calculations of $a\sqrt{\sigma}$ are obtained at a number of discrete values of β within some finite range $\beta_0 \leq \beta \leq \beta_1$ and the β value of interest may lie outside this range, or may be within this range but not at one of the discrete values where $a\sqrt{\sigma}$ has been calculated. In the latter case one needs to find an interpolating function that will work in the range $\beta \in [\beta_0, \beta_1]$ and since $a\sqrt{\sigma}$ typically varies smoothly in this range this is easy to do: a few sensibly chosen terms from almost any complete set of functions will work adequately. However if the β value of interest lies outside the range $[\beta_0, \beta_1]$ and, in particular, if it is at some weaker coupling, then extrapolating such a 'random' interpolating fit will invariably work badly unless the original interpolating function has a form motivated by weak coupling perturbation theory, in which case it should (in principle) be reasonably accurate. In the section above we have used precisely such functions. We will here present a fit in an explicit form so that the reader can readily employ it.

Our fit will be in terms of the mean-field improved coupling g_I^2 defined in eq. (4.2). This requires that one know the value of the average plaquette; this is always calculated in a Monte Carlo but one needs to record the average, which is normally done so as to provide a first check on the calculation. (And if not, one can obtain a value with adequate accuracy very quickly using small lattices and modest statistics.) The interpolating function we will use is a variation on the ones used above and is as follows:

$$a\sqrt{\sigma}(a) = c_0 \left(1 + c_\sigma a^2 \sigma(a)\right) F_{2l+}(g_I), \quad (4.10)$$

where

$$F_{2l+}(g_I) = e^{-\frac{1}{2b_0 g_I^2}} \left(\frac{b_1}{b_0^2} + \frac{1}{b_0 g_I^2} \right)^{\frac{b_1}{2b_0^2}} e^{-\frac{b_2^I}{2b_0^2} g_I^2}. \tag{4.11}$$

The first two factors of $F_{2l+}(g_I)$ constitute the exact dependence when $\beta(g)$ is truncated to the first two terms. The last factor on the right is the extra dependence if one keeps in the exponent the leading $O(b_2^I)$ term to $O(g_I^2)$. That is to say, it is 'more' than 2 loops, but 'less' than 3 loops. Hence the subscript $2l+$ on $F(g)$. This is of course an arbitrary truncation with no guarantee that it does indeed do better than the 2-loop one; however we use it because, as we shall see below, it turns out to be very close to the 3-loop result, but without the need to perform any numerical integrations. Note that here we choose to use in the $\propto a^2\sigma$ correction term the value given by fitting the formula to our data since this is the mode in which it needs to be used in an extrapolation.

To make use of eq. (4.11) we need to fit the constants c_0 and c_σ to our calculated values of $a\sqrt{\sigma}$, at each N. Once the constants c_0 and c_σ have been fitted we can solve eq. (4.10), which is quadratic in $a\sqrt{\sigma}$, at any value of β_I:

$$a\sqrt{\sigma}(a) = \frac{1}{2c_0 c_\sigma F_{2l+}(\beta_I)} \left(1 - \left[1 - 4c_0^2 c_\sigma F_{2l+}(\beta_I)^2 \right] \right). \tag{4.12}$$

In eq. (4.11) the values of b_0, b_1, b_2^I need to be specified. The values of b_0 and b_1 are universal and are given in eq. (A.12). The value of b_2^I is as given in eq. (A.18)

$$b_2^I = b_2^L + w_2 b_0 - w_1 b_1, \tag{4.13}$$

where we use eqs. (A.13), (A.15) in eq. (A.14) to obtain the explicit expression for b_2^L and then inserting that together with the functions in eq. (A.17) and eq. (A.12) into eq. (4.13) we obtain the explicit expression for b_2^I for any N.

It only remains now to give our fitted values of c_0 and c_σ for each of the SU(N) groups for which we have calculated the string tension. This we do in table 16. There we show for each N our best fits to these two parameters as well as the fitted range and the χ^2 per degree of freedom of the fit. In performing these fits we systematically drop the largest values of $a\sqrt{\sigma}$ from the fit until we obtain an acceptable χ^2. This is appropriate since our interpolating function is based on weak-coupling perturbation theory. Note that being based on weak coupling the resulting function is not designed to work for values of a or g^2 greater than the range within which it provides a good fit.

As an aside it needs to be emphasised that all the above fits are only relevant if one uses the Wilson plaquette action. As a second aside, we note that if one wants $a(\beta)$ in terms of some physical scale μ instead of $\sqrt{\sigma}$ then one can straighforwardly modify the above formula for $a\sqrt{\sigma}$ to one for $a\mu$ by using the relation $\mu/\sqrt{\sigma} = d_0 + d_1 a^2\sigma$ if it accurately holds in the range of couplings of interest.

5 Glueball masses

5.1 Quantum numbers

The glueballs are colour singlets and so our glueball operator is obtained by taking the ordered product of $SU(N)$ link matrices around a contractible loop and then taking the trace. To retain the exact positivity of the correlators we use loops that contain only spatial links. The real part of the trace projects on $C = +$ and the imaginary part on $C = -$. We sum all spatial translations of the loop so as to obtain an operator with momentum $p = 0$. We take all rotations of the loop and construct the linear combinations that transform according to the irreducible representations, R, of the rotational symmetry group of our cubic spatial lattice. We always choose to use a cubic lattice volume that respects these symmetries. For each loop we also construct its parity inverse so that taking linear combinations we can construct operators of both parities, $P = \pm$. The correlators of such operators will project onto glueballs with $p = 0$ and the R^{PC} quantum numbers of the operators concerned.

The irreducible representations R of our subgroup of the full rotation group are usually labelled as A_1, A_2, E, T_1, T_2. The A_1 is a singlet and rotationally symmetric, so it will contain the $J = 0$ state in the continuum limit. The A_2 is also a singlet, while the E is a doublet and T_1 and T_2 are both triplets. In section 5.7 we will outline the detailed relationship between these representations and the continuum spin J. Since, for example, the three states transforming as the triplet of T_2 are degenerate on the lattice, we average their values and treat them as one state in our tables of glueball masses and we do the same with the T_1 triplets and the E doublets. (Just as we would treat the 5 states of a continuum $J = 2$ glueball as one entry.)

5.2 Finite volume effects

For reasons of computational economy we wish to calculate on lattice sizes that are small but, at the same time, large enough that any finite volume corrections remain smaller than our typical statistical errors. Since the computional cost of calculating in $SU(N)$ gauge theories grows roughly $\propto N^3$ (the multiplication of two $N \times N$ matrices) and since finite volume corrections are expected to decrease as powers of $1/N$, we reduce the size in physical units of our lattices as we increase N, as shown in tables 1–8.

There are two important types of finite volume corrections. The first can be thought of as arising when the propagating glueball emits a virtual glueball which propagates around the spatial torus. The resulting shift in the mass of the propagating glueball decreases exponentially in $m_G l$ where m_G is the mass gap and l is the length of the spatial torus [19]. As we see from tables 1–8 the value of $am_G \times l/a$ is quite large in all of our calculations, so we can expect this correction to be small.

The second type of finite volume correction consists of states composed of multiple flux tubes winding around a spatial torus in a (centre) singlet state. The lightest of these will be a state composed of one winding flux tube together with a conjugate winding flux tube, which we refer to as a 'ditorelon'. (A single winding flux tube is usually referred to as a 'torelon'.) Since it can have a non-zero overlap onto the contractible loops that we use as our glueball operators, it can appear as a state in our calculated glueball spectrum.

Neglecting interactions, the lightest ditorelon will consist of each flux tube in its ground state with zero momentum and will have an energy, E_d, that is twice that of the flux tube ground state, $E_d = 2E_f$. Interactions will shift the energy but this shift should be small on our volumes so we shall use $E_d \simeq 2E_f$ as a rough guide in searching for these states. This ground state ditorelon has simple rotational properties and only contribute to the A_1^{++} and E^{++} representations. If we allow one or both of the component flux tubes to be excited and/or to have non-zero equal and opposite transverse momenta we can populate other representations and produce towers of states. However these excited ditorelon states will be considerably heavier on the lattice volumes we employ and so we will not consider them any further in this paper, although they certainly warrant further study.

The first of the above corrections leads to small shifts in the masses of the glueballs. The second leads to extra states in the glueball spectrum. The signature of such an extra ditorelon state is that its mass grows roughly linearly with the lattice size: $aE_D \simeq 2aE_f \simeq 2a^2\sigma_f L$ where L is the relevant spatial size in lattice units and σ_f is the (fundamental) string tension. So to test for finite volume effects we perform calculations at the same value of β on different lattice sizes and compare the glueball spectra. To identify any ditorelon states we look for extra states in the A_1^{++} and E^{++} spectra whose masses increase roughly linearly with the volume. Since the mass shift associated with the first kind of correction decreases exponentially with the lattice size any shift on a significantly larger volume should be much smaller than on the smaller volume; so to check that it is negligible compared to our statistical errors we simply compare the masses of the states that are not ditorelons on the different volumes. As we see from tables 1–8 the lattice sizes we use fall into three groups: $l\sqrt{\sigma} \sim 4.0$ for $SU(2), SU(3), SU(4)$; $l\sqrt{\sigma} \sim 3.1$ for $SU(5), SU(6)$; $l\sqrt{\sigma} \sim 2.6$ for $SU(8), SU(10), SU(12)$. We will exhibit a finite volume analysis for a representative of each of these three groups.

We begin with $SU(2)$. In table 17 we list the low-lying glueball spectra that we obtain on 3 lattice sizes, together with the energies of the ground and first excited states of the winding flux tubes. In physical units the $L = 12, 14, 20$ spatial lattice sizes correspond to $l\sqrt{\sigma} \simeq 2.9, 3.4, 4.8$ respectively and we recall that the typical lattice size we use in $SU(2)$ is $l\sqrt{\sigma} \simeq 4$. For the glueball states we list the effective energy at $t = 2a$ or, where applicable, the energy of the fit to the effective energy plateau when that begins at $t = 2a$. (These two measures differ very little in practice.) These are obtained from the correlators of our variationally selected best operators. For most of our lighter states the value of $aE_{\text{eff}}(t = 2a)$ is very close to our best estimate of the mass. For these finite volume comparisons we prefer this measure to the mass itself because it serves to minimise the statistical errors and makes any finite volume corrections more visible. Putting aside the $R^P = A_1^+$ and the E^+ spectra for the moment, we see that most of the glueball energies on the $L = 14$ and $L = 20$ lattices are consistent within one standard deviation and all within two standard deviations. The energies from the $L = 12$ lattice are broadly consistent but there are now some examples, such as the A_2^+ and E^- ground states, where there appear to be significant differences. We now return to the A_1^+ and the E^+ spectra listed in table 17 to see if there is any evidence of the extra ditorelon states. We do indeed see these on the $L = 12$ and $L = 14$ lattices in both the A_1^+ and the E^+ spectra: these states are displayed in the table with no corresponding

entries at other lattice sizes. Their effective energies increase with L and are just a little heavier than twice the flux tube energy. For the $L = 20$ lattice any ditorelon state would be much heavier than any of the states shown: at such energies the spectrum is denser, the errors are larger, and so identifying an 'extra' state becomes ambiguous. The remaining states in the A_1^+ and the E^+ spectra are broadly consistent across the lattice sizes, except for the lightest E^+ on $L = 12$ and the first excited A_1^+ on $L = 14$, both of which are quite close to their respective ditorelons and possibly mixing with them. Also the 4th state in the $L = 12$ A_1^+ spectrum shows a shift. Since the typical lattice size we use in SU(2) is $l\sqrt{\sigma} \sim 4$ (except for the relatively unimportant calculations at the largest values of $a(\beta)$) we can estimate the ditorelon states to have energies $E_D \sim 2\sigma l \sim 2(l\sqrt{\sigma})\sqrt{\sigma} \sim 8\sqrt{\sigma}$ and we shall therefore only perform continuum extrapolations of A_1^+ and E^+ states that are lighter than $\sim 8\sqrt{\sigma}$, although it is still the case that the heaviest states in these channels may be perturbed by ditorelon contributions. As for the other channels, since the size $l\sqrt{\sigma} \sim 4$ falls between our $L = 14$ and $L = 20$ lattices at $\beta = 2.427$, we can conclude from the above that there should be no finite volume corrections that would be visible outside our statistical errors. We have performed similar finite volume checks in SU(3) in our earlier paper [11] and we refer the reader to that paper for details, in particular for a check of the $C = -$ states. In the case of SU(4) we have performed a finite volume analysis comparing the spectra on $18^3 20$ and 22^4 lattices at $\beta = 11.02$, which has helped us identify the positions of the ditorelon states in the spectra at other values of β, and to remove these states from our spectra. With all these checks we have some confidence that our SU(2), SU(3) and SU(4) continuum spectra will not be afflicted by significant finite volume corrections.

Our SU(5) and SU(6) calculations are on significantly smaller volumes, typically with $l\sqrt{\sigma} \sim 3.1$, and therefore deserve a separate finite volume study to the one above. To do so we compare the low-lying glueball spectra that we obtain in SU(5) on $14^3 20$ and $18^3 18$ lattices at $\beta = 17.46$, together with the energies of the ground and first excited states of the fundamental and $k = 2$ winding flux tubes. In physical units these $L = 14$ and $L = 18$ spatial lattice sizes correspond to $l\sqrt{\sigma} \simeq 3.06$ and 3.93 respectively and we recall that the typical lattice size we use in SU(5) and SU(6) is $l\sqrt{\sigma} \simeq 3.1$ i.e. close to that of the smaller of our two lattices. As in SU(2) we readily identify the extra ditorelon states in the A_1^{++} and E^{++} representations, which have energies very close to twice that of the winding fundamental flux tube. (The ditorelon on the $L = 18$ lattice will lie outside our energy range.) They appear to be well separated from neighbouring glueball states and so we can readily identify and exclude them from our SU(5) and SU(6) glueball spectra and exclude them from our continuum limits. The other energies on our two lattice sizes are mostly within errors of each other, with a few out by up to two standard deviations, and two states a little more than that. Given the large number of states being compared, such rare discrepancies are inevitable and we can claim that we see no significant finite volume corrections to any of our listed states.

We now turn to our largest N calculations where we use the even smaller spatial lattice size $l\sqrt{\sigma} \simeq 2.6$. Our finite volume study is in SU(12) on $12^3 20$ and $14^3 20$ lattices at $\beta = 103.03$, where the $12^3 20$ lattice represents our typical physical size, and the energies are listed in table 18. In contrast to the previous tables, we list under the A_1^{++} and E^{++}

representations our best estimate of the true glueball spectrum with the ditorelons removed. We will return to the identification of the latter shortly. We observe that most of the energies are the same within errors and all are within two standard deviations. That is to say, any finite volume shifts in the energies are within our statistical errors at these values of N, despite the fact that the $L = 12$ lattice volume is quite small.

The situation with respect to the ditorelons is more complex. The first complication is that on the $12^3 20$ lattice the A_1^{++} ditorelon is nearly degenerate with the first excited A_1^{++} glueball, so that these states may well mix even if the overlaps are small due to the large-N suppression. Moreover the same occurs in the E^{++} representation where the ditorelon is nearly degenerate with the ground state E^{++} glueball. The second complication arises from the fact that the overlap of the ditorelon double trace operators onto the single trace operators that we used to calculate the glueball spectrum is suppressed since N is large. This should be an advantage and indeed if the overlap is small enough then the ditorelon will not appear in the spectrum obtained from the single trace operators so that there is no issue. However it may well appear as a minor component of a state that at first sight is quite massive but then its $aE_{\text{eff}}(t)$ drops towards the ditorelon energy as t increases and the more massive components die away. This can lead to ambiguities and indeed does on both our lattice sizes.

Since all our SU(12) glueball calculations, and also those in SU(10) and SU(8), are on lattices of roughly the same physical size as our $12^3 20$ one at $\beta = 103.03$, we need to address these problems with the ditorelons. We do so as follows. First we find that if in constructing our glueball operators we use blocked links whose extent is smaller than the lattice size then the overlap of ditorelons onto these operators is small enough that we do not see any ditorelon state in the A_1^{++} spectrum but we do see it embedded as a small component in more massive states in the E^{++} spectrum. Since a link at blocking level bl joins sites that are $2^{bl-1}a$ apart, this means keeping to blocking levels $bl = 1 - 4$ on our $l = 12a$ and $l = 14a$ lattices. If we now do something that may appear less reasonable and include $bl = 5$ blocked links, which join lattice sites $16a$ apart, so that the operators formed out of these links wrap multiply around the spatial torus in all spatial directions, we find that the ditorelon overlaps are much larger and the ditorelon states now appear quite clearly in the resulting spectrum. The results of these various calculations are shown in table 19. As usual the energies shown are $aE_{\text{eff}}(t = 2a)$ and so are often slightly higher than the value of the effective energy plateau. Consider first the A_1^{++} spectra on the $12^3 20$ lattice. We see that the second and third states in the $bl = 1 - 5$ spectrum are nearly degenerate, with masses close to what one might expect for the ditorelon, i.e. $2aE_f \sim 0.96$, but only one of them appears in the $bl = 1 - 4$ spectrum. Thus we infer that one of those two (or a mixture of the two) is a ditorelon. On the $14^3 20$ lattice we also see an extra state in the $bl = 1 - 5$ spectrum, as compared to the $bl = 1 - 4$ spectrum, but now the state is heavier, as we would expect for a ditorelon since $2aE_f \sim 1.2$ on this lattice. Turning to the E^{++} representation on the $14^3 20$ lattice we find an extra state using the $bl = 1 - 5$ basis, as compared to using the $bl = 1 - 4$ basis, with roughly the expected mass of a ditorelon. On the $12^3 20$ lattice things are a bit different: the second state in the $bl = 1 - 5$ spectrum has no obvious partner in the $bl = 1 - 4$ spectrum, but there is a state in the latter spectrum

where $aE_{ff}(t)$ decreases rapidly with increasing t to a comparable value. This is the second entry in the table and the mass from the 'plateau', indicated in square brackets, is similar to the energy of the second state in the $bl = 1 - 5$ spectrum. We interpret this as follows: the E^{++} ditorelon has a substantial overlap onto the $bl = 1 - 5$ basis and only a small overlap onto the $bl = 1 - 4$ basis, but large enough to appear within what appears to be a higher excited state. This mass is somewhat smaller than that of the state we identified as a ditorelon on the $14^3 20$ lattice which is what one expects. We note that unlike the states we identify as ditorelons, most of the other states have nearly the same energies on the two lattice sizes, as one expects for states that are not ditorelons. Recalling that the lattice sizes we use in our $N \geq 8$ calculations are of the same physical size as our $12^3 20$ lattice at $\beta = 103.03$, we can use the above results in all those cases to identify ditorelon states and remove them from our glueball spectra. The same type of technique is useful for $N = 5, 6$.

A final comment is that the rotational symmetries of the ditorelon states — and indeed multitorelon states — remain those of our finite volume, i.e. $\pi/2$ rotations, even in the continuum limit. That is to say, even in that limit they will fall into the representations of the cubic subgroup of the continuum rotation group. The genuine glueballs, on the other hand, will fall into representations of the full continuum rotation group in the continuum limit once the volume is large enough, up to corrections that are exponentially small in the spatial size, and this difference can also be useful in distinguishing ditorelons from genuine glueballs.

5.3 Lattice masses

As described earlier, we calculate glueball masses from the correlators of suitable $p = 0$ operators. These operators are chosen to have the desired R^{PC} quantum numbers, where $R \in \{A_1, A_2, E, T_1, T_2\}$ labels the irreducible representation of the cubic subgroup of the rotation group and $P = \pm$ and $C = \pm$ label parity and charge conjugation. We typically start with a set of 12 different closed loops on the lattice. (For $N = 2, 3$ we used 27, but we then observed that we can get almost equally good spectra by using a suitable subset of 12 loops.) We calculate all 24 rotations of the loop and construct linear combinations of the traces that transform as R. We do so separately using the real and imaginary parts of the traces, which gives us operators with $C = \pm$ respectively. We also calculate the parity inverses of each of these twelve loops, and of their rotations, and by adding and subtracting appropriate operators from these two sets we form operators for each R with $P = \pm$. To ensure that we have non-trivial operators for each set of quantum numbers it is useful to include some loops that have no symmetry under rotations and parity inversion. With our particular choice of 12 (or 27) closed loops we are able to construct the number of independent operators shown in table 20. This is the number of operators at each blocking level and we typically use 4 or 5 blocking levels in our calculations. This makes for quite a large basis of operators for all R^{PC} quantum numbers, and indeed a very large number for most of them. However this large number is slightly deceptive as at any given β only two or perhaps three blocking levels make an important contribution to the low-lying spectrum. In addition the states in the E representation are doubly degenerate and in the T_1 and T_2 are triply degenerate, so one should divide the corresponding numbers in table 20 by 2 or 3 in order to estimate the number of different energy levels accessible to the basis.

For completeness we list our 12 basic loops in table 21. The links are labelled by $1, 2, 3$ to indicate their spatial directions, with negative signs for backward going links, and the path ordering is from left to right. So, for example, the plaquette in the $2-3$ plane would appear as $\{2, 3, -2, -3\}$. Our list includes the plaquette, three 6 link loops, four 8 link loops and four 10 link loops. We also show for each loop which representations it contributes to once we include all the rotations and the inverses, doing so for the real $(C = +)$ and imaginary $(C = -)$ parts of the traces separately. This basis is used for $N \geq 4$. For SU(2) and SU(3) we use a larger basis of 27 loops that includes the 12 listed here. For some finite size studies we have used a reduced set of 8 loops.

We use these bases of operators in our variational calculations of the glueball spectra. In each R^{PC} sector we calculate a number of the lowest masses from the correlation functions of the operators that our variational procedure selects as being the best operators for those states within our basis. This relies on identifying an effective mass plateau in the correlator, as described in section 2.2, and performing an exponential fit to the data points on that plateau. So an important question is: how reliably can we identify such a plateau? We will illustrate this with our calculations in SU(8) on the $20^3 30$ lattice at $\beta = 47.75$. This is at our smallest value of $a(\beta)$ which, being the closest to the continuum limit, is one of the most important values in our subsequent extrapolations to the continuum theory. Also it provides the best resolution in t of our correlation functions. We begin with the effective masses, $aE_{\text{eff}}(t = an_t)$, of the three lightest A_1^{++} states and of the two lightest A_1^{-+} states, as shown in figure 7. As we will see below, the lightest two A_1^{++} and A_1^{-+} states become the lightest two $J^{PC} = 0^{++}$ and 0^{-+} glueballs in the continuum limit. The third A_1^{++} state is most likely part of the nonet of spin states making up the 4^{++} glueball ground state (see below), although if not then it would probably be the third scalar glueball. It is clear from figure 7 that we have plausible effective mass plateaux for all the states, with the weakest case being the excited A_1^{-+} state. The solid lines show our best mass estimates as obtained from fits to the correlation functions, together with their error bands. The error band on the lightest A_1^{++} state, which is the mass gap of the gauge theory, is invisible on this plot, so given the importance of this state we replot it in figure 8 with an axis rescaling that exposes the errors. Here the solid line is the best mass estimate and the dahsed lines bound the ± 1 stadard deviation error band. Figure 7 illustrates the obvious fact that as the masses get larger, the error to signal ratio grows at any fixed value of n_t, so that at large enough masses the effective energies becomes too imprecise to unambiguously indicate the values of n_t where the effective mass plateau begins. In this case we can turn to our calculations of the excited A_1^{-+} state at the smallest lattice spacings in SU(2) and SU(3), where there is much better evidence for the effective mass plateau beginning at $aM_{\text{eff}}(n_t = 3a)$, and use that in estimating that the effective mass plateau in this SU(8) calculations begins at $n_t = 3a$. This is the type of argument we use for a number of the heavier states at larger values of N where our calculations do not extend to very small values of $a(\beta)$.

As an aside, we also show in this plot the effective mass plot for the ditorelon. It shows every sign of plateauing to a value not far from $\sim 2aE_f \simeq 0.59$ as one would expect. It is clearly important to make sure that one excludes such a state from the scalar glueball

spectrum, as we have done here, since it is located near the first excited glueball state and would create a false level ordering if included.

We turn next to states which become $J = 2$ glueballs in the continuum limit. As we shall see below, the five components of a $J = 2$ state are spread over the two components of an E energy level and the three of a T_2. As always we average the masses of the 'degenerate' doublets of $R = E$ and the triplets of $R = T_1$ and T_2 to provide single effective masses in each case. What we show in figure 9 are the resulting effective mass plots for a number of such pairs of E and T_2 states. The equality of the E^{++} and T_2^{++} masses for the lightest two pairs is convincing, as it is for the lightest E^{-+} and T_2^{-+}. It is also plausible for the lightest E^{--}, T_2^{--} pair, and the lightest E^{+-}, T_2^{+-} pair, and there is some convergence for the second E^{-+}, T_2^{-+} pair, even if these more massive states do not show unambiguous plateaux. Again we show the ditorelon, this time in the E^{++} representation. In this spectrum it is nearly degenerate with the E^{++} ground state. The fact that it does not appear in a nearly degenerate T_2^{++} state confirms that it is a finite volume state, reflecting the limited rotational symmetries of the spatial volume.

If we examine the effective mass plots for the T_1^{PC} states that we shall later argue approach $J = 1$ in the continuum limit, we see that while the lightest T_1^{+-} glueball has a well-defined effective mass plateau, this is less evident for the more massive states. Finally we remark that if we plot the effective masses of our heaviest states, such as those of the lightest five A_1^{--} states, the evidence for the effective mass plateaux is not strong, although one can speculate on the presence of some the plateaux. This will clearly result in substantial systematic errors on the corresponding mass estimates, which we cannot readily quantify.

One lesson of the effective mass plots is that the heavier the state the less reliable will be our error estimate. However these plots also tell us at what $t = an_t$ the effective mass plateau begins for those states where this can be identified. Since the iterative blocking means that when we vary β our variationally selected operators are of roughly constant physical size and shape, we can assume that the overlap of a given state onto our basis will be roughly independent of β and hence that the effective mass plateau will begin at a value of $t = a(\beta)n_t$ that is roughly constant in physical units, i.e. at smaller n_t as $a(\beta)$ grows. So at larger values of $a(\beta)$ where $aE_{\text{eff}}(t)$ may be too large for us to identify a plateau, we can nonetheless use the value of $aE_{\text{eff}}(t_0)$, where t_0 is the value where our above calculations tell us that a plateau begins, as an estimate of the mass. This is something we do in our calculations, where appropriate.

We turn now to the glueball spectra that we obtain by the methods described above. We obtain the spectra for the lightest glueballs in each R^{PC} sector for each of our gauge groups. As an example we display in 22 our results for SU(8). Here we have removed the finite volume ditorelon states in the A_1^{++} and E^{++} sectors whenever they are present, as discussed in section 5.2, so that what we present in the table is our best estimate of the infinite volume glueball spectrum. A similar table for SU(3) has been published separately in [11]. All this assumes of course that none of these states is a multiglueball state. Since we use single trace operators, their overlap onto multiglueball states should decrease with increasing N and in any case they would be quite heavy. Some explicit calculations that provide evidence that such mutliglueball states do not appear in our spectra are described in section 5.8.

The reader will note that in some cases what we list as a higher excited state has a lower mass than what is listed as a lower excited state. This typically involves states that are nearly degenerate. Our procedure is to order the states according to the values of their effective masses at $t = a$ which is the value of t at which our variational calculation typically operates. This nearly always corresponds to final mass estimates (from the plateaux) that are in the same order, but very occasionally this not the case. In the very few cases where the difference is well outside the statistical errors we invert the ordering, but otherwise we do not. In addition it may be that the continuum extrapolation leads to a level inversion; again we only take that on board if the difference is well outside the errors. We have a good number of states that are nearly degenerate with a neighbouring state and in these cases the variational procedure itself is likely to mix them, and if that is done differently at different values of β it can lead to poor extrapolations to the continuum limit.

Finally we remark that the ensembles of lattice fields used at each N and β have a reasonable distribution of topological charge, either because the tunnelling between topological charge sectors is sufficiently frequent, or because we have imposed such a distribution on the initial lattice fields of the collection of sequences that make up the total ensemble, as discussed in section 2.4.

5.4 Strong-to-weak coupling transition

Before moving on to the continuum extrapolation of the lattice masses that we have calculated above, we briefly remark on the 'bulk' transition that interpolates in $\beta \propto 1/g^2$ between the strong and weak coupling regimes. From eqs. (2.1), (2.2) we see that the naive expectation is that at strong coupling, $\beta \to 0$, the natural expansion of a lattice quantity is in positive powers of β while at weak coupling, $\beta \to \infty$, the natural expansion is in positive powers of $1/\beta$. On the weak coupling side asymptotic freedom promotes the dependence of physical quantities to exponentials, $\propto \exp\{-c\beta\}$, and it is important to make sure that our calculations are indeed in the weak coupling regime.

As remarked in section 2.1, for SU($N \leq 4$) the transition is known to be a smooth crossover, while for SU(5) it is weakly first order, and for SU($N \geq 6$) it is strongly first order. For SU($N \leq 4$) the location of the crossover coincides with a dip in the mass gap which then drives a peak in the specific heat. (The specific heat is proportional to the sum of the plaquette-plaquette correlator and so peaks where the correlation length has a peak, i.e. where the mass gap has a dip.) For SU(2) this peak is around $\beta \sim 2.15$ as we see, for example, in figure 8 of [50], while for SU(3) the peak is around $\beta \sim 5.4$ as we see, for example, in figure 4a of [51]. For SU(4) the dip in the mass gap can be seen in figure 1 of [1] and is located around $\beta \sim 10.45$. For larger N the transition has been shown in [14] to be first order, and strongly first order for $N \geq 6$. In that case we have a strong hysteresis, i.e. if we lower β slowly from large values then the transition occurs at $\beta = \beta_b^\downarrow$, while if we increase β slowly from small values then the transition occurs at $\beta = \beta_b^\uparrow$, with $\beta_b^\uparrow$ significantly larger than $\beta_b^\downarrow$. Values for these transitions can be found listed in table 16 of [14]. As described in that paper, calculations performed in the weak coupling false vacuum just above $\beta = \beta_b^\downarrow$, and well below $\beta = \beta_b^\uparrow$, show no sign of being affected by the simultaneous presence of the deeper true vacuum elsewhere in field space. This fact has

been exploited in previous large N calculations. For example all but one of the β values in the SU(8) calculations in [2] lie within this hysteresis window, as does the SU(8) calculation in [3]. As is clear from tables 1–8 all our calculations have been performed on the weak coupling side of the cross-over or transition. In addition we note that none of our SU(5) or SU(6) calculations fall within the hysteresis window, only one of our SU(8) calculations lies within this window, while some of the SU(10) and about half of the SU(12) calculations lie within the window.

As remarked above, the main effect of the crossover at smaller N is an anomalous dip in the value of the mass gap, i.e. that of the lightest scalar glueball am_{0++}. This dip is caused by a nearby critical point which lies at the end of a first-order transition line in an extended fundamental and adjoint coupling plane, at which critical point the scalar glueball mass vanishes. For a detailed calculation in SU(3) see for example [52]. (The fundamental coupling is the one that which appears in our path integral.) As N increases the first-order line intersects the fundamental axis and provides the first-order bulk transition separating weak and strong coupling. However until the critical point has moved far away from the fundamental axis there may still be a dip in the mass gap near the first-order transition. Indeed one can see some plausible evidence for this occuring in the behaviour of the SU(6) and SU(8) mass gaps listed in [2]. Since there is no theoretical reason to expect that this dip can be encoded in the weak coupling expansion of the lattice action in powers of a^2, we minimise the risk to the continuum extrapolation of the scalar glueball mass by simply excluding from the continuum fit the value obtained at the largest value of β when including this value would require adding an additional a^4 correction to the fit. As it turns out, we need to do this for all our SU(N) groups except for SU(2).

5.5 Continuum masses

For each of our SU(N) lattice gauge theories we now have the low-lying glueball spectra for a range of values of $a(\beta)$. These are all given in lattice units as aM, and to transform that to physical units we can take the ratio to the string tension, $a\sqrt{\sigma}$, that we have simultaneously calculated. We can then extrapolate this ratio to the continuum limit using the standard Symanzik effective action analysis [53] that tells us that for our lattice action the leading correction at tree-level is $O(a^2)$:

$$\frac{aM(a)}{a\sqrt{\sigma(a)}} = \frac{M(a)}{\sqrt{\sigma(a)}} = \frac{M(0)}{\sqrt{\sigma(0)}} + a^2\sigma(a) + O(a^4). \tag{5.1}$$

Here we have used the calculated string tension, $a^2\sigma(a)$, as the $O(a^2)$ correction. Clearly we could use any other calculated energy, and this would differ at $O(a^4)$ in eq. (5.1). It is convenient to use $a^2\sigma(a)$ since its calculated value has very small errors.

The results of these continuum extrapolations are listed in tables 23–30 for the gauge groups ranging from $SU2$ to SU(12). (As always, each E doublet, and each T_2 or T_1 triplet appears as a single state in our tables and discussions.) A few entries are accompanied by a star denoting a poor fit, $2.5 < \chi^2/n_{df} < 3.5$, or a double star denoting a very poor fit, $\chi^2/n_{df} \geq 3.5$. For SU(10) and SU(12) we have only 5 values of β and since the masses at the coarsest value of β often have to be discarded from the fit (not surprisingly) and

since we are fitting 2 parameters, we often have only 2 degrees of freedom. For lower N we usually have 3 and sometimes 4 degrees of freedom, which gives much more confidence in the extrapolations. All of which is to say that while the fits for larger N are certainly not trivial, it would be good to be able to do better in future calculations.

We now illustrate the quality of these linear continuum extrapolations for our most interesting glueball states. We do so for SU(4). In figure 10 we show our extrapolations of the lightest two A_1^{++}, E^{++} and T_2^{++} states. These states are of particular importance because, as we shall see latter on, they correspond to the lightest two $J^{PC} = 0^{++}$ and 2^{++} states. We see that all the linear fits are convincing, even if in some cases we have to exclude from the fit the value at the largest $a(\beta)$. In figure 11 we show the corresponding plot for $P = -$ which, as we shall see latter on, correspond to the lightest two $J^{PC} = 0^{-+}$ and 2^{-+} states. The lightest states have very plausible continuum extrapolations, although the excited states, which are heavier than those for $P = +$, begin to show a large scatter indicating a poor fit. In figure 12 we show the extrapolations of various T_1^{PC} states that we shall later argue correspond to $J = 1$, and again we see fits that appear convincing for the lighter states and quite plausible for the heavier states. Even for the heaviest states to which we can plausibly assign a continuum spin, such as the states that pair up to give the $J^{PC} = 2^{--}$ and 2^{+-} ground states and the states that provide the seven components of the 3^{+-} ground state, where the larger errors lead to a greater scatter of points, continuum fits linear in $a^2\sigma$ are still plausible.

5.6 $N \to \infty$ extrapolation

Amongst the various SU(N) calculations, the one that is most interesting from a phenomenological point of view is the SU(3) one, and that is why we devoted a separate paper to that case [11]. From a theoretical point of view however the most interesting glueball spectra are those of the SU($N \to \infty$) theory since the theoretical simplifications in that limit make it the most likely case to be accessible to analytic solution, whether complete or partial.

To obtain the $N = \infty$ spectrum from our results so far, we use the fact that in the pure gauge theory the leading correction is $O(1/N^2)$. So we can extrapolate the continuum mass ratios in tables 23–30 using

$$\left.\frac{M_i}{\sqrt{\sigma}}\right|_N = \left.\frac{M_i}{\sqrt{\sigma}}\right|_\infty + \frac{c_i}{N^2} + O\left(\frac{1}{N^4}\right). \tag{5.2}$$

The results of these extrapolations are presented in table 31. In this table the stars point to poor fits exactly as described earlier for the continuum fits. The very poor fit for the first excited A_1^{++} is due to a large mismatch between the SU(5) and SU(6) mass estimates which may well be due to an inadequate treatment of the ditorelon influence. (We can obtain a good fit to $N \geq 6$ and this gives a mass $\sim 5.85(9)$ which is the same within errors.) Most of the fits are to $N \geq 2$ or $N \geq 3$ but some are over a more restricted range of N and this is indicated by a dagger. These states are the A_2^{++} ground state, fitted to $N \geq 4$, the T_2^{-+} second excited state, also fitted to $N \geq 4$, the T_2^{--} ground state, again fitted to $N \geq 4$, and finally the A_2^{+-} ground state which is more arguable since it was fitted to $N \leq 8$. From the practical point of view the most important extrapolations are for those

states to which we are able to assign a continuum spin (in the next section). We therefore show these extrapolations in figures 13, 14, 15 for states with $J = 0, 2, 1$ respectively.

5.7 Continuum spins

So far we have used the representations of the rotational symmetry of our cubic spatial lattice to label our glueball states. However as we approach the continuum limit these states will approach the continuum glueball states and these belong to representations of the continuum rotational symmetry, i.e. they fall into degenerate multiplets of $2J + 1$ states where J is the spin. In determining the continuum limit of the low-lying glueball spectrum, it is clearly more useful to be able to assign the states to a given spin J, rather than to the representations of the cubic subgroup which have a much less fine 'resolution' since all of $J = 0, 1, 2, \ldots, \infty$ are mapped to just 5 cubic representations. How the $2J + 1$ states for a given J are distributed amongst the representations of the cubic symmetry subgroup is given, for the relevant low values of J, in table 32. So, for example, we see that the seven states corresponding to a $J = 3$ glueball will be distributed over a singlet A_2, a degenerate triplet T_1 and a degenerate triplet T_2, so seven states in total. These A_2, T_1 and T_2 states will be split by $O(a^2)$ lattice spacing corrections, generated by irrelevant operators. So once a is small enough these states will be nearly degenerate and one can use this near-degeneracy to identify the continuum spin.

This strategy works for the lightest states but becomes rapidly unrealistic for heavier states. The latter will have larger statistical errors and will fall amongst other states that become more densely packed as the energy increases, so that identifying apparent near-degeneracies between states in different representations becomes highly ambiguous. There exist more sytematic ways of assigning continuum spin to lattice states, such as [8, 9, 54], but these are beyond the scope of this work. Accordingly we shall limit ourselves to the lightest states where any ambiguity in identifying near-degeneracies is either small or non-existent.

The states whose spin J we feel confident in identifying are listed in table 33 and the resulting continuum masses are listed in table 34 and table 35. We will now briefly illustrate the argument for the assignments, taking SU(8) as a typical example. Consider the masses in the SU(8) column of table 35. We have obtained these by interpreting the masses listed in table 28 as follows. The ground state of $R^{PC} = A_1^{++}$ is much lighter than any other mass and so must be the singlet $J^{PC} = 0^{++}$ ground state. The first excited A_1^{++} state certainly has no 'nearly-degenerate' partners amongst all the other $P, C = +, +$ states and so it must be the first excited 0^{++} glueball. The ground states of the doubly degenerate E^{++} and the triply degenerate T_2^{++} states are nearly degenerate and there are no other states with similar masses, so together they must provide the five components of the $J^{PC} = 2^{++}$ ground state. Similarly the first excited E^{++} doublet and T_2^{++} triplet have no nearly degenerate companion states elsewhere, and so they provide the first excited $J^{PC} = 2^{++}$ state. The argument for the ground and first excited 0^{-+} states is equally straightforward, as it is for the E^{-+} and the T_2^{-+} ground states forming the 2^{-+} ground state. The first excited E^{-+} and the T_2^{-+} states are consistent with forming the first excited 2^{-+} state, but here there is some ambiguity: it is also possible that these states pair with the second excited A_1^{-+} state and the T_1^{-+} ground state to make up the 4^{-+} ground state. This ambiguity

arises because the errors are sufficiently large that both possibilities can be entertained. Here we can resolve the ambiguity by observing that for neighbouring values of N, SU(6) and SU(10), the ambiguity is not present and the first excited E^{-+} and the T_2^{-+} states form the first excited 2^{-+} state, strongly suggesting that this is also the case for SU(8). This choice is not as solid as the earlier choices and fortunately it is not an argument we need to make very often in coming to our choices of J. With this choice we can plausibly assign the lightest T_1^{-+} state to the 1^{-+} ground state. (The second excited A_1^{-+} state has a similar mass but there are no further partners allowing us to assign it elsewhere according to table 32.) Similar arguments to the above lead to the J^{+-} and J^{--} choices in table 33 and the corresponding masses in table 35. Determining the spin J in the above way, clearly requires us not to miss any intermediate states in the mass range of interest. For this one needs a good enough overlap onto all the low-lying states and for that one needs a large basis of operators, which has been our goal in these calculations.

Using the arguments sketched above we infer the J^{PC} glueball masses listed in tables 34, 35, from the various masses listed in tables 23–30. In addition by inspecting the remaining states in tables 23–30 we can infer some lower bounds on the ground states in some other channels, and these are listed in table 36. These estimates are fairly rough and at that level apply to all our SU(N) theories.

The most interesting glueball spectra are those for SU(3) and for SU(∞): the former for its potential phenomenological relevance and the latter for its potential theoretical accessibility. The SU(3) theory is sufficiently close to the real world of QCD that it makes sense to attempt to present the masses in physical units, using scales that one believes to be relatively insensitive to the presence of quarks. We refer the reader to [11] for a more detailed discussion. Here we simply recall from our earlier discussion that the Sommer scale r_0, which is defined by the heavy quark potential at intermediate distances, is believed to vary weakly with quark masses, with a physical value of $r_0 \simeq 0.472(5)$fm [47]. One can extract from the published data the value $r_0\sqrt{\sigma} = 1.160(6)$ [11] This allows us to translate masses in units of $\sqrt{\sigma}$ to units of r_0 and finally to units of GeV. Doing so we obtain the masses listed in table 37. This table is similar to that in [11] except that we have included lower bounds for most of the masses where we previously lacked entries.

We now turn to our main focus: the $N \to \infty$ limit. We extrapolate the masses in tables 34, 35 with $O(1/N^2)$ corrections, as in eq. (5.2). The extrapolations for most of these states are displayed in figures 13, 14, 15. This leads to the masses (in units of the string tension) listed in table 38. In making these extrapolations we have sometimes excluded the mass for the smallest value of N ($N = 2$ for $C = +$ and $N = 3$ for $C = -$), in order to achieve a significantly better fit. This we have done for the 2^{++}, 1^{-+} and 1^{--} ground states. This presumably reflects the need for at least a further $1/N^4$ correction, but our number of data points is too small for this. In some cases we obtain better fits by excluding the $N = 12$ values, and although this could be argued for on the basis that our range of a for the continuum extrapolation is relatively limited in that case, the danger of 'cherry-picking' has led us to avoid doing so.

The main features of these continuum spectra are that the lightest glueball is the $J^{PC} = 0^{++}$ scalar, with the $J^{PC} = 2^{++}$ tensor about 50% heavier, and with the $J^{PC} = 0^{-+}$

pseudoscalar just slightly above that. The next state is the $J^{PC} = 1^{+-}$ vector, which is special in that it is the only relatively light $C = -$ glueball, with most $C = -$ states being very heavy. Just a little heavier than this vector is the first excited 0^{++} and then the 2^{-+} ground state. The N dependence of nearly all these states is weak and readily absorbed into a $O(1/N^2)$ correction down to at least SU(3); all this confirming that the SU(3) gauge theory is indeed 'close to' SU(∞).

5.8 Scattering states

A given operator will project onto all states with the quantum numbers of that operator. In particular our single trace glueball operators will project onto multi-glueball states in addition to the glueballs that we are interested in. This means that some of the states in the 'glueball' spectra that we have calculated may in fact be multi-glueball states. In the ideal case of a very large spatial volume these will be scattering states where at sufficiently large times the states are far apart

There is some ambiguity here of course. Sufficiently heavy glueballs will be unstable, and will decay into multiglueball states but to the extent that their decay width is not too large, we still regard them as glueball states. Indeed as N increases the decay widths and the overlap of multiglueball states onto our single trace basis of glueball operators should decrease. So although we expect this to be an issue primarily at smaller N, it is clearly important to address. We do so here in some detail because it has been addressed only briefly and occasionally in past glueball calculations.

A full analysis of scattering states and glueball decays would involve different techniques to those used in this paper and so are outside the scope of this work. Here we will, instead, perform some exploratory calculations to obtain an indication of the impact of multiglueball states on our calculated glueball spectra. We limit ourselves to considering states consisting of two glueballs since these are the lightest ones and our calculated glueball spectra do not extend to masses that are much higher. If there is weak mixing between double trace and single trace operators then we can introduce two glueball scattering states by using double trace operators, such as

$$\phi_{ab}(t) = (\phi_a(t) - \langle\phi_a\rangle)(\phi_b(t) - \langle\phi_b\rangle) - \langle(\phi_a - \langle\phi_a\rangle)(\phi_b - \langle\phi_b\rangle)\rangle. \tag{5.3}$$

Here ϕ_a and ϕ_b are single trace operators. The vacuum subtractions ensure that ϕ_{ab} does not have a projection onto the vacuum or a 'trivial' projection onto single glueball states through terms such as $\langle\phi_a\rangle\phi_b(t)$. One can calculate the mass spectrum obtained when one adds such double trace operators to the basis of single trace operators and compare it to that obtained using just the single trace operators. If the resulting spectra are the same then this strongly suggests that the spectrum obtained using single trace operators already includes two glueball states. If, on the other hand, the spectrum obtained using the expanded basis produces extra states that can be plausibly interpreted as two glueball scattering states, then this suggests that the states obtained with our original basis of single trace operators does not contain such states and that categorising them as single glueball states is probably correct.

The potential number of operators ϕ_{ab} is clearly too huge to be practical here and so we severely limit the number for our study as follows. Firstly, we take both ϕ_a and ϕ_b to have zero momentum, so both the total and relative momenta are zero. Of course this does not mean that the relative momentum of the two glueballs has to be zero, since the relative momentum is not a conserved quantum number in an interacting system, but one naively expects that the main overlap will be onto zero relative momentum. Secondly we only keep the 2 or 3 blocking levels that are most important at the β we calculate. (We systematically avoid using the largest blocking levels so as to exclude unwanted ditorelon states.) Thirdly, we take the same blocking levels for ϕ_a and ϕ_b. For ϕ_a we use only the rotationally invariant sum of (blocked) plaquettes. That is to say it is in the A_1^{++} representation. So ϕ_{ab} will be in the same representation as ϕ_b. For ϕ_b we take 3 different loops chosen so that we can have projections onto all representations including $P = \pm$ and $C = \pm$. The lightest energy of the corresponding asymptotic two glueball state would be the sum of the lightest A_1^{++} mass plus the lightest mass in the representation of ϕ_b if we were in an infinite spatial volume. Since our spatial volume is finite the glueballs are interacting at all times and there will be a shift in the total energy. However, to the extent that our spatial volume is not very small, this shift should be small and we will use the naive sum as the quantity against which to compare our supposed scattering states.

We perform calculations in SU(3), which is the most physically interesting case amongst our lower N calculations, and in SU(8) which is representative of our large N calculations. In SU(3) we work at $\beta = 6.235$ on the same 26^4 lattice used in our above glueball calculations. For completeness we have also carried out some calculations on $18^3 26$ and $34^3 26$ lattices at the same value of β. In SU(8) we work at $\beta = 46.70$ on a $16^3 24$ lattice which, again, is the same as that used in our glueball calculations. The spatial volumes at larger N are smaller than those at smaller N, taking advantage of the expected suppression of finite volume corrections with increasing N, and this is the reason for this additional calculation in SU(8).

We calculate correlators of the double trace operators with each other as well as with the single trace operators, since all of these are needed in the variational calculation using the basis that combines single and double trace operators. Because we need high statistics for glueball calculations, we calculate the correlators at the same time as we generate the lattice fields. At that stage we do not know the values of the vacuum subtractions in eq. (5.3) and so we need to calculate a number of other correlators so that at the later analysis stage we can reconstruct the desired subtracted correlators. The relevant expressions are given in appendix B.

We begin with our SU(3) calculation. In figure 16 we show the effective masses of the lightest few states in the A_1^{++} representations obtained using the basis of single trace operators (open circles) and the same basis extended with our double trace operators (filled points). We see quite clearly that the two sets of states match each other well except for one state, whose effective masses are represented by a ♦, and which clearly has no partner amongst the states from the single trace basis. This state appears to asymptote, at larger t, to an energy that is close to twice the lightest A_1^{++} mass, i.e. that of the lightest free two glueball state, and so we infer that this is indeed the lightest two glueball state. Apart from

this state, the lightest 4 states in the two bases match each other quite precisely. That is to say, we have good evidence that the A_1^{++} continuum masses listed in table 24 are indeed those of single glueball states.

It is interesting to ask what kind of A_1^{++} energy spectrum one obtains if one uses a basis consisting only of the double trace operators. The result is shown in figure 17. We see that the state that is lightest at small t is consistent with being the lightest 2 glueball state, and that our variational wave-functional has a good overlap onto that state. What is equally interesting is the state that is the first excited state at small t and whose effective mass drops monotonically below that of our two glueball state as t increases, consistent with heading towards the mass of the lightest glueball. This presumably represents the overlap of our double trace basis onto the lightest glueball. A rough estimate suggests that this variationally selected operator has an overlap (squared) of $\sim 10\%$ which again points to little mixing of scattering states into our low-lying glueball spectrum.

Clearly we would like to repeat our above analysis of the A_1^{++} spectrum for all the other representations. However once the lightest state in some R^{PC} representation is much heavier than in the above case the energy of the predicted scattering state lies in a dense part of the spectrum, all the energies have much larger statistical errors and we cannot follow the effective energies beyond the smallest values of t. That is to say, the analysis becomes hopelessly ambiguous. We will therefore restrict ourselves to a few cases where the energies are still manageably small. That is to say, we will look at the T_2^{++} which contains 3 components of the lightest $J = 2^{++}$ state, the A_1^{-+} where the lightest state is the interesting 0^{-+} pseudoscalar (the lightest $P = -$ glueball), the E^{-+} where the lightest state is the 2^{-+} pseudotensor, and the T_1^{+-} which is the lightest $C = -$ state and where the lightest 3 component state is the $C = -$ vector. We do not analyse any R^{--} states since they are all too heavy.

We begin with the T_2^{++} representation. Here our double trace operator would project onto a two glueball state consisting of the lightest A_1^{++} and T_2^{++} glueballs if there were no mixing. Neglecting interactions its energy is just the sum of these masses. This case differs from the A_1^{++} representation discussed above because this is not the lightest scattering state one can construct. Two A_1^{++} glueballs with two units of angular momentum are lighter, although one can expect an angular momentum threshold suppression factor that would need to be quantified. Such a state requires the use of operators with non-zero momentum which would mean extending our basis of operators well beyond our choice for this exploratory study. It is plausible that what we learn using our heavier two glueball states would also apply to these lighter ones. So we carry out for the T_2^{++} representation the analogue of the analysis in figure 16 for the A_1^{++}. Once again we find that the inclusion of our double trace operators leads to an extra state although because of the denser packing of the states it is less prominent than in the A_1^{++} case. However the effective energy of this state is consistent with decreasing towards that of a scattering state composed of the lightest A_1^{++} and T_2^{++} glueball, albeit with substantial statistical uncertainty. So it is very plausible that it is a scattering state composed of the lightest A_1^{++} and T_2^{++} glueballs. The spectrum from the double trace basis shows quite clearly that the state that is lightest at small t has an energy roughly equal to the sum of the lightest A_1^{++} and T_2^{++} glueballs,

showing it to be a scattering state. It is also clear that the projection of these double trace operators onto the lightest T_2^{++} glueball is very small. All this makes it plausible that the five or six lightest states in the T_2^{++} channel are single glueballs. However we recall our above caveat that there are lighter scattering states that could, in principle, behave differently.

With the T_1^{+-} representation our double trace operators project onto the lightest two glueball state since the lightest T_1^{+-} is the lightest $C = -$ state. Here we again find that the addition of the double trace operators to the single trace basis does produce an extra state and that the effective energy of that state appears to be decreasing towards the energy of the lightest scattering state, up to the point where the errors grow too large to allow a statement. From this we infer that the lightest five T_1^{+-} states obtained using the single trace basis are not scattering states. In addition we find that in the spectrum obtained using just the double trace operators the lightest state appears to approach the expected scattering state and that there apears to be no significant component of the lightest single glueballs present in this basis, providing further evidence for little overlap between our single and double trace operators.

In the case of the A_1^{-+} representation our double trace operators naturally project onto a state with both an A_1^{++} and an A_1^{-+} glueball. Just as for the A_1^{++} this should be the lightest possible scattering state: although one can obtain $P = -$ through unit angular momentum one would need a glueball with non-zero spin to take us back to an overall A_1 state. We show in figure 18 how the inclusion of our double trace operators affects the spectrum. While the ground and first excited states are unaffected, there is clearly an extra state just above these, and a significant shift in the mass of the next state above this. The effective energy of the (probable) extra state descends rapidly towards the energy of the free scattering state, but the rapidly growing errors prevent us from telling if it asymptotes to this value or continues to decrease. For further evidence we plot in figure 19 the spectrum obtained in the basis with only the double trace operators. Here we have a quite dramatic contrast to what we have seen above in the A_1^{++}, T_2^{++} and T_1^{+-} representations: the lightest state is clearly the ground state of the single trace spectrum. This tells us that here we have a large overlap between single trace and double trace operators. So here we can have legitimate concerns about the presence of multiglueball states in the low-lying spectrum obtained using single trace operators.

The E^{-+} representation contains the second lightest state in the $P, C = -, +$ sector, after the A_1^{-+} ground state. Neglecting interactions, our double trace operators would project onto the two glueball states composed of an A_1^{++} and an E^{-+} glueball. There are scattering states that are slightly lighter but they should have angular momentum threshold factors that effectively cancel that advantage. (For example, the lightest A_1^{++} and A_1^{-+} glueballs with two units of angular momentum.) We find, when plotting the effective masses, that the addition of the double trace operators to the single trace basis does produce an extra state. However this state is nearly degenerate with another state so it is unclear which is the extra one. (It is quite possible that our variational procedure mixes the two.) In either case the effective energy of that state appears to be decreasing towards the energy of the lightest scattering state, up to the point where the errors grow too large to allow a

statement. The spectrum of states with just the double trace basis shows quite clearly that the lightest state is the scattering state and that there is no significant overlap of our double trace operators onto the low-lying spectrum obtained with the single trace operators.

In summary, the above study in SU(3) shows that two glueball states have very little overlap onto most of the spectrum one obtains from single trace operators for the lighter and hence most interesting states in our calculated glueball spectra. This is something of a surprise in SU(3) since one would not expect to be able to invoke a large-N suppression for $N = 3$. The one apparent exception concerns the A_1^{-+} representation which contains the 0^{-+} pseudoscalar which is of particular theoretical interest. This clearly merits a much more detailed investigation.

We now turn to a similar study in SU(8). This we should do since for $N \geq 8$ we use considerably smaller spatial volumes than for SU(3), taking advantage of the expected large-N suppression of finite volume corrections. We perform our study on a $16^3 24$ lattice at $\beta = 46.70$ which corresponds to a lattice spacing that is slightly larger than that of the above SU(3) study if measured in units of the string tension, σ, although equal when measured in units of the mass gap. Our results are very much the same as for SU(3): in the $A_1^{++}, T_2^{++}, T_1^{+-}$ and E^{-+} representations there appear to be very small overlaps between our would-be two glueball operators and the single trace operators in the low-lying part of the spectrum that is of interest to us in this paper. The striking exception, as in the case of SU(3), is the A_1^{-+} representation. This is intriguing both because this representation contains the interesting $J^{PC} = 0^{-+}$ pseudoscalar glueball and because one would have naively expected the large-N suppression of such overlaps between single and double trace operators to have taken effect by $N = 8$. There is perhaps some hint of this in comparing the approaches to the respective A_1^{-+} masses of the ground states.

These results for SU(3) and SU(8) provide some reassurance that our spectra in the glueball calculations of this paper are indeed those of single glueballs, at least for the lower lying spectrum that is of the greatest physical and theoretical interest.

5.9 Some comparisons

It is useful to compare our glueball results against those of earlier calculations both as a check on the reliability of our errors, particularly the systematic errors that are the most difficult to control. To reduce the comparison to manageable proportions we limit ourselves to the continuum limit of the $J^{PC} = 0^{++}, 2^{++}, 0^{-+}, 2^{-+}, 1^{+-}, 3^{+-}, 2^{--}$ ground states and to calculations that have appeared after the year 2000. The first five states are the lightest ground states and are easy to identify, while the sixth involves a more challenging identification of near-degeneracies amongst the cubic irreducible representations, and the last is an example of the much heavier states over which we have less control. We will also limit ourselves to SU(3), where there are several calculations, and to SU(8) as a representative of our larger N calculations.

We list the SU(3) and SU(8) comparisons in tables 39 and 40. The calculations in [1, 2, 9] are broadly of the same type as those in the present paper, making a comparison straightforward. The calculations of [1, 2] were designed to explore the approach to the large N limit and focussed upon the masses of the $J^{PC} = 0^{++}, 2^{++}$ ground states and the string

tension. The primary goal of [9] was to calculate the masses of higher spin glueballs which cannot be identified using the naive approach of searching for near-degeneracies, as used in the present paper, and this required the application of novel dedicated techniques. The calculations in [10] are significantly different to all of these, in that they use an alternative 'improved' lattice action and anisotropic lattices with a temporal lattice spacing, a_t, smaller than the spatial lattice spacing, a_s, by a factor of (roughly) 3 or 5. In addition the continuum glueball masses are expressed in units of the Sommer scale r_0 rather than the string tension σ. We have used the value $r_0\sqrt{\sigma} = 1.160(6)$, as fitted in [11], to translate the values given for $r_o M_G$ in [10] to the values $M_G/\sqrt{\sigma}$ listed in table 39.

We begin with the SU(3) comparison in table 39. Overall we see that the results of the different calculations agree within about 2 standard deviations for all the states. In particular the values in [9] are within one standard deviation of our values. On the lighter ground states our errors are far smaller than those of the earlier calculations. However on the two heaviest states the errors in [10] are similar to ours, demonstrating the expected advantage of highly anisotropic lattices for calculating the masses of heavy glueballs. Focussing now on possible differences, we note that all the mass estimates from [10] are slightly above ours, and indeed above those of [9] It is possible that this has to do with the scale r_0. This scale is determined as the spatial distance at which the heavy quark potential has a certain value of its derivative. Thus its value is expressed in units of the spatial lattice spacing, i.e. as r_0/a_s, and this has to be expressed as r_0/a_t in order to serve as a scale for a lattice glueball mass, $a_t M_G$. This rescaling is clearly sensitive to even small shifts of the anisotropy from the tree level values of 3 or 5. Moreover the values of a_s used in [10] are large which means that r_0/a_s is not large, and this makes the accurate determination of its value more delicate. So it is possible that all this is enough to lead to a $1-2\%$ shift in the estimates of $M/\sqrt{\sigma}$ in this calculation. Turning now to [1, 2] we see that the 0^{++} mass is about two standard deviations higher than our value (or that of [9]). A possible source of this is the fact that these older calculations have a more limited range of higher β values and include in their continuum extrapolations the smaller values of β where there is some effect of the dip in the mass gap associated with the strong-to-weak coupling bulk transition, as discussed in section 5.4. This dip in the mass at larger lattice spacings may then bias the straight line fit in $a^2\sigma$ so that its $a = 0$ intercept is a little too high. In the present calculations the statistical errors are small enough that a good straight line fit is no longer possible if one includes such large a values and by excluding them any such bias becomes smaller and the continuum intercept is a little lower. This discussion is only relevant to the mass gap, since the other glueballs appear to be insensitive to the bulk transition and have, for the most part, a small dependence on the size of the lattice spacing.

Turning now to the SU(8) comparison in table 40, we see that for the states other than the 0^{++} the masses from the different calculations agree within one standard deviation, although the errors on the earlier calculations are typically about ten times larger than ours, leaving room for potential discrepancies. The mass gap shows a signficant discrepancy but both of the earlier calculations include masses calculated close to the bulk transition at $\beta = \beta_b^{\downarrow}$ where the mass gap appears to have a significant dip, as discussed in section 5.4, which may well explain this minor difference.

The above comparisons naturally raise the question of why we chose to use the traditional Wilson plaquette action instead of some alternative 'improved' action, such as the one used in [10]. In glueball calculations the main improvement observed, for SU(3), is to largely remove the dip in the mass gap as one transitions from strong to weak coupling. This means that calculations at coarser lattice spacings, and so on smaller lattices, may be used in the continuum extrapolation of the mass gap. However a larger lattice spacing means that the correlator signals tends to disappear into the statistical noise before one has a well defined effective mass plateau. To remedy this one can use an anisotropic lattice action with the temporal spacing a_t much less than the spatial a_s. However using contemporary resources there is no need to worry about the dip in the mass gap: one can easily do calculations far from the dip, at much weaker coupling, as we have seen in this paper. Moreover if one works at coarse lattice spacings using such an improved action one does not know in advance whether the behaviour of other glueballs will be improved or worsened. And in any case, as we have seen in figures 10, 11, 12, the lattice corrections to the glueball masses are already quite modest with the standard Wilson plaquette action. An advantage of the simple plaquette action is that it is known to have exact reflection positivity and hence the transfer matrix has real positive eigenvalues between zero and one, just as if it was the exponential of a Hamiltonian. This means that one does not need to be cautious in applying a variational calculation of the glueball spectrum. Of course one can use an anisotropic plaquette action, which will also possess reflection positivity. Such a calculation would produce a finer resolution in time of the correlator and so could be very useful for calculating heavier glueball masses. However it has a disadvantage in setting the scale as described just above. One needs to know the relation between a_s and a_t and since the chosen tree level anisotropy will receive corrections, this need to be estimated, and the error on this estimate may be significant. Thus our suggestion for a better calculation than the present one is that one does two calculations in parallel. One calculation should be with an isotropic action, and this will provide very accurate continuum values for the light glueballs, including the mass gap M_G, in units of, for example, the string tension, σ, or the Sommer scale r_0. The second calculation should be with a strongly anisotropic action and provided that one has a large enough basis of operators, this should provide accurate calculations of the heavier glueball masses in units of, say, the mass gap. Here it is important that the spatial lattice spacings should extend to small values, just as in the isotropic calculations, in order to guarantee the credibility of the continuum extrapolations. Putting together both calculations allows all the masses to be expressed in units of σ or r_0. The action used could be either the plaquette action or some improved action, although maintaining reflection positivity is desirable from a practical point of view.

6 Topological fluctuations

Euclidean $D = 4$ SU(N) gauge fields possess non-trivial topological properties, characterised by a topological charge Q which is integer-valued in a space-time volume with periodic boundary conditions. This charge can be expressed as the integral over Euclidean space-time

of a topological charge density, $Q(x)$, where

$$Q(x) = \frac{1}{32\pi^2}\epsilon_{\mu\nu\rho\sigma}\mathrm{Tr}\{F_{\mu\nu}(x)F_{\rho\sigma}(x)\}. \tag{6.1}$$

Since the plaquette matrix $U_{\mu\nu}(x) = 1 + a^2 F_{\mu\nu}(x) + \dots$ on sufficiently smooth fields, one can write a lattice topological charge density $Q_L(x)$ on such fields as

$$Q_L(x) \equiv \frac{1}{32\pi^2}\epsilon_{\mu\nu\rho\sigma}\mathrm{Tr}\{U_{\mu\nu}(x)U_{\rho\sigma}(x)\} = a^4 Q(x) + O(a^6). \tag{6.2}$$

However this definition lacks the reflection antisymmetry of the continuum operator in eq. (6.1), since all the plaquettes $U_{\mu\nu}(x)$ are defined as forward going in terms of our coordinate basis, so to recover these symmetry properties we use the version of this operator that is antisymmetrised with respect to forward and backward directions [55] (although this is unnecessary on smooth fields).

The fluctuations of $Q_L(x)$ are related to the expectation value of the composite operator $Q_L^2(x)$ whose operator product expansion contains the unit operator [55], so these fluctuations are powerlike in $1/\beta$. On the other hand, the average of $Q_L(x)$ is $O(a^4)$ and hence exponentially suppressed in β. Thus as β increases the fluctuations around $Q_L(x)$ and $Q_L = \sum_x Q_L(x)$ diverge compared to the physically interesting mean values. In addition the composite operator $Q_L(x)$ also receives a multiplicative renormalisation $Z(\beta)$ such that $Z(\beta) \ll 1$ at accessible values of β [56].

In practice all this means that one cannot extract the topological charge of a typical lattice gauge field by directly calculating $Q_L = \sum_x Q_L(x)$ on that gauge field. However we note that the fluctuations obscuring the value of Q are ultraviolet, while the physically relevant topological charge is on physical length scales. Thus if we perform a very limited local smoothening of the fields to suppress the ultraviolet fluctuations, this should not affect physics on long distance scales, and the value of $Q_L = \sum_x Q_L(x)$ calculated on these smoothened fields should provide a reliable estimate of Q. Moreover, recalling that the total topological charge of a gauge field is unchanged under smooth deformations, we can expect that even under a moderately large amount of continued smoothening the value of Q_L will not change, even though $Q_L(x)$ itself does gradually change. One convenient way to smoothen the gauge fields is to locally minimise the action. Such a 'cooling' of the original 'hot' lattice gauge field [57] involves sweeping through the lattice one link at a time, precisely like the Monte Carlo except that one chooses the new link matrix to be the one that minimises the total action of the plaquettes containing that link matrix. This is a standard technique that one can find described in more detail in, for example, [58]. An alternative and attractive smoothing method with perturbatively proven renormalisation properties is the gradient flow [59–61] which has been shown to be numerically equivalent to cooling [62–64]. Cooling typically performs nearly two orders of magnitude faster than the gradient flow and since we are aiming for large statistics we adopt the simplest cooling method. After the first couple of cooling sweeps the fields are already quite smooth, as we shall see below. Since we are minimising the action and since in the continuum the minimum action field with a given Q is a multi-instanton field, we expect that under systematic cooling the lattice field will be driven to become some multi-instanton field, which one

can see by calculating the distribution $Q_L(x)$ on such a field. Of course, because of the discretisation of space-time the topological properties of lattice fields are only approximately like those of a continuum field. One can deform a large instanton by gradually shrinking its non-trivial core and on a lattice this core can shrink to within a hypercube. At this point what was an instanton has been transformed into a gauge singularity and the value of Q will now differ from its original value by one unit. (Equally, one can gradually grow an instanton out of a hypercube.) This process can occur during cooling but it can equally occur during the course of our Monte Carlo. In the latter case, it is these changes in Q that allow us to sample all possible values of Q and hence maintain the ergodicity in Q of our Markov process. As $\beta \uparrow$ the distance between physical and ultraviolet scales grows and these changes in Q become increasingly suppressed — in fact more strongly than the usual critical slowing down (see below). This is as it should be: after all, the changes in topological charge are no more than a (useful) lattice artifact.

We have outlined in section 2.4 the specific reasons for the suppression of changes in Q_L when $a(\beta) \to 0$ at fixed N and when $N \to \infty$ at fixed $a(\beta)$, and how we deal with this problem in our glueball and string tension calculations. Below, in section 6.1, we will give some evidence that the value of Q_L on a cooled lattice field does indeed reflect the topology of the original lattice field. Then, in section 6.2, we will give some results on the rate of critical slowing down, both as $a(\beta) \to 0$ and as $N \to \infty$. In section 6.3 we present our results for the continuum topological susceptibility in those cases, $2 \leq N \leq 6$, where the topological freezing is not too serious an obstacle. Finally in section 6.4 we present our numerical results for the factor $Z(\beta)$ that relates the value of Q_L before cooling to its value, Q_I, after cooling. Our study of lattice topology has some limitations of course: it is not a dedicated study but is constrained by being a byproduct of our glueball and string tension calculations. Finally we remark that it is only in the calculations of the topological susceptibility that the topological freezing is an obstacle; in our other calculations in this section it does not matter whether the topological charge we study is introduced by hand or appears spontaneously.

6.1 Topology and cooling

As we cool our lattice fields the fluctuations in the measured value of Q_L decrease and it rapidly settles down to a value that is close to an integer. As a typical example we plot in figure 20 the number of fields with a given topological charge Q_L after 2 coolings sweeps and the number after 20 cooling sweeps, taken from sequences of SU(5) fields on a $16^3 20$ lattice at $\beta = 17.63$. With respect to the calculations in this paper, this corresponds to an intermediate value of N, and of $a(\beta)$, and of the lattice volume. As we see, after 20 cooling sweeps the values of Q_L are very strongly peaked close to integer values. The reason that the peak is not at an integer, even when the cooling has erased the high frequency fluctuations, is that for an instanton of size ρ on a lattice, we only obtain $Q_L \to 1$ in the limit $\rho/a \to \infty$, with deviations from unity that are powers of a/ρ. However, as is clear from figure 20, there is no significant ambiguity in assigning to each field after 20 cooling sweeps an integer valued topological charge which we label Q_I. We can expect Q_I to provide our most reliable estimate of the topological charge Q of the original lattice gauge

field. For the calculations with the largest values of $a(\beta)$ identifying the value Q_I can be less clear-cut, but such lattices are of little importance in determining continuum physics. We also see from figure 20 that even after only 2 cooling sweeps the fields fall into groups that only overlap slightly. Since 2 sweeps cannot affect anything other than the most local fluctuations, we can assume that this segregation into differing topological sectors directly reflects the topology of the gauge fields prior to any cooling.

As a second example we show in figure 21 the same type of plot for several sequences of SU(8) fields generated at $\beta = 47.75$ on a $20^3 30$ lattice. This corresponds to our smallest lattice spacing in SU(8). Here we see an even sharper peaking after 20 cooling sweeps and, more interestingly, a very clear separation between the various sectors even after only 2 cooling sweeps. In contrast to the SU(5) example, in this case there is essentially no tunnelling between topological sectors, and the observed distribution of Q has been imposed on the starting configurations for the various sequences.

The loss of ergodicity with respect to the topological charge is illustrated for SU(8) in figure 22 where we show the values of Q_L after 2 and 20 cooling sweeps taken every 100 Monte Carlo sweeps for two sequences of 50000 sweeps generated at $\beta = 47.75$. In one sequence we have $Q_L \sim 1$ and in the other we have $Q_L \sim 2$. It is interesting that even after only 2 cooling sweeps the separation in the measured values of Q_L is unambiguous. A similar plot for SU(5) fields generated at $\beta = 17.63$ is shown in figure 23. Here the value of Q_L remains unchanged over subsequences that are typically a few thousand sweeps long, but the changes are sufficiently frequent that in our overall ensemble of $\sim 2 \times 10^6$ fields we may regard Q_L as ergodic. But just as for SU(8) the values of Q_L after only 2 cooling sweeps track the values after 20 cooling sweeps.

The close relationship that we observe in figure 22 and figure 23 between the values of Q_L after 2 and 20 cooling sweeps is confirmed explicitly in figure 24. Here we have taken all the $\beta = 47.75$ SU(8) fields on which we have calculated Q_L and we have extracted the three subsets that correspond to $Q_L \simeq 1, 2, 3$ after 20 cooling sweeps. For each subset we plot the values that Q_L takes on fields after 2 cooling sweeps. As we see in figure 24 the three distributions do not overlap. So we can assign to each field a value of Q that is completely unambiguous (at least for our statistics) on the basis of the value of Q_L measured after only 2 cooling sweeps, where the long-distance physics should be essentially unchanged from that of the original uncooled lattice fields. As an aside, we show in figure 25 the same plot as in figure 24, but with values of Q_L calculated after only 1 cooling sweep. Here the distributions are broader, so that one can no longer use the value of Q_L to unambiguously assign the field its value of Q, but the fact that even after 1 cooling sweep the values of Q_L strongly reflect the value of Q after 20 cooling sweeps is evident.

It is instructive to see how the measured values of Q_L vary with the number of cooling sweeps n_c. As an example, we take an ensemble of fields that have a topological charge $Q = 2$, as determined by the value of Q_L after 20 cooling sweeps. For this same ensemble we calculate how the average value of Q_L varies with n_c and also how the standard deviation of its fluctuations vary with n_c. These quantities, labelled $\overline{Q}_L$ and σ_{Q_L} respectively, are shown in table 41 for three different values of β in SU(8). As we see, in the uncooled ($n_c = 0$) fields the fluctuations σ_{Q_L} are so large compared to the average charge $\bar{Q}_L(n_c = 0)$

of those fields, that one cannot hope to estimate for individual fields the true value of Q from the value of Q_L at $n_c = 0$. However we also see that even after only 1 cooling sweep the value of $\bar{Q}_L/\sigma_{Q_L}$ increases by a factor ~ 20 and after 2 cooling sweeps by ~ 80, so that one can, with rapidly increasing reliability, assign a value of Q to an individual field on the basis of the value of $Q_L(n_c)$ at the first few cooling sweeps. What we also see in table 41 is that beyond the lowest few values of n_c there is little difference between the 3 ensembles, despite the fact that the lattice spacing changes by a factor ~ 1.7. For larger n_c the value of $Q_L(n_c)$ decreases slightly with decreasing β as one expects because the typical instanton size will decrease in lattice units and the discretisation corrections are negative. For $n_c = 0$ the decrease in Q_L is larger and reflects the β-dependence of the renormalisation factor $Z(\beta)$ which is driven by high frequency fluctuations, as analysed more quantitatively in section 6.4. The rapid increase of σ_{Q_L} with increasing β is driven by two competing factors: the high frequency fluctuations per lattice site decrease as an inverse power of β, but since these fluctuations are roughly uncorrelated across lattice sites, there is a factor proportional to the square root of the lattice volume in lattice units which increases exponentially with β if our volumes are roughly constant in physical units. At larger β the latter factor will dominate and it therefore becomes rapidly harder to relate Q from $Q_L(n_c = 0)$ as we approach the continuum limit. On the other hand, after the first few cooling sweeps the high frequency fluctuations have been largely erased and the fluctuations of Q_L no longer increase with increasing β, so that it becomes easier to identify the value of Q from the value of Q_L.

As a footnote to the above we have calculated the same quantities as in table 41 but now for different SU(N) groups. The calculations are at roughly the same value of $a\sqrt{\sigma}$ as for the SU(8) fields at $\beta = 46.70$ in table 41, i.e. at roughly the same value of the 't Hooft coupling, so that the contribution of the high frequency fluctuations is roughly the same. We find that the variation in $\sigma_{Q_L}(n_c = 0)$ with N is consistent with being due to the difference in the square root of the lattice volumes. At larger n_c the value of $\sigma_{Q_L}(n_c)$ decreases with increasing N, which tells us that larger-scale non-perturbative fluctuations, such as in the instanton size, are decreasing. Finally, the main practical point is that there is very little variation with N of $\overline{Q}_L$ at any value of n_c.

6.2 Tunneling between topological sectors

In the continuum theory Q cannot change under continuous deformations of the fields unlike most other quantities, such as glueball correlation functions, so one expects to lose ergodicity in Q much faster than in such other quantities as one approaches the continuum limit in a lattice calculation using a local Monte Carlo algorithm such as the heat bath. In this section we shall provide our data on this 'freezing' of Q as a function of a and N and then compare this to some theoretical expectations.

As described earlier, the value of Q changes if the core of an instanton shrinks and disappears within a hypercube (or the reverse of this process). When a is small enough such instantons can be described by dilute gas calculations since these very small instantons are very rare and the effect on them of other background field fluctuations that exist on physical length scales will be negligible. So the basic process is for Q to change by one

unit. Therefore we use as our measure of topological freezing the average number of sweeps between changes of Q by one unit. We call this τ_Q. Since the probability of such a process is clearly proportional to the space-time volume, which is not something we have tried to keep constant in our calculations, we rescale our measured values of τ_Q to a standard physical volume, which we choose to be $V_0 = l^4$ with $l\sqrt{\sigma} = 3.0$, so that we can compare the results of different calculations. Our calculations of Q have not been performed after every sweep, but typically with gaps of 25 or 50 or 100 sweeps depending on the calculation. Our estimates of τ_Q can only be reliable if they are much larger than this gap, since otherwise there could be multiple changes of Q within the gaps that we are missing, and so we do not includes those ensembles where this issue arises — typically at the coarser lattice spacings. However even if τ_Q appears to be much larger than the gap, we will occasionally see that ΔQ, the change in Q across a gap, is greater than unity. In this case we assume that there have been $|\Delta Q|$ jumps within the gap and we make that part of our final estimate of τ_Q. In practice this makes a very small difference to our results. By counting the number of changes of Q in our total sequence of lattice fields we can obtain the average distance between such changes, τ_Q, once we have renormalised to our standard volume V_0.

As $\tau_Q \to \infty$ the above definition is adequate. However when τ_Q is not very large one can worry about the unwanted contribution of near-dislocations that occur across a measurement of Q. We have in mind a small instanton that appears out of a hypercube shortly before a measurement, survives the cooling (because of its environment) and so contributes to the value of Q, but then quickly disappears without becoming a larger physical instanton long before the next measurement. In a sequence of measurements of Q such an event would be characterised by a jump $\Delta Q = \pm 1$ at one measurement followed by the opposite jump, $\Delta Q = \mp 1$, at the next measurement. Of course it could be that when this happens we are seeing two independent events, with an instanton appearing from one hypercube and after the measurement an anti-instanton appearing out of a quite different hypercube. The characteristic of the latter events is that the signs of the changes in Q at neighbouring measurements are uncorrelated. Correcting for these we obtain the measure $\tilde{\tau}_Q$ (normalised to our standard volume) which excludes this estimate of near-dislocations. Whether this estimate is entirely reliable is arguable, so it is reassuring that the differences between $\tilde{\tau}_Q$ and τ_Q are not large, and which one we use does not alter our conclusions below.

We present in table 42 our results for τ_Q and $\tilde{\tau}_Q$ from the sequences of fields generated in our glueball and string tension calculations. The excluded values of β either correspond to cases where τ_Q is not much larger than the gap between measurements, and this includes all of our SU(2) calculations, or where τ_Q has become so large that we see no changes in Q at all, which includes almost all of our SU(10) and SU(12) calculations. The prominent qualitative features of our results are that for any given gauge group both τ_Q and $\tilde{\tau}_Q$ increase rapidly as $a(\beta)$ decreases and, at roughly equal values of $a(\beta)$, they increase rapidly as N increases.

One can formulate some theoretical expectations for the behaviour of τ_Q as one decreases a and increases N. Just before shrinking through a hypercube an instanton will be very small with size $\rho \sim a$ where the number density, $D(\rho)d\rho$ can be estimated using the standard

semiclassical formula [21]

$$D(\rho) \propto \frac{1}{\rho^5} \frac{1}{g^{4N}} \exp\left\{-\frac{8\pi^2}{g^2(\rho)}\right\} \stackrel{N \to \infty}{\propto} \frac{1}{\rho^5} \left\{\exp\left\{-\frac{8\pi^2}{g^2(\rho)N}\right\}\right\}^N \stackrel{\rho=a}{\propto} (a\Lambda)^{\frac{11N}{3}-5}, \qquad (6.3)$$

where Λ is the dynamical length scale of the theory. This is of course a very asymptotic expression: we have neglected the powers of g because they only contribute powers of $\log(a\Lambda)$, and we have used the 1-loop expression for $g^2(a)$ which is, as we have seen in section 4, inadequate for our range of bare couplings. We also note that this expression only tells us what is the probability of a very small instanton. In addition there will be a factor for the small instanton with $\rho \sim O(a)$ to finally shrink completely within a hypercube: this 'tunneling event' may contribute an important factor depending on the lattice action being used.

The first qualitative feature of eq. (6.3) is that if we increase N at fixed a, we should find

$$\tau_Q \propto \frac{1}{D(\rho)} \propto \left\{\frac{1}{a\Lambda}\right\}^{\frac{11N}{3}-5} \longrightarrow \ln\{\tau_Q\} = b + cN, \qquad (6.4)$$

where c depends on the value of a and b is some undetermined constant. In our simulations we have some that correspond to almost equal values of $a\sqrt{\sigma}$, and hence of $a\Lambda$, across several values of N. These are for $N = 3, 4, 5, 6$ at $a\sqrt{\sigma} \simeq 0.15$ and for $N = 8, 10, 12$ at $a\sqrt{\sigma} \simeq 0.33$. In figure 26 we plot the values of $\ln\{\tilde{\tau}_Q\}$ against N and we see that the behaviour is roughly linear as predicted from eqs. (6.3), (6.4).

The second qualitative feature of eq. (6.4) is that if we vary a at fixed N, we should find

$$\tau_Q \propto \frac{1}{D(\rho)} \propto \left\{\frac{1}{a\Lambda}\right\}^{\frac{11N}{3}-5} \longrightarrow \ln\{\tau_Q\} = b + \left\{\frac{11N}{3} - 5\right\} \ln\left\{\frac{1}{a\Lambda}\right\}. \qquad (6.5)$$

In figure 27 we show plots of $\ln\{\tau_Q\}$ versus $\ln\{1/a\sqrt{\sigma}\}$ for $N \in [3, 8]$ and we see that the plots are roughly linear as predicted by eqs. (6.3), (6.5). (As an aside, the fact that the SU(2) values of τ_Q never become large enough to be useful is no surprise given that the asymptotic dependence predicted by eq. (6.5) is quite weak, $\tau_Q \propto a^{7/3}$.) The fitted coefficients of the $\ln\{1/a\sqrt{\sigma}\}$ term are listed in table 43 and compared to the value in eq. (6.5). We do not expect a good agreement since we know that the one loop expression for $g^2(a)$ is a poor approximation in our range of bare couplings but it is interesting that our calculated values listed in table 43 do reflect the trend of the asymptotic theoretical values.

6.3 Topological susceptibility

The simplest topological quantity that one can calculate is the topological susceptibility, $\chi_t = \langle Q^2 \rangle / V$, where V is the space-time volume. This is a particularly interesting quantity because of the way it enters into estimates of the physical η' mass through the Witten-Veneziano sum rule [66, 67]. There have been many calculations of this quantity and here we will add to these our calculations for the gauge groups SU(2), SU(3), SU(4), SU(5) and for those of our SU(6) ensembles where there are enough fluctuations in the value of Q to make an estimate plausible.

We typically calculate the topological charge Q after every 25 or 50 or 100 Monte Carlo sweeps on most of the lattice ensembles that we use for our glueball and/or string tension

calculations. We estimate the value of Q from the value of the lattice Q_L after 20 cooling sweeps. The assignment of an integer value, Q_I, after 20 cooling sweeps is, as we have seen, largely unambiguous. In tables 44, 45 and 46 we list our values for Q^2 on the lattices and at the couplings shown.

To obtain the continuum limit we perform a conventional extrapolation

$$\left.\frac{\chi_t^{\frac{1}{4}}}{\sqrt{\sigma}}\right|_a = \left.\frac{\chi_t^{\frac{1}{4}}}{\sqrt{\sigma}}\right|_0 + ca^2\sigma, \tag{6.6}$$

where we systematically remove from the fit the values corresponding to the largest a until we get an acceptable fit. We show the resulting continuum extrapolations for $N = 2, 3, 4, 5$ in figure 28 and list the resulting continuum values in table 47. For SU(2) and SU(3) we do not include the value at the smallest a since it is clearly too low and it is plausible that it is due to a gradual loss of ergodicity in Q accompanied by an increasingly unreliable estimate of the errors. We see from figure 28 that As we increase N our fits are able to include values from increasingly coarse $a(\beta)$. This is presumably related to the fact that the 'bulk' cross-over/transition between strong and weak coupling becomes rapidly sharper as N increases [15]. (It is particularly smooth for SU(2).) As shown in table 47 all the fits are acceptable. We have performed separate continuum extrapolations of the susceptibilities obtained from the non-integer lattice charges, Q_L, and the integer charges, Q_I, labelling these χ_L and χ_I respectively. In the continuum limit these should be the same and we see from table 47 that this is indeed so, within errors, for all except the case of SU(2), where the difference between the two values can be taken as a systematic error that is additional to the statistical errors.

Once we have the continuum susceptibilites we can extrapolate them to $N = \infty$ as shown in figure 29:

$$\left.\frac{\chi_I^{\frac{1}{4}}}{\sqrt{\sigma}}\right|_N = 0.3681(28) + \frac{0.471(15)}{N^2}, \tag{6.7}$$

and

$$\left.\frac{\chi_L^{\frac{1}{4}}}{\sqrt{\sigma}}\right|_N = 0.3655(27) + \frac{0.448(15)}{N^2}. \tag{6.8}$$

The two are within errors as one would expect. We note that this value is consistent within errors with the $N = \infty$ extrapolation in [68] which uses a novel technique [69] for ameliorating the problem of topological freezing.

Finally we return to the case of SU(3) since it also has some phenomenological interest. Here our analysis differs slightly from our earlier analysis in [11] and our final result

$$\left.\frac{\chi_I^{\frac{1}{4}}}{\sqrt{\sigma}}\right|_{\text{SU}(3)} = 0.4246(36) \tag{6.9}$$

is about one standard deviation higher. To transform this into physical units we translate from units in terms of $\sqrt{\sigma}$ to the standard scale r_0 and then to MeV units just as we did in

eq. (4.9) of section 4.2, giving

$$r_0\sqrt{\sigma} = 1.160(6) \implies \chi_I^{\frac{1}{4}} = 206(4)\text{MeV}. \tag{6.10}$$

This is within errors of the value we presented in [11] and the value $\chi_I^{\frac{1}{4}} \overset{\text{SU3}}{=} 208(6)\text{MeV}$ obtained in [70] using the gradient flow technique. As an aside we note that the value of $\chi_I^{\frac{1}{4}}/\sqrt{\sigma}$ at $N = \infty$, as given in eq. (6.7), is $\sim 13\%$ lower than the SU(3) value, i.e. ~ 179'MeV' if we simply rescale the value in eq. (6.10).

6.4 $Z_Q(\beta)$ and lattice θ parameter

Consider the ensemble of Monte Carlo lattice gauge fields that correspond to an integer valued topological charge Q. If we calculate the charge Q_L of each of these fields, prior to any cooling, the average value will be related to Q by [56]

$$<Q_L> = Z_Q(\beta)Q, \tag{6.11}$$

where $Z_Q(\beta)$ will depend (weakly) on N and negligibly on the lattice volume (as long as it is not very small). Since the deviation of $Z_Q(\beta)$ from unity is driven by high frequency lattice fluctuations, it is of little physical interest in itself. However its value is important if, for example, one wishes to study the θ dependence of the theory by adding a term $i\theta Q$ to the continuum action and, correspondingly, a term $i\theta_L Q_L$ to the lattice action, since one sees that [71]

$$\theta_L \simeq Z_Q^{-1}(\beta)\theta. \tag{6.12}$$

Primarily for this reason we have calculated $Z_Q(\beta)$ in our lattice calculations and will also provide interpolating functions that will give $Z_Q(\beta)$ at values of β that lie between our measured values.

A first estimate for $Z_Q(\beta)$ can be obtained in perturbation theory, giving at one loop [56]

$$Z_Q(\beta) \overset{\beta\to\infty}{=} 1 - (0.6612N^2 - 0.5)\frac{1}{\beta} + O(\beta^{-2}) \tag{6.13}$$

which already tells us that for our range of β we will have $Z_Q(\beta) \ll 1$. The fact that the one loop correction is so large tells us that the one loop estimate is likely to be not very accurate, and indeed that proves to be the case. Moreover as we increase the lattice spacing the typical instanton becomes smaller and the value of Q_L acquires significant corrections that are powers of $a(\beta)$ and which are additional to any perturbative corrections. So in constructing our interpolating function for Z_Q we simply use the form

$$Z_Q^{\text{int}}(\beta) = 1 - z_0 g^2 N - z_1(g^2 N)^2; \quad g^2 N = \frac{2N^2}{\beta}, \tag{6.14}$$

where $g^2 N$ is the 't Hooft coupling, and we make no attempt to constrain the parameters z_0 and z_1 to perturbative values. This turns out to be an adequate fitting function to our values of $Z_Q(\beta)$. It is however important to note that while this works as an interpolating

function, it is likely to fail increasingly badly the further one uses it away from the fitted range of β as an extrapolating function.

Our values for $Z_Q(\beta)$ are obtained from fits such as those shown in figure 30, and are listed in tables 48 and 49. Interpolating these values with eq. (6.14) gives the values for z_0 and z_1 listed in table 50. Physically the most relevant interpolating function is the one for SU(3):

$$Z_Q^{\text{int}}(\beta) \stackrel{su3}{=} 1 - 0.162(10)g^2N - 0.0425(31)(g^2N)^2, \quad \chi^2/n_{df} = 0.62 \qquad (6.15)$$

In the case of SU(2) we have only a few entries because most of our earliest calculations did not include calculating Q_L on the fields prior to cooling. In addition in the case of SU(2) the identification of an integer Q after 20 cooling sweeps possesses small but significant ambiguities, which rapidly disappear as N increases. We can also fit our interpolating functions in N, thus obtaining

$$z_0 = 0.179(12) - \frac{0.08(15)}{N^2}, \quad \chi^2/n_{df} = 1.00 \qquad (6.16)$$

and

$$z_1 = 0.0482(46) - \frac{0.072(50)}{N^2}, \quad \chi^2/n_{df} = 1.13 \qquad (6.17)$$

which should be reliable over a wide range of N as long as we are not too far outside the range of the t'Hooft coupling $\lambda = g^2N$ of our calculations in tables 48 and 49. Finally we remind the reader that all these results for $Z_Q(\beta)$ only apply to calculations with the standard Wilson plaquette action and with the definition of the lattice topological charge Q_L used here.

7   Conclusions

Our primary goal in this paper has been to calculate the glueball spectra of a range of SU(N) gauge theories, in the continuum limit, with enough precision to obtain plausible extrapolations to the theoretically interesting $N = \infty$ limit. This provides the first calculation of the masses of the ground states in all the R^{PC} channels, as well as some excited states in most channels, in the continuum limit of the $N \to \infty$ gauge theory.

Our results, for $N = 2, 3, 4, 5, 6, 8, 10, 12$, were obtained using standard lattice gauge theory methods. Although the issue of topological freezing at larger N in SU(N) gauge theories is not expected to be important for glueball spectra [28, 29], we confirmed this explicitly in some extensive SU(8) calculations, and in addition we chose to minimise any remnant bias at larger N by modifying the usual update algorithm, explicitly imposing the expected distribution of topological charge on the starting lattice fields of our ensemble of Monte Carlo sequences. We employed a large basis of single-trace glueball operators, which allowed us to calculate the ground state and some excited states for each of the R^{PC} channels, where R labels the representation of the rotation symmetry group appropriate to our cubic lattice, and P, C label the parity and charge conjugation. The large basis gives us confidence that we are not missing any low-lying states and this in turn allows us to match near-degeneracies between states with different R so as to assign continuum spin quantum numbers to a significant number of glueball states.

Our results have greatly extended existing calculations while largely confirming existing results; in particular the important conclusion that SU(3) is 'close to' SU(∞). As before, one finds that the lightest glueball is the $J^{PC} = 0^{++}$ scalar ground state, with a mass that ranges from $M_{0^{++}} \sim 3.41\sqrt{\sigma}$ for SU(3) to $M_{0^{++}} \sim 3.07\sqrt{\sigma}$ for SU(∞), where σ is the string tension, and that the next heavier glueballs are the tensor with a mass $M_{2^{++}} \simeq 1.5 M_{0^{++}}$, and the pseudoscalar, 0^{-+}, which is nearly degenerate with the tensor. One then has the 1^{+-} with $M_{1^{+-}} \sim 1.85 M_{0^{++}}$, and this is the only relatively light $C = -$ state. At roughly the same mass is the first excited 0^{++} and then the lightest pesudotensor with $M_{2^{-+}} \sim 1.95 M_{0^{++}}$. All other states are heavier than twice the lightest scalar, with most of the $C = -$ ground states being very much heavier than that. One sees a number of near-degeneracies which may or may not be significant. The continuum glueball masses (in units of the string tension) for the various R^{PC} channels are listed in tables 23–31 and for the J^{PC} channels in tables 34–38.

Since our calculations are on a finite spatial volume we have had to identify and exclude the 'ditorelon' states composed of a pair of mutually conjugate flux tubes that wind around our periodic spatial torus. These are states whose projection onto our single trace operators will vanish as $N \to \infty$. We also need to exclude any multiglueball scattering states. Our (albeit partial) explicit calculations using the corresponding double trace operators strongly suggest that these states do not appear in the glueball spectra that we claim to obtain using our single trace basis.

In calculating the glueball spectra we have also calculated a number of other quantities that could be calculated simultaneously. Our calculations of the string tension were primarily intended to provide a scale in which to express our glueball masses. However they also provided a scale for the lattice spacing a at each value of the bare lattice coupling, $g_L(a)$, which we were able to use to obtain values of the dynamical scale $\Lambda_{\overline{MS}}$ for all our values of N. These improved upon earlier calculations of this kind and for SU(3) provided a value in physical units of $\Lambda_{\overline{MS}} \simeq 263(4)[9]$MeV which is consistent with values obtained using more dedicated methods At the same time we were able to confirm that keeping fixed the running 't Hooft coupling $g^2(a)N$, with a being kept fixed in units of the string tension, is the way to approach the $N = \infty$ limit along lines of constant physics.

In addition to the fundamental string tension we calculate the tension of $k = 2$ flux tubes, in order to analyse the way that $\sigma_{k=2}/\sigma$ approaches $N = \infty$. We find that a leading $O(1/N)$ correction works better than the $O(1/N^2)$ expected from standard large-N counting, but that the latter cannot be completely excluded. We speculate that the $O(1/N)$ behaviour is sub-asymptotic, with the $O(1/N^2)$ correction settling in for flux tubes of length $l \leq l_c$ once N is large enough that the $k = 2$ flux tube becomes a pair of weakly interacting fundamental flux tubes for $l \leq l_c$ with $l_c \uparrow$ as $N \uparrow$. That is to say, the $l, N \to \infty$ limit is not uniform.

Since for our glueball calculations we need to monitor the onset of the freezing of the topology of our lattice fields, we have performed extensive calculations of the topological charge along with the glueball calculations. Using these calculations we obtain values for the continuum limit of the topological susceptibility for the SU($N \leq 6$) gauge theories. The freezing of topology means that we have no values for $N > 6$ or for our smaller SU(6)

lattice spacings. Nonetheless this does not prevent us achieving a usefully precise value of the $N = \infty$ topological suseptibility, $\chi_I^{\frac{1}{4}}/\sqrt{\sigma} = 0.3681(28)$. We have also calculated the renormalisation factor $Z_Q(\beta)$ that relates the value of our particular (but standard) lattice topological charge, as obtained on the Monte carlo generated lattice gauge fields, to the true integer valued topological charge of those fields. This is useful if one wishes to include a topological θ-term in the action, and so we also include functions that interpolate between our values of β. We can do so for all our SU(N) groups because these calculations can be equally well determined using ensembles of fields where the topological charge has been inserted through the initial fields of the Markovian chains.

The present study could be improved in several ways. A definitive study of ditorelon states and the lightest multiglueball states for all R^{PC} sectors would be useful. The heaviest states need a finer resolution in the correlation functions for the mass identification to become completely unambiguous: this could be achieved by using an anisotropic lattice such that the timelike lattice spacing is much smaller than the spacelike one, a technique that has occasionally been put to good purpose in the past [7, 10, 50, 51]. Perhaps most important would be the incorporation of more effective techniques for determining the continuum spins of the glueball states, as for example in [54] for 2 space dimensions and in [9] for our case here of 3 spatial dimensions.

Acknowledgments

A Lattice running couplings

For pure gauge theories the perturbative β function for the running coupling in a coupling scheme s is given by

$$\beta(g_s) = -a\frac{\partial g_s}{\partial a} = -b_0 g_s^3 - b_1 g_s^5 - b_2^s g_s^7 + \dots, \tag{A.1}$$

where a is the length scale on which the coupling is calculated and on which it depends. The first two coefficients b_0 and b_1 are scheme independent while the coefficients $b_{j\geq 2}^s$ depend on the scheme. Integrating between scales a_0 and a, we obtain

$$\frac{a}{a_0} = \exp\left(-\int_{g(a_0)}^{g(a)} \frac{dg}{\beta(g)}\right). \tag{A.2}$$

(The label s on g is to be understood.) The integrand is singular as $g \to 0$ and for any calculations it is convenient to separate out the singular pieces. Since the issue arise for

$g \to 0$ we can expand $1/\beta(g)$ in powers of g and we then readily see that we can separate out the singular terms as follows,

$$\frac{a}{a_0} = e^{+\int_{g(a_0)}^{g(a)} dg\left(-\frac{b_1}{b_0^2 g} + \frac{1}{b_0 g^3}\right)} e^{-\int_{g(a_0)}^{g(a)} dg\left(\frac{1}{\beta(g)} - \frac{b_1}{b_0^2 g} + \frac{1}{b_0 g^3}\right)}$$

$$= \left(\frac{g^2(a)}{g^2(a_0)}\right)^{-\frac{b_1}{2b_0^2}} e^{-\frac{1}{2b_0}\left(\frac{1}{g^2(a)} - \frac{1}{g^2(a_0)}\right)} e^{-\int_{g(a_0)}^{g(a)} dg\left(\frac{1}{\beta(g)} - \frac{b_1}{b_0^2 g} + \frac{1}{b_0 g^3}\right)}. \tag{A.3}$$

In the second line we have integrated the 'singular' terms, and the remaining integral will now be finite as $g(a_0) \to 0$. So we can break up the integral as

$$e^{-\int_{g(a_0)}^{g(a)} dg\left(\frac{1}{\beta(g)} - \frac{b_1}{b_0^2 g} + \frac{1}{b_0 g^3}\right)} = e^{+\int_0^{g(a_0)} dg\left(\frac{1}{\beta(g)} - \frac{b_1}{b_0^2 g} + \frac{1}{b_0 g^3}\right)} e^{-\int_0^{g(a)} dg\left(\frac{1}{\beta(g)} - \frac{b_1}{b_0^2 g} + \frac{1}{b_0 g^3}\right)} \tag{A.4}$$

where each integral will be well-defined since the singularities at $g = 0$ have been removed. Separating the terms in a and a_0 in eqs. (A.3), (A.4) we can write

$$\frac{a}{a_0} = \frac{F(g(a))}{F(g(a_0))}, \tag{A.5}$$

where we define

$$F(g) \equiv \left(b_0 g^2\right)^{-\frac{b_1}{2b_0^2}} e^{-\frac{1}{2b_0 g^2}} e^{-\int_0^g dg\left(\frac{1}{\beta(g)} - \frac{b_1}{b_0^2 g} + \frac{1}{b_0 g^3}\right)}. \tag{A.6}$$

Note that the factor of b_0 that we have inserted in the first term on the right of eq. (A.6) will cancel in eq. (A.5) so we are free to insert it if we wish. We see from eq. (A.5) that $a/F(g^2(a))$ is independent of the scale a on which the coupling is defined and is a constant. So we can now define a dynamical energy scale Λ by

$$\Lambda \equiv \frac{a_0}{F(g(a_0))} \implies a = \frac{1}{\Lambda} F(g(a))$$

$$= \frac{1}{\Lambda} \left(b_0 g^2\right)^{-\frac{b_1}{2b_0^2}} e^{-\frac{1}{2b_0 g^2}} e^{-\int_0^{g(a)} dg\left(\frac{1}{\beta(g)} - \frac{b_1}{b_0^2 g} + \frac{1}{b_0 g^3}\right)}. \tag{A.7}$$

The scale Λ defined here coincides with the conventional Λ parameter that appears in the standard 2-loop expression for the running coupling. (It is to ensure this equality that we inserted the factor of b_0 above.) This scale will clearly depend on the coupling scheme and within a given scheme the value we obtain for it will depend on our approximation to $\beta(g)$.

For our lattice action only the first 3 coefficients in the β-function are known. In that case, collecting terms, it is convenient to rewrite eq. (A.7) as

$$a \stackrel{3\text{loop}}{=} \frac{1}{\Lambda} \left(b_0 g^2(a)\right)^{-\frac{b_1}{2b_0^2}} e^{-\frac{1}{2b_0 g^2(a)}} e^{-\frac{1}{2}\int_0^{g^2(a)} dg^2 \left(\frac{b_0 b_2 - b_1^2 - b_1 b_2 g^2}{b_0^3 + b_0^2 b_1 g^2 + b_0^2 b_2 g^4}\right)} \equiv \frac{1}{\Lambda} F_{3l}(g(a)), \tag{A.8}$$

where we denote by $F_{3l}(g)$ the 3-loop approximation to $F(g)$. The integrand is a smooth function of g^2 and so the integral can be calculated accurately for any given $g(a)$ using any

elementary numerical integration method. If we retain only the first 2 coefficients of $\beta(g)$ then we can do the integral analytically to obtain

$$a \overset{\text{2loop}}{=} \frac{1}{\Lambda} e^{-\frac{1}{2b_0 g(a)^2}} \left(\frac{b_1}{b_0^2} + \frac{1}{b_0 g^2(a)} \right)^{\frac{b_1}{2b_0^2}} \equiv \frac{1}{\Lambda} F_{2l}(g(a)) \tag{A.9}$$

as the exact 2-loop result, where we denote by $F_{2l}(g)$ the 2-loop approximation to $F(g)$.

The above perturbative expressions for $a\Lambda$ can be turned into expressions for $a\mu$ where μ is some physical mass or energy:

$$a\mu = a\Lambda \frac{\mu}{\Lambda}\bigg|_a = \frac{\mu}{\Lambda}\bigg|_{a=0} (1 + c_\mu a^2 \mu^2 + O(a^4)) F(g(a)), \tag{A.10}$$

where $F(g(a))$ is defined in eq. (A.6) and c_μ is an unknown constant. Here we use the standard tree-level expansion for a dimensionless ratio of physical energy scales, which here is μ/Λ. This expression marries perturbative (logarithmic) and power-like dependences on a in a plausible way. It is of course arguable: for example the perturbative expansion is at best asymptotic and this can introduce other power-like corrections. In practice we shall use this for the string tension, $\mu = \sqrt{\sigma}$, and we will drop $O(a^4)$ and higher order terms. That is to say we will attempt to fit the calculated string tensions with

$$a\sqrt{\sigma} = \frac{\sqrt{\sigma}}{\Lambda}\bigg|_{a=0} (1 + c_\sigma a^2 \sigma) F_{3l}(g(a)) \tag{A.11}$$

and we shall be doing so in the mean-field coupling scheme $s = I$. To calculate $F_{3l}(g(a))$ in that scheme we only need to know the coefficient $b_2^{s=I}$, since b_0 and b_1 are scheme independent with values

$$b_0 = \frac{1}{(4\pi)^2} \frac{11}{3} N, \quad b_1 = \frac{1}{(4\pi)^4} \frac{34}{3} N^2. \tag{A.12}$$

We can begin with the well-known value of $b_2^{s=\overline{MS}}$ [72]

$$b_2^{\overline{MS}} = \frac{1}{(4\pi)^6} \frac{2857}{54} N^3. \tag{A.13}$$

To obtain b_2^s in the improved lattice coupling scheme I we first transform to the plaquette action lattice coupling scheme, $s = L$, using [73]

$$b_2^L = 2b_2^{\overline{MS}} - b_1 l_0 + b_0 l_1, \tag{A.14}$$

where

$$l_0 = \frac{1}{8N} - 0.16995599 N, \qquad l_1 = -\frac{3}{128 N^2} + 0.018127763 - 0.0079101185 N^2. \tag{A.15}$$

The lattice coupling, g_L^2, satisfies the β-function in eq. (A.1) with $s = L$, and the mean-field coupling will satisfy a β-function with the same b_0 and b_1 coefficients but with a different coefficient, b_2^I, of the g^7 power. To determine b_2^I one can use the expression for $\langle \text{Tr} U_p \rangle$ as a power series in g_L^2 to write g_I^2 as

$$g_I^2 = g_L^2 \langle \frac{1}{N} \text{Tr} U_p \rangle = g_L^2 \left(1 - w_1 g_L^2 - w_2 g_L^4 - \ldots \right), \tag{A.16}$$

where [74]

$$w_1 = \frac{(N^2 - 1)}{8N}, \qquad w_2 = \left(N^2 - 1\right)\left(0.0051069297 - \frac{1}{128N^2}\right). \tag{A.17}$$

We now insert the expression for g_I^2 in eq. (A.16) into the β-function for g_L^2 in eq. (A.1) giving us, after some elementary manipulation,

$$b_2^I = b_2^L + w_2 b_0 - w_1 b_1. \tag{A.18}$$

So: using eqs. (A.13), (A.15) in eq. (A.14) we obtain the explicit expression for b_2^L and then inserting that together with the functions in eq. (A.17) and eq. (A.12) into eq. (A.18) we obtain the explicit expression for b_2^I for any N. We now have the explicit expressions for b_0, b_1 and b_2^I which allow us to calculate the value of $F_{3l}(g_I(a))$ in eq. (A.11) for any value of N and $g_I(a)$.

B Scattering states

We will restrict ourselves to states of two glueballs. We probe such states with product operators $\phi_a(t)\phi_b(t)$ where ϕ_a and ϕ_b are typical single loop zero momentum operators that are expected to project primarily onto single glueballs with chosen quantum numbers. Both the individual and product operators will in general need vacuum subtraction for this to be the case. As usual we will have some basis of single loop operators so the generic correlator will be of the form

$$C_4(t) = \langle \phi_a'(t)\phi_b'(t)\phi_c'(0)\phi_d'(0)\rangle - \langle \phi_a'\phi_b'\rangle\langle \phi_c'\phi_d'\rangle, \tag{B.1}$$

where $\phi_a'(t) = \phi_a(t) - \langle\phi_a\rangle$ etc. This equation subtracts any vacuum contribution to the individual operators as well as to their products. We have taken the operators to be real. If, for example, we were to include operators $\phi_i(t), \phi_j(t)$ with opposite non-zero momenta then these would be complex. In that case we should change $\phi_a(t), \phi_b(t) \to \phi_a^\dagger(t), \phi_b^\dagger(t)$ in eq. (B.1) and below.

Our glueball calculations require high statistics so we calculate our correlators during the generation of the sequence of lattice fields. At this stage we can only calculate the correlators of the fields ϕ without any vacuum subtraction — we will only be able to calculate the vacuum expectation values at the end of the computer simulation. A short calculation tells us that the correlator of the ϕ_i' fields in eq. (B.1) can be written in terms of the correlators of the unsubtracted ϕ_i fields as follows:

$$\begin{aligned}
C_4(t) = &\langle \phi_a(t)\phi_b(t)\phi_c(0)\phi_d(0)\rangle \\
&- \langle\phi_a\rangle\langle\phi_b(t)\phi_c(0)\phi_d(0)\rangle - \langle\phi_b\rangle\langle\phi_a(t)\phi_c(0)\phi_d(0)\rangle \\
&- \langle\phi_c\rangle\langle\phi_a(t)\phi_b(t)\phi_d(0)\rangle - \langle\phi_d\rangle\langle\phi_a(t)\phi_b(t)\phi_c(0)\rangle \\
&+ \langle\phi_a\rangle\langle\phi_c\rangle\langle\phi_b(t)\phi_d(0)\rangle + \langle\phi_b\rangle\langle\phi_c\rangle\langle\phi_a(t)\phi_d(0)\rangle \\
&+ \langle\phi_a\rangle\langle\phi_d\rangle\langle\phi_b(t)\phi_c(0)\rangle + \langle\phi_b\rangle\langle\phi_d\rangle\langle\phi_a(t)\phi_c(0)\rangle \\
&- \langle\phi_a\phi_b\rangle\langle\phi_c\phi_d\rangle + 2\langle\phi_a\phi_b\rangle\langle\phi_c\rangle\langle\phi_d\rangle + 2\langle\phi_c\phi_d\rangle\langle\phi_a\rangle\langle\phi_b\rangle - 4\langle\phi_a\rangle\langle\phi_b\rangle\langle\phi_c\rangle\langle\phi_d\rangle.
\end{aligned} \tag{B.2}$$

Of course when some of the operators have non-vacuum quantum numbers, then the corresponding vacuum expectation values will vanish and the above expression will simplify in obvious ways.

In addition to the above we may also be interested in the overlap of single loop operators, which mainly project onto single glueballs, with the above product operators, which one expects to mainly project onto two glueballs. That is to say correlators such as

$$C_3(t) = \langle \phi_a'(t)\phi_b'(t)\phi_c'(0)\rangle - \langle \phi_a'\phi_b'\rangle\langle\phi_c'\rangle = \langle\phi_a'(t)\phi_b'(t)\phi_c'(0)\rangle \tag{B.3}$$

since $\langle\phi_c'\rangle = 0$ by definition. In terms of the unsubtracted operators we find

$$\begin{aligned}
C_3(t) = \langle\phi_a(t)\phi_b(t)\phi_c(0)\rangle - \langle\phi_a\rangle\langle\phi_b(t)\phi_c(0)\rangle - \langle\phi_b\rangle\langle\phi_a(t)\phi_c(0)\rangle \\
- \langle\phi_c\rangle\langle\phi_a\phi_b\rangle + 2\langle\phi_a\rangle\langle\phi_b\rangle\langle\phi_c\rangle.
\end{aligned} \tag{B.4}$$

In this paper we can only calculate light masses with any reliability so we restrict ourselves to double loop operators where one loop is in the A_1^{++} representation and therefore has some projection onto the lightest glueball. The second operator will then be in the representation R^{PC} in which we happen to be interested. If $R^{PC} \neq A_1^{++}$ then eq. (B.2) simplifies drastically

$$\begin{aligned}
C_4(t) = \langle\phi_a(t)\phi_b(t)\phi_c(0)\phi_d(0)\rangle - \langle\phi_a\rangle\langle\phi_b(t)\phi_c(0)\phi_d(0)\rangle \\
- \langle\phi_c\rangle\langle\phi_a(t)\phi_b(t)\phi_d(0)\rangle + \langle\phi_a\rangle\langle\phi_c\rangle\langle\phi_b(t)\phi_d(0)\rangle - \langle\phi_a\phi_b\rangle\langle\phi_c\phi_d\rangle
\end{aligned} \tag{B.5}$$

since with ϕ_a, ϕ_c being A_1^{++} and ϕ_b, ϕ_d not being A_1^{++} means that not only $\langle\phi_b\rangle = \langle\phi_d\rangle = 0$ but also that products like $\langle\phi_a\phi_b\rangle$ are zero. Similarly if ϕ_a in eq. (B.3) is A_1^{++} and ϕ_b is in some $R^{PC} \neq A_1^{++}$ then ϕ_c must be in the same $R^{PC} \neq A_1^{++}$ for $C_3(t)$ not to be zero. In that case we will have

$$C_3(t) = \langle\phi_a(t)\phi_b(t)\phi_c(0)\rangle - \langle\phi_a\rangle\langle\phi_b(t)\phi_c(0)\rangle. \tag{B.6}$$

If however ϕ_b and ϕ_c are in A_1^{++} then we need the full expression.

SU(2) ; $l\sqrt{\sigma} \sim 4$				
β	$l^3 l_t$	$\frac{1}{2}\mathrm{ReTr}\langle U_p \rangle$	$a\sqrt{\sigma}$	am_G
2.2986	$12^3 16$	0.6018259(46)	0.36778(69)	1.224(16)
2.3714	$14^3 16$	0.6226998(36)	0.29023(50)	1.025(12)
2.427	$20^3 16$	0.6364293(15)	0.24013(41)	0.8469(76)
2.509	$22^3 20$	0.6537214(10)	0.18011(22)	0.6563(56)
2.60	30^4	0.6700089(5)	0.13283(30)	0.5001(41)
2.70	40^4	0.6855713(3)	0.09737(23)	0.3652(35)

Table 1. Parameters of the main SU(2) calculations: the inverse coupling, β, the lattice size, the average plaquette, the string tension, σ, and the mass gap, m_G.

SU(3) ; $l\sqrt{\sigma} \sim 4$				
β	$l^3 l_t$	$\frac{1}{3}\mathrm{ReTr}\langle U_p \rangle$	$a\sqrt{\sigma}$	am_G
5.6924	$10^3 16$	0.5475112(71)	0.3999(58)	0.987(9)
5.80	$12^3 16$	0.5676412(36)	0.31666(66)	0.908(12)
5.8941	$14^3 16$	0.5810697(18)	0.26118(37)	0.7991(92)
5.99	18^4	0.5925636(11)	0.21982(77)	0.7045(65)
6.0625	20^4	0.6003336(10)	0.19472(54)	0.6365(43)
6.235	26^4	0.6167723(6)	0.15003(30)	0.4969(29)
6.3380	30^4	0.6255952(4)	0.12928(27)	0.4276(37)
6.50	38^4	0.6383531(3)	0.10383(24)	0.3474(22)

Table 2. Parameters of the main SU(3) calculations: the inverse coupling, β, the lattice size, the average plaquette, the string tension, σ, and the mass gap, m_G.

SU(4) ; $l\sqrt{\sigma} \sim 4$				
β	$l^3 l_t$	$\frac{1}{4}\mathrm{ReTr}\langle U_p \rangle$	$a\sqrt{\sigma}$	am_G
10.70	$12^3 16$	0.5540665(24)	0.3021(5)	0.8406(48)
10.85	$14^3 20$	0.5664268(15)	0.25426(38)	0.7611(54)
11.02	$18^3 20$	0.5782610(11)	0.21434(28)	0.6605(33)
11.20	22^4	0.5893298(6)	0.18149(49)	0.5709(34)
11.40	26^4	0.6004374(4)	0.15305(34)	0.4864(30)
11.60	30^4	0.6106057(3)	0.13065(21)	0.4132(44)

Table 3. Parameters of the main SU(4) calculations: the inverse coupling, β, the lattice size, the average plaquette, the string tension, σ, and the mass gap, m_G.

SU(5) ; $l\sqrt{\sigma} \sim 3.1$				
β	$l^3 l_t$	$\frac{1}{5}\mathrm{ReTr}\langle U_p\rangle$	$a\sqrt{\sigma}$	am_G
16.98	$10^3 16$	0.5454873(28)	0.3033(8)	0.8241(68)
17.22	$12^3 16$	0.5587002(18)	0.2546(6)	0.7517(51)
17.43	$14^3 20$	0.5685281(10)	0.22217(37)	0.6751(44)
17.63	$16^3 20$	0.5769707(9)	0.19636(35)	0.5961(79)
18.04	$20^3 24$	0.5924012(6)	0.15622(38)	0.4783(44)
18.375	$24^3 30$	0.6036547(4)	0.13106(30)	0.4078(38)

Table 4. Parameters of the main SU(5) calculations: the inverse coupling, β, the lattice size, the average plaquette, the string tension, σ, and the mass gap, m_G.

SU(6) ; $l\sqrt{\sigma} \sim 3.1$				
β	$l^3 l_t$	$\frac{1}{6}\mathrm{ReTr}\langle U_p\rangle$	$a\sqrt{\sigma}$	am_G
24.67	$10^3 16$	0.5409011(28)	0.30658(34)	0.8240(41)
25.05	$12^3 16$	0.5557062(13)	0.25177(23)	0.7395(50)
25.32	$14^3 20$	0.5646185(10)	0.22208(35)	0.6673(32)
25.55	$16^3 20$	0.5715585(9)	0.20153(34)	0.6112(41)
26.22	$20^3 24$	0.5894540(4)	0.15480(36)	0.4751(53)
26.71	$24^3 30$	0.6009861(3)	0.12867(27)	0.3886(37)

Table 5. Parameters of the main SU(6) calculations: the inverse coupling, β, the lattice size, the average plaquette, the string tension, σ, and the mass gap, m_G.

SU(8) ; $l\sqrt{\sigma} \sim 2.6$				
β	$l^3 l_t$	$\frac{1}{8}\mathrm{ReTr}\langle U_p\rangle$	$a\sqrt{\sigma}$	am_G
44.10	$8^3 16$	0.5318034(31)	0.32589(62)	0.8246(66)
44.85	$10^3 16$	0.5497960(15)	0.25791(40)	0.7461(53)
45.50	$12^3 20$	0.5622253(9)	0.21851(45)	0.6409(38)
46.10	$14^3 20$	0.5723242(8)	0.18932(38)	0.5617(43)
46.70	$16^3 24$	0.5815072(5)	0.16557(38)	0.4909(43)
47.75	$20^3 30$	0.5959878(3)	0.13253(26)	0.4075(28)

Table 6. Parameters of the main SU(8) calculations: the inverse coupling, β, the lattice size, the average plaquette, the string tension, σ, and the mass gap, m_G.

SU(10) ; $l\sqrt{\sigma} \sim 2.6$				
β	$l^3 l_t$	$\frac{1}{10}\mathrm{ReTr}\langle U_p \rangle$	$a\sqrt{\sigma}$	am_G
69.20	$8^3 16$	0.5292925(29)	0.33024(35)	0.8282(60)
70.38	$10^3 16$	0.5478565(13)	0.25987(30)	0.7435(42)
71.38	$12^3 20$	0.5602903(9)	0.21988(32)	0.6451(44)
72.40	$14^3 20$	0.5713707(6)	0.18845(20)	0.5549(59)
73.35	$16^3 24$	0.5807004(4)	0.16399(19)	0.4952(44)

Table 7. Parameters of the main SU(10) calculations: the inverse coupling, β, the lattice size, the average plaquette, the string tension, σ, and the mass gap, m_G.

SU(12) ; $l\sqrt{\sigma} \sim 2.6$				
β	$l^3 l_t$	$\frac{1}{12}\mathrm{ReTr}\langle U_p \rangle$	$a\sqrt{\sigma}$	am_G
99.86	$8^3 16$	0.5275951(27)	0.33341(40)	0.8243(52)
101.55	$10^3 16$	0.5464461(12)	0.26162(32)	0.7384(51)
103.03	$12^3 20$	0.55936304(61)	0.21915(25)	0.6432(32)
104.55	$14^3 20$	0.57087665(49)	0.18663(38)	0.5521(42)
105.95	$16^3 24$	0.58043063(32)	0.16197(27)	0.4920(37)

Table 8. Parameters of the main SU(12) calculations: the inverse coupling, β, the lattice size, the average plaquette, the string tension, σ, and the mass gap, m_G.

$aE_{\text{eff}}(t = 2a)$: SU(8) at $\beta = 45.50$ on $14^3 20$					
R^{PC}	all Q	Q = 0	R^{PC}	all Q	Q = 0
A_1^{++}	0.6512(21)	0.6497(25)	A_1^{-+}	1.119(8)	1.098(9)
	1.199(9)	1.209(9)		1.581(23)	1.587(21)
	1.243(12)	1.236(11)		1.908(43)	1.937(51)
	1.565(21)	1.551(23)			
A_2^{++}	1.668(27)	1.642(25)	A_2^{-+}	2.21(8)	2.51(11)
	1.983(48)	2.037(48)		2.30(9)	2.23(11)
E^{++}	1.020(4)	1.020(5)	E^{-+}	1.354(9)	1.356(11)
	1.230(8)	1.233(8)		1.757(24)	1.765(25)
	1.435(10)	1.424(9)		2.060(51)	2.157(50)
T_1^{++}	1.670(14)	1.673(18)	T_1^{-+}	1.841(25)	1.861(24)
	1.728(20)	1.708(19)		1.976(27)	1.950(26)
	2.011(27)	2.041(35)		1.925(28)	1.928(28)
	2.053(35)	2.037(31)			
T_2^{++}	1.032(4)	1.033(3)	T_2^{-+}	1.360(8)	1.356(9)
	1.460(9)	1.447(8)		1.727(15)	1.714(17)
	1.670(15)	1.648(18)		1.881(20)	1.900(24)
	1.692(14)	1.691(17)			
A_1^{+-}	2.10(7)	2.10(8)	A_1^{--}	2.10(7)	2.10(8)
	2.33(9)	2.41(12)		2.41(12)	2.40(13)
A_2^{+-}	1.557(18)	1.577(21)	A_2^{--}	2.00(5)	2.06(7)
	1.852(29)	1.754(26)		2.15(8)	2.25(9)
	2.13(6)	2.27(10)			
E^{+-}	1.980(35)	1.981(33)	E^{--}	1.690(18)	1.686(21)
	2.155(48)	2.119(41)		2.072(39)	1.998(42)
	2.198(54)	2.087(50)		2.198(57)	2.204(66)
T_1^{+-}	1.266(5)	1.271(6)	T_1^{--}	1.738(18)	1.734(18)
	1.542(9)	1.557(10)		1.973(29)	1.920(26)
	1.656(13)	1.648(11)		2.088(32)	2.001(31)
	1.859(18)	1.860(19)			
T_2^{+-}	1.571(11)	1.543(11)	T_2^{--}	1.721(15)	1.715(21)
	1.880(19)	1.881(20)		1.888(23)	1.889(28)
	1.900(20)	1.915(27)		2.043(27)	2.006(26)
	1.996(34)	1.994(30)			
$l_{k=1}$	0.5963(11)	0.5932(14)	$l_{k=2}$	1.1204(33)	1.1235(28)
	1.2954(33)	1.2918(42)		1.3876(57)	1.3810(64)

Table 9. Comparison of glueball and flux tube energies obtained on fields with topological charge $Q = 0$ against fields with a 'normal' distribution of Q. In SU(8) on a $14^3 20$ lattice at $\beta = 45.50$. Energies extracted from best (variationally selected) correlators between $t = a$ and $t = 2a$. Glueballs labelled by representation of cubic rotation symmetry R, parity P and charge conjugation C. Flux tubes are fundamental, $l_{k=1}$, and $k = 2$, $l_{k=2}$.

SU(2) $\beta = 2.427$		SU(3) $\beta = 6.235$		SU(6) $\beta = 25.35$	
l	$a\sqrt{\sigma}$	l	$a\sqrt{\sigma}$	l	$a\sqrt{\sigma}$
12	0.2380(3)	18	0.1491(5)	12	0.2196(5)
14	0.2387(4)	26	0.1499(4)	14	0.2200(7)
16	0.2390(8)	34	0.1506(6)	18	0.2181(17)
20	0.2399(10)				
24	0.2396(16)				
SU(4) $\beta = 11.02$		SU(4) $\beta = 11.60$		SU(8) $\beta = 45.50$	
l	$a\sqrt{\sigma}$	l	$a\sqrt{\sigma}$	l	$a\sqrt{\sigma}$
18	0.2143(3)	24	0.1301(5)	12	0.2187(4)
22	0.2142(6)	30	0.1307(3)	14	0.2189(4)
SU(10) $\beta = 71.38$		SU(12) $\beta = 103.03$			
l	$a\sqrt{\sigma}$	l	$a\sqrt{\sigma}$		
12	0.2199(4)	12	0.2198(2)		
14	0.2195(5)	14	0.2202(7)		

Table 10. String tensions obtained using eq. (3.3), for (fundamental) flux tubes of length l for various groups. A test of finite volume corrections.

SU(4) $\beta = 11.02$		SU(4) $\beta = 11.60$		SU(6) $\beta = 25.35$	
l	$a\sqrt{\sigma_{k=2}}$	l	$a\sqrt{\sigma_{k=2}}$	l	$a\sqrt{\sigma_{k=2}}$
18	0.2490(12)	24	0.1523(5)	12	0.2779(9)
22	0.2480(24)	30	0.1534(5)	14	0.2846(6)
				18	0.2841(8)
SU(8) $\beta = 45.50$		SU(10) $\beta = 71.38$		SU(12) $\beta = 103.03$	
l	$a\sqrt{\sigma_{k=2}}$	l	$a\sqrt{\sigma_{k=2}}$	l	$a\sqrt{\sigma_{k=2}}$
12	0.2833(9)	12	0.2901(10)	12	0.2925(11)
14	0.2885(24)	14	0.2946(22)	14	0.2987(23)

Table 11. String tensions obtained using eq. (3.3) for $k = 2$ flux tubes of length l for various groups. Testing finite volume corrections.

SU(2)				
β	lattice	$\frac{1}{2}\mathrm{ReTr}\langle U_p\rangle$	aE_f	$a\sqrt{\sigma}$
2.2986	$8^3 16$	0.6018323(78)	0.9310(55)	0.36590(93)
2.3714	$10^3 16$	0.6227129(41)	0.7159(41)	0.28779(71)
2.427	$12^3 16$	0.6364295(26)	0.5831(32)	0.23750(56)
2.452	$14^3 20$	0.6420346(28)	0.5852(51)	0.21791(83)
2.509	$16^3 20$	0.6537206(12)	0.4399(15)	0.17857(26)
2.60	$22^3 30$	0.6700085(8)	0.3370(17)	0.13279(29)
2.65	$26^3 34$	0.6780431(5)	0.2914(15)	0.11342(26)
2.70	$28^3 40$	0.6855710(4)	0.2228(13)	0.09698(24)
2.75	$34^3 46$	0.6926656(2)	0.2048(16)	0.08375(21)
2.80	$40^3 54$	0.6993804(2)	0.1817(16)	0.07242(28)

Table 12. Energies of periodic flux tubes of length l in SU(2) and derived string tensions at the couplings $\beta = 4/g^2$ on the lattices $l^3 l_t$.

SU(3)				
β	lattice	$\frac{1}{3}\mathrm{ReTr}\langle U_p\rangle$	aE_f	$a\sqrt{\sigma}$
5.6924	$8^3 16$	0.547503(7)	1.1588(37)	0.4010(23)
5.80	$10^3 16$	0.567642(5)	0.8862(26)	0.31603(84)
5.8941	$12^3 16$	0.581069(4)	0.7298(47)	0.2613(14)
5.99	$14^3 20$	0.5925655(13)	0.5984(26)	0.21959(76)
6.0625	$14^3 20$	0.6003331(21)	0.4517(25)	0.19509(65)
6.235	$18^3 26$	0.6167715(13)	0.3369(26)	0.14899(59)
6.338	$22^3 30$	0.6255948(8)	0.3182(19)	0.12948(44)
6.50	$26^3 38$	0.6383532(5)	0.2334(17)	0.10319(41)
6.60	$32^3 40$	0.64566194(21)	0.2255(15)	0.09024(26)
6.70	$36^3 44$	0.65260033(18)	0.1933(16)	0.07898(28)

Table 13. Energies of periodic flux tubes of length l in SU(3) and derived string tensions at the couplings $\beta = 6/g^2$ on the lattices $l^3 l_t$.

continuum $k = 2$ string tensions			
group	σ_k/σ_f:NG	σ_k/σ_f:$l \to \infty$	Casimir scaling
SU(4)	1.381(14)	1.381(14)	1.333
SU(5)	1.551(11)	1.551(11)	1.500
SU(6)	1.654(13)	1.654(13)	1.600
SU(8)	1.731(11)	1.794(28)	1.714
SU(10)	1.733(15)	1.796(29)	1.778
SU(12)	1.792(16)	1.857(29)	1.818

Table 14. Ratio of the $k = 2$ string tension to the fundamental for various SU(N) gauge theories. Values labelled NG are obtained using eq. (3.3). Values labelled $l \to \infty$ denote our best estimates in that limit. The values corresponding to 'Casimir scaling' are shown for comparison.

N	$a\sqrt{\sigma} \in$	$\sqrt{\sigma}/\Lambda_I^{3\text{loop}}$	χ^2/n_{df}	$\sqrt{\sigma}/\Lambda_I^{2\text{loop}}$	$\Lambda_{\overline{MS}}^{3\text{loop}}/\sqrt{\sigma}$
2	[0.133,0.072]	4.535(16)	0.42	4.914(16)	0.5806(21)[570]
3	[0.195,0.079]	4.855(11)	1.40	5.210(20)	0.5424(13)[185]
4	[0.254,0.131]	5.043(10)	0.48	5.532(11)	0.5222(11)[230]
5	[0.255,0.131]	5.090(14)	0.31	5.622(15)	0.5174(15)[245]
6	[0.252,0.129]	5.105(11)	1.62	5.664(48)*	0.5158(11)[250]
8	[0.258,0.133]	5.148(17)	0.13	5.727(20)	0.5115(17)[250]
10	[0.260,0.164]	5.221(40)*	3.30	5.845(44)*	0.5044(20)[270]
12	[0.262,0.162]	5.193(13)	0.45	5.823(15)	0.5071(13)[270]

Table 15. Results for Λ_I in units of the string tension using the exact 3-loop β-function, with the 2-loop result for comparison. Poor fits denoted by $*$. Resulting $\Lambda_{\overline{MS}}$ is shown with statistical errors and an estimate of the (correlated) systematic error in square brackets.

N	c_0	c_σ	$a\sqrt{\sigma} \in$	$\beta \in$	χ^2/n_{df}	n_{df}
2	4.510(15)	4.98(25)	[0.133,0.072]	[2.60,2.80]	0.40	3
3	4.827(12)	2.48(11)	[0.195,0.079]	[5.99,6.70]	1.29	4
4	5.017(8)	1.622(40)	[0.302,0.131]	[10.70,11.60]	0.98	4
5	5.068(11)	1.435(56)	[0.303,0.131]	[16.98,18.375]	0.38	4
6	5.064(12)	1.541(68)	[0.252,0.129]	[25.05,26.71]	1.45	3
8	5.143(9)	1.265(34)	[0.326,0.133]	[44.10,47.75]	1.75	4
10	5.176(10)	1.285(35)	[0.260,0.164]	[70.38,73.35]	3.06	2
12	5.148(12)	1.387(43)	[0.262,0.162]	[101.55,105.95]	0.41	2

Table 16. Fitted values of the coefficients c_0 and c_σ that determine the interpolation function in eq. (4.12) for each of our SU(N) lattice gauge theories. In each case the range in $a\sqrt{\sigma}$ and of β of the fit is shown as is the χ^2 per degree of freedom and the number of degrees of freedom.

$aE_{\text{eff}}(t = 2a)$: SU(2) at $\beta = 2.427$			
R^P	$12^3 16$	$14^3 16$	$20^3 16$
A_1^+	0.840(11)	0.854(8)	0.847(8)
	1.225(26)		
	1.418(17)	1.367(15)	1.408(19)
		1.593(27)	
	1.611(36)	1.721(51)	1.780(45)
	1.871(40)	1.839(46)	1.872(46)
A_2^+	1.680(40)	1.805(38)	1.942(72)
E^+	1.220(9)	1.254(14)	1.284(13)
	1.317(17)		
		1.549(20)	
	1.632(30)	1.672(33)	1.672(40)
	1.774(31)	1.820(39)	1.832(42)
T_1^+	1.925(42)	1.875(27)	1.855(37)
	1.977(48)	1.972(34)	1.916(50)
T_2^+	1.297(12)	1.278(14)	1.289(11)
	1.739(20)	1.701(30)	1.672(21)
	1.774(34)	1.849(22)	1.877(30)
A_1^-	1.471(30)	1.540(30)	1.526(36)
	1.71(4)	1.87(9)	1.94(9)
A_2^-	2.31(16)	2.21(17)	2.04(12)
E^-	1.585(31)	1.680(28)	1.652(34)
	2.00(6)	2.04(7)	2.02(7)
T_1^-	2.18(6)	2.15(6)	2.09(7)
T_2^-	1.665(25)	1.632(33)	1.620(21)
	2.04(5)	2.00(4)	2.01(6)
$l_{k=1}$	0.5804(38)	0.7140(41)	1.0996(39)
	1.367(23)	1.428(32)	1.677(9)

Table 17. Comparison of glueball effective energies from $t = 2a$ and flux tube energies ($l1$) obtained on $12^3 16$, $14^3 16$ and $20^3 16$ lattices at $\beta = 2.427$ in SU(2). Unmatched states are ditorelons. Glueballs labelled by representation of cubic rotation symmetry R and parity P. Fundamental flux tube energies, $l_{k=1}$, are ground and first excited states.

$aE_{\text{eff}}(t = 2a)$: SU(12) at $\beta = 103.03$					
R^{PC}	$12^3 20$	$14^3 20$	R^{PC}	$12^3 20$	$14^3 20$
A_1^{++}	0.6434(32)	0.6499(50)	A_1^{-+}	1.079(8)	1.097(12)
	1.190(9)	1.200(14)		1.567(22)	1.591(33)
	1.495(19)	1.579(25)		1.859(38)	2.037(91)
	1.604(26)	1.585(33)			
	1.660(26)	1.687(43)			
A_2^{++}	1.629(30)	1.639(39)	A_2^{-+}	2.14(10)	2.21(11)
	1.91(5)	2.11(10)		2.20(9)	2.30(13)
E^{++}	1.021(5)	1.026(7)	E^{-+}	1.346(10)	1.355(15)
	1.429(14)	1.464(16)		1.723(21)	1.747(32)
	1.610(19)	1.632(28)		2.105(33)	2.178(74)
T_1^{++}	1.635(17)	1.692(21)	T_1^{-+}	1.865(21)	1.885(39)
	1.712(19)	1.776(26)		1.945(30)	1.930(36)
	2.090(32)	2.062(47)		2.012(28)	2.026(49)
T_2^{++}	1.040(4)	1.031(7)	T_2^{-+}	1.357(8)	1.366(12)
	1.465(9)	1.473(16)		1.730(16)	1.748(23)
	1.597(14)	1.659(21)		1.891(26)	1.905(44)
	1.652(14)	1.676(25)		1.932(29)	1.975(40)
A_1^{+-}	2.001(52)	2.06(11)	A_1^{--}	2.18(8)	2.09(11)
	2.12(8)	2.23(13)		2.23(10)	2.30(12)
A_2^{+-}	1.564(22)	1.603(30)	A_2^{--}	1.932(52)	2.026(70)
	1.823(36)	1.882(53)		2.209(85)	2.33(17)
	1.97(8)	2.19(10)			
E^{+-}	1.903(29)	2.011(43)	E^{--}	1.682(17)	1.677(30)
	2.140(51)	2.044(70)		2.053(44)	2.087(54)
				2.11(5)	2.26(9)
T_1^{+-}	1.269(6)	1.268(8)	T_1^{--}	1.696(18)	1.693(22)
	1.543(12)	1.546(16)		1.921(25)	1.897(44)
	1.678(16)	1.690(18)		1.976(33)	2.023(45)
	1.850(21)	1.880(27)		2.21(6)	2.18(6)
T_2^{+-}	1.534(13)	1.541(15)	T_2^{--}	1.719(20)	1.766(27)
	1.878(24)	1.870(27)		1.893(29)	1.935(31)
	1.850(22)	1.896(36)		2.014(32)	2.035(37)
	1.988(32)	1.987(43)		2.19(5)	2.19(6)
$l_{k=1}$	0.4812(13)	0.5993(40)	$l_{k=2}$	0.935(8)	1.172(18)

Table 18. Comparison of glueball effective energies from $t = 2a$ and flux tube energies ($l1,l2$) obtained on $12^3 20$ and $14^3 20$ lattices at $\beta = 103.03$ in SU(12). Glueballs labelled by representation of cubic rotation symmetry R, parity P and charge conjugation C. Flux tube energies are fundamental, $l_{k=1}$, and $k = 2$, $l_{k=2}$.

$aE_{\text{eff}}(t=2a)$: SU(12) at $\beta = 103.03$				
R^{PC}	$12^3 20$		$14^3 20$	
	$bl = 1-4$	$bl = 1-5$	$bl = 1-4$	$bl = 1-5$
A_1^{++}	0.6434(32)	0.6432(32)	0.6499(50)	0.6497(50)
		1.172(10)		
	1.190(9)	1.179(14)	1.200(14)	1.200(14)
				1.424(23)
	1.462(20)	1.495(19)	1.588(23)	1.433(29)
	1.604(26)	1.601(29)	1.585(33)	1.571(35)
	1.660(26)	1.666(30)	1.687(43)	1.659(40)
	1.753(25)	1.780(31)	1.786(54)	1.780(52)
E^{++}	1.021(5)	1.019(5)	1.026(7)	1.026(7)
	1.525(13)[1.01(14)]	1.118(7)		
				1.273(20)
	1.429(14)	1,373(12)	1.464(16)	1.446(16)
	1.610(19)	1.610(18)	1.635(29)	1.632(28)
	1.657(19)	1.650(18)	1.663(24)	1.666(25)

Table 19. Comparison of A_1^{++} and E^{++} glueball effective energies from $t = 2a$ obtained on $12^3 20$ and $14^3 20$ lattices at $\beta = 103.03$ in SU(12). Using operators up to blocking levels 4 and 5 respectively, as shown.

number of operators: $N \in [4, 12]$				
R	P=+,C=+	P=-,C=+	P=+,C=-	P=-,C=-
A_1	12	7	6	8
A_2	7	5	7	7
E	36	24	24	30
T_1	48	54	66	51
T_2	60	60	60	54
number of operators: $N = 2, 3$				
R	P=+,C=+	P=-,C=+	P=+,C=-	P=-,C=-
A_1	27	9	8	11
A_2	14	6	13	11
E	80	30	40	44
T_1	78	84(75)	132	81
T_2	108	96(87)	108	84

Table 20. Number of operators in rotational representation, R, with parity, P, and charge conjugation, C, as used in our various SU(N) calculations, at each blocking level. Some numbers for SU(2) differ from SU(3) and are in brackets; also no $C = -$ for SU(2).

operator loops	
loop	R^{PC}
{2,3,-2,-3}	A_1^{++}, E^{++}
	T_1^{+-}
{1,2,2,-1,-2,-2}	$A_1^{++}, A_2^{++}, E^{++}$
	T_1^{+-}, T_2^{+-}
{1,2,3,-1,-2,-3}	A_1^{++}, T_2^{++}
	A_2^{+-}, T_1^{+-}
{1,3,2,-3,-1,-2}	$A_1^{++}, E^{++}, T_2^{++}, T_1^{-+}, T_2^{-+}$
	$T_1^{+-}, T_2^{+-}, A_1^{--}, E^{--}, T_2^{--}$
{1,2,2,-1,3,-2,-3,-2}	$A_1^{++}, A_2^{++}, E^{++}, T_1^{++}, T_2^{++}, A_1^{-+}, A_2^{-+}, E^{-+}, T_1^{-+}, T_2^{-+}$
	$A_1^{+-}, A_2^{+-}, E^{+-}, T_1^{+-}, T_2^{+-}, A_1^{--}, A_2^{--}, E^{--}, T_1^{--}, T_2^{--}$
{1,3,-1,-3,-1,-2,1,2}	$A_1^{++}, E^{++}, T_1^{++}, T_2^{++}, A_1^{-+}, E^{-+}, T_1^{-+}, T_2^{-+}$
	$A_1^{+-}, E^{+-}, T_1^{+-}, T_2^{+-}, A_1^{--}, E^{--}, T_1^{--}, T_2^{--}$
{1,2,3,-1,-3,-3,-2,3}	$A_1^{++}, E^{++}, T_1^{++}, T_2^{++}, A_1^{-+}, E^{-+}, T_1^{-+}, T_2^{-+}$
	$A_2^{+-}, E^{+-}, T_1^{+-}, T_2^{+-}, A_2^{--}, E^{--}, T_1^{--}, T_2^{--}$
{1,3,1,2,-3,-1,-1,-2}	$A_1^{++}, A_2^{++}, E^{++}, T_1^{++}, T_2^{++}, A_1^{-+}, A_2^{-+}, E^{-+}, T_1^{-+}, T_2^{-+}$
	$A_1^{+-}, A_2^{+-}, E^{+-}, T_1^{+-}, T_2^{+-}, A_1^{--}, A_2^{--}, E^{--}, T_1^{--}, T_2^{--}$
{1,2,2,2,-1,3,-2,-3,-2,-2}	$A_1^{++}, A_2^{++}, E^{++}, T_1^{++}, T_2^{++}, A_1^{-+}, A_2^{-+}, E^{-+}, T_1^{-+}, T_2^{-+}$
	$A_1^{+-}, A_2^{+-}, E^{+-}, T_1^{+-}, T_2^{+-}, A_1^{--}, A_2^{--}, E^{--}, T_1^{--}, T_2^{--}$
{1,2,2,2,-1,-2,3,-2,-3,-2}	$A_1^{++}, A_2^{++}, E^{++}, T_1^{++}, T_2^{++}, T_1^{-+}, T_2^{-+}$
	$T_1^{+-}, T_2^{+-}, A_1^{--}, A_2^{--}, E^{--}, T_1^{--}, T_2^{--}$
{-3,1,3,1,2,-3,-1,3,-1,-2}	$A_1^{++}, A_2^{++}, E^{++}, T_1^{++}, T_2^{++}, A_1^{-+}, A_2^{-+}, E^{-+}, T_1^{-+}, T_2^{-+}$
	$A_1^{+-}, A_2^{+-}, E^{+-}, T_1^{+-}, T_2^{+-}, A_1^{--}, A_2^{--}, E^{--}, T_1^{--}, T_2^{--}$
{-3,1,3,1,2,3,-1,-3,-2,-1}	$A_1^{++}, A_2^{++}, E^{++}, T_1^{++}, T_2^{++}, A_1^{-+}, A_2^{-+}, E^{-+}, T_1^{-+}, T_2^{-+}$
	$A_1^{+-}, A_2^{+-}, E^{+-}, T_1^{+-}, T_2^{+-}, A_1^{--}, A_2^{--}, E^{--}, T_1^{--}, T_2^{--}$

Table 21. The 12 loops used as the basis of our glueball calculations for $N \geq 4$. These generate contributions to the representations as shown.

	SU(8) : aM_G					
R^{PC}	$\beta = 44.10$	$\beta = 44.85$	$\beta = 45.50$	$\beta = 46.10$	$\beta = 46.70$	$\beta = 47.75$
	$8^3 16$	$10^3 16$	$12^3 20$	$14^3 20$	$16^3 24$	$20^3 30$
A_1^{++}	0.8246(66)	0.7461(53)	0.6409(38)	0.5617(43)	0.4909(43)	0.4075(28)
	1.615(26)	1.191(50)	1.112(37)	1.081(22)	0.930(13)	0.755(10)
	2.01(6)	1.764(39)	1.42(9)	1.252(41)	1.146(27)	0.936(18)
A_2^{++}	2.42(11)	1.828(46)	1.615(25)	1.408(26)	1.180(27)	0.969(16)
E^{++}	1.504(13)	1.184(8)	1.0063(51)	0.8813(48)	0.7676(67)	0.6192(69)
	2.145(41)	1.689(18)	1.442(11)	1.299(34)	1.070(16)	0.831(8)
		1.855(28)	1.579(15)	1.393(13)	1.184(22)	0.954(11)
T_1^{++}	2.50(8)	1.970(29)	1.517(27)	1.397(40)	1.204(21)	0.982(7)
		1.932(29)	1.536(90)	1,392(43)	1.238(29)	0.996(10)
T_2^{++}	1.536(12)	1.191(22)	1.033(10)	0.8795(58)	0.7725(64)	0.6195(22)
	2.092(41)	1.689(15)	1.428(39)	1.188(21)	1.101(12)	0.870(16)
	2.41(8)	1.875(28)	1.621(76)	1.357(34)	1.162(14)	0.963(8)
		1.889(30)	1.52(8)	1.344(35)	1.201(18)	0.975(24)
A_1^{-+}	1.618(33)	1.256(13)	1.009(20)	0.902(17)	0.8021(95)	0.6365(81)
	2.21(10)	1.75(5)	1.42(8)	1.23(5)	1.074(82)	0.963(35)
A_2^{-+}		2.27(13)	2.07(6)	1.857(38)	1.588(32)	1.257(33)
E^{-+}	1.994(56)	1.573(17)	1.295(41)	1.131(21)	1.013(11)	0.8082(65)
	2.72(14)	2.019(54)	1.734(20)	1.498(14)	1.320(9)	1.101(15)
T_1^{-+}		2.29(15)	1.844(23)	1.571(65)	1.324(32)	1.108(11)
c			1.990(24)	1.639(12)	1.447(39)	1.142(18)
T_2^{-+}	1.959(26)	1.47(5)	1.271(24)	1.146(16)	0.982(10)	0.807(10)
	2.62(11)	2.043(43)	1.741(18)	1.506(11)	1.298(25)	1.065(11)
A_1^{+-}		2.47(16)	2.103(73)	1.831(40)	1.552(19)	1.209(32)
A_2^{+-}	2.25(10)	1.834(37)	1.529(18)	1.275(44)	1.176(26)	0.928(13)
E^{+-}		2.196(52)	1.921(33)	1.659(26)	1.463(38)	1.117(18)
T_1^{+-}	1.898(26)	1.510(12)	1.281(7)	1.102(6)	0.9556(82)	0.7706(46)
	2.23(6)	1.812(27)	1.539(13)	1.328(6)	1.1724(41)	0.9269(78)
		1.914(21)	1.648(14)	1.437(10)	1.221(16)	0.980(8)
T_2^{+-}	2.33(6)	1.781(21)	1.544(15)	1.294(30)	1.133(14)	0.922(7)
	2.53(12)	2.237(46)	1.811(22)	1.50(6)	1.327(32)	1.093(15)
	2.53(10)	2.265(50)	1.815(20)	1,618(18)	1.343(33)	1.119(13)
A_1^{--}		2.62(18)	2.05(7)	1.888(35)	1.633(23)	1.254(36)
A_2^{--}		2.22(10)	1.94(6)	1.74(17)	1.368(67)	1.114(24)
E^{--}	2.42(9)	2.012(40)	1.663(19)	1.441(11)	1.250(31)	1.009(14)
T_1^{--}	2.55(9)	1.906(30)	1.564(69)	1.414(42)	1.186(22)	0.974(29)
T_2^{--}	2.48(7)	1.981(32)	1.709(16)	1.473(10)	1.2920(56)	1.037(9)
		2.24(5)	1.896(22)	1.601(13)	1.4108(81)	1.109(14)
aE_f	0.7067(33)	0.5506(21)	0.4778(24)	0.4204(20)	0.3674(20)	0.2943(14)
$aE_{k=2}$	1.268(20)	0.9948(85)	0.8716(61)	0.7923(69)	0.6735(46)	0.5483(29)

Table 22. SU(8) lattice glueball masses for all R^{PC} representations, with the fundamental, aE_f, and $k = 2$, $aE_{k=2}$, flux tube energies.

SU(2): $M_G/\sqrt{\sigma}$ continuum limit		
R	P=+,C=+	P=-,C=+
A_1	3.781(23)	6.017(61)
	6.126(38)	8.00(15)
	7.54(10)	
A_2	7.77(18)	9.50(18)*
	8.56(21)	
E	5.343(30)	7.037(67)
	6.967(62)	8.574(83)
	7.722(82)	9.58(16)
T_1	8.14(10)	9.06(13)
	8.46(12)	9.40(13)
	9.67(9)	9.83(16)
T_2	5.353(23)	6.997(65)
	7.218(52)	8.468(86)
	8.23(10)	9.47(10)

Table 23. SU(2) continuum limit of glueball masses in units of the string tension, for all representations, R, of the rotation symmetry of a cube, for both values of parity, P. Ground states and some excited states. Stars indicate poor fits (see text).

SU(3): $M_G/\sqrt{\sigma}$ continuum limit				
R	P=+,C=+	P=−,C=+	P=+,C=−	P=−,C=−
A_1	3.405(21)	5.276(45)	9.32(28)	9.93(49)
	5.855(41)	7.29(13)		10.03(47)
	7.38(11)	9.18(26)		
	7.515(50)	9.37(22)		
A_2	7.705(85)	9.80(22)	7.384(90)	8.96(15)
	8.61(20)	11.17(30)	8.94(10)	10.21(20)
			8.90(21)	
E	4.904(20)	6.211(56)	8.77(12)	7.91(10)
	6.728(47)	8.23(9)	9.03(23)	9.39(18)
	7.49(9)	9.47(16)	10.39(21)	10.40(22)
	7.531(60)			
T_1	7.698(80)	8.48(12)	6.065(40)	8.31(10)
	7.72(11)	8.57(13)	7.21(8)	9.30(14)**
	9.31(11)*	8.66(15)	7.824(56)	9.72(15)
		9.56(28)	8.92(10)	
T_2	4.884(19)	6.393(45)	7.220(86)	8.198(80)
	6.814(31)	8.15(7)	8.72(11)	8.99(11)**
	7.716(70)**	9.23(12)*	9.060(80)	9.69(13)
	7.677(71)			

Table 24. SU(3) continuum limit of glueball masses in units of the string tension, for all representations, R, of the rotation symmetry of a cube, for both values of parity, P, and charge conjugation, C. Ground states and some excited states. Stars indicate poor fits (see text).

SU(4): $M_G/\sqrt{\sigma}$ continuum limit				
R	P=+,C=+	P=-,C=+	P=+,C=-	P=-,C=-
A_1	3.271(27)	5.020(46)	9.22(22)*	10.27(28)
	5.827(62)	7.33(11)	10.43(21)	9.95(29)
	7.50(11)	8.98(23)		
	7.73(8)			
A_2	7.32(12)	9.67(19)	6.87(26)	8.89(13)
	8.42(22)	10.69(45)*	8.66(16)	10.99(35)
			9.57(19)	
E	4.721(27)	6.130(52)	8.73(20)	7.80(11)
	6.702(45)	7.91(13)	9.28(19)	9.55(13)*
	7.271(86)	9.13(22)	9.58(20)	10.06(26)
	7.586(84)			
T_1	7.42(12)	8.47(11)	5.956(42)	7.603(84)
	7.50(9)	8.59(16)	7.11(8)	8.92(12)**
	9.10(18)	8.62(17)**	7.508(74)	9.86(22)
	9.54(23)		8.91(13)	
T_2	4.750(16)	6.203(33)	7.010(68)	7.787(96)
	6.687(51)	8.05(10)**	8.53(11)	8.42(14)
	7.411(81)	8.25(16)	8.86(8)	9.80(17)
	7.492(68)		8.94(20)	

Table 25. SU(4) continuum limit of glueball masses in units of the string tension, for all representations, R, of the rotation symmetry of a cube, for both values of parity, P, and charge conjugation, C. Ground states and some excited states. Stars indicate poor fits (see text).

SU(5): $M_G/\sqrt{\sigma}$ continuum limit				
R	P=+,C=+	P=-,C=+	P=+,C=-	P=-,C=-
A_1	3.156(31)	4.832(40)	9.04(22)	10.36(18)
	5.689(53)	7.38(11)	9.48(30)	9.70(36)
	7.36(14)	8.03(30)*		
	7.53(14)			
A_2	7.31(14)	9.80(20)	7.333(59)	8.05(23)
	8.85(32)	9.93(57)	8.75(19)	11.03(37)
E	4.692(22)	6.152(60)	8.54(19)	8.000(51)
	6.590(62)	8.19(23)	9.45(18)	9.02(22)
	7.31(10)	9.51(17)	9.53(20)	10.22(13)**
	7.28(10)			
T_1	7.396(73)	8.29(13)	5.915(45)	7.62(15)
	7.19(12)	8.56(15)	7.018(62)	8.53(17)**
	8.99(22)	8.59(16)	7.624(74)	9.91(26)
			8.36(14)	
T_2	4.686(30)	6.208(47)	7.051(72)	7.87(11)
	6.621(55)	7.97(11)	8.28(15)*	8.52(9)
	7.338(84)	8.45(16)	8.44(16)	10.17(9)*
	7.53(10)		9.18(13)	

Table 26. SU(5) continuum limit of glueball masses in units of the string tension, for all representations, R, of the rotation symmetry of a cube, for both values of parity, P, and charge conjugation, C. Ground states and some excited states. Stars indicate poor fits (see text).

SU(6): $M_G/\sqrt{\sigma}$ continuum limit				
R	P=+,C=+	P=-,C=+	P=+,C=-	P=-,C=-
A_1	3.102(32)	4.967(43)	9.37(22)	10.46(17)
	6.020(57)	7.14(13)	10.58(21)	10.53(20)**
	7.51(12)	8.72(31)		
	7.59(13)*			
A_2	7.46(13)	9.37(25)	7.169(96)	8.71(16)*
	9.58(24)**	10.48(43)	9.00(11)	10.87(38)
			9.12(20)	
E	4.706(30)	6.098(55)	8.80(11)	8.106(50)
	6.43(11)	7.93(15)	8.95(17)	9.48(33)
	7.06(13)	9.58(19)	9.34(19)	9.88(11)
	7.19(17)			
T_1	7.435(80)	8.405(88)	5.847(43)	7.41(13)
	7.57(10)	8.75(11)	7.066(80)	8.90(11)
	9.17(19)	9.23(11)*	7.552(85)	9.86(26)*
			8.46(11)	
T_2	4.649(28)	6.157(50)	6.997(80)	7.64(14)
	6.577(71)	7.92(14)	8.20(19)	8.51(9)
	7.189(72)	8.25(11)*	8.864(61)	10.20(9)
	7.02(10)*		9.15(11)	

Table 27. SU(6) continuum limit of glueball masses in units of the string tension, for all representations, R, of the rotation symmetry of a cube, for both values of parity, P, and charge conjugation, C. Ground states and some excited states. Stars indicate poor fits (see text).

SU(8): $M_G/\sqrt{\sigma}$ continuum limit			
R	P=+,C=+	P=-,C=+	P=+,C=-	P=-,C=-
A_1	3.099(26)	4.755(58)	8.97(31)	9.69(35)
	5.87(7)	6.90(24)	10.06(24)	9.50(39)
	7.18(13)	8.25(26)		
	7.61(7)			
A_2	7.28(14)	9.80(29)	7.00(12)	8.26(28)
	9.06(34)	11.28(25)	8.60(18)	11.40(23)
			8.87(48)	
E	4.658(32)	6.091(59)	8.53(19)	7.60(11)
	6.32(7)*	8.23(13)	8.94(24)**	9.18(25)
	7.26(11)	9.46(24)	8.81(35)	9.57(29)
T_1	7.318(74)	8.24(15)	5.801(38)	7.09(17)
	7.51(11)	8.60(27)	7.089(55)	8.35(18)
	9.21(22)	8.46(22)	7.43(9)*	9.60(25)
	9.21(25)		8.43(12)	
T_2	4.661(21)	5.995(61)	6.908(67)	7.863(66)
	6.599(84)	8.00(11)	8.01(16)	8.31(12)
	7.16(8)	8.38(16)	8.51(12)*	9.40(24)
	7.23(16)		8.92(15)	

Table 28. SU(8) continuum limit of glueball masses in units of the string tension, for all representations, R, of the rotation symmetry of a cube, for both values of parity, P, and charge conjugation, C. Ground states and some excited states. Stars indicate poor fits (see text).

SU(10): $M_G/\sqrt{\sigma}$ continuum limit				
R	P=+,C=+	P=-,C=+	P=+,C=-	P=-,C=-
A_1	3.102(37)	4.835(60)	8.92(37)	10.04(36)
	5.99(13)	7.03(14)	8.73(60)	9.79(55)
	7.15(17)	8.90(68)		
	7.87(13)			
A_2	7.20(18)	8.99(35)	6.78(15)	9.06(44)
	8.35(50)	11.74(70)	7.83(44)	10.70(70)
			8.29(103)?	
E	4.587(27)	6.12(10)	8.64(20)	7.60(14)
	6.49(9)	8.03(12)	9.04(30)	9.59(33)
	7.34(12)	9.36(46)	9.05(30)	9.92(22)
T_1	7.14(17)	8.49(28)	5.776(41)	7.27(17)
	7.84(27)	8.11(62)	7.039(62)	9.00(24)*
	9.32(18)**	9.53(100)*	7.79(13)	10.17(52)
	9.69(22)**		8.75(21)**	
T_2	4.600(30)	5.94(8)	7.071(55)	7.89(16)
	6.638(82)	7.52(17)	7.60(24)	7.82(26)*
	7.00(18)	7.88(30)**	8.60(13)	9.26(36)
	7.19(22)		8.77(28)	

Table 29. SU(10) continuum limit of glueball masses in units of the string tension, for all representations, R, of the rotation symmetry of a cube, for both values of parity, P, and charge conjugation, C. Ground states and some excited states. Stars indicate poor fits (see text).

SU(12): $M_G/\sqrt{\sigma}$ continuum limit				
R	P=+,C=+	P=−,C=+	P=+,C=−	P=−,C=−
A_1	3.151(33)	4.696(65)	9.63(25)	9.57(32)
	5.914(82)	6.94(19)	10.50(51)	9.90(58)
	7.07(18)	9.56(44)*		
	7.61(19)			
A_2	7.74(22)	10.16(26)	6.49(17)	9.03(22)
	9.64(26)	12.09(74)	8.90(22)	10.66(60)
			9.46(46)	
E	4.647(33)	6.22(10)	8.52(22)	7.80(14)
	6.613(80)	8.28(12)*	9.56(43)	9.88(20)
	7.67(13)			10.24(29)
T_1	6.64(27)	8.59(12)	5.741(60)	7.50(17)*
	7.59(21)	8.95(16)	7.005(78)	8.83(14)
	9.34(18)**	9.30(30)*	7.48(14)	9.51(48)
			8.80(23)	
T_2	4.645(33)	5.97(7)	6.88(10)	8.20(13)
	6.764(57)	8.05(15)	8.16(25)	8.27(31)*
	7.35(15)*	8.89(22)	8.48(25)	10.52(21)**
	7.20(19)		8.21(30)	

Table 30. SU(12) continuum limit of glueball masses in units of the string tension, for all representations, R, of the rotation symmetry of a cube, for both values of parity, P, and charge conjugation, C. Ground states and some excited states. Stars indicate poor fits (see text).

SU(∞): $M_G/\sqrt{\sigma}$			
R	P=+,C=+	P=-,C=+	P=+,C=-	P=-,C=-
A_1	3.072(14)	4.711(25)	9.26(16)	10.10(18)
	5.805(31)**	7.050(68)		10.14(23)
	7.294(63)			
A_2	7.40(12)†	9.73(12)	7.142(75)†*	8.61(13)*
	9.14(14)*	11.12(24)	8.77(10)	11.38(21)
E	4.582(14)	6.108(44)	8.63(10)	7.951(53)**
	6.494(33)*	8.051(60)	9.14(15)	9.55(13)
	7.266(50)*			9.84(12)
T_1	7.250(47)	8.412(76)	5.760(25)	7.134(86)
	7.337(60)*	8.79(10)	7.020(39)	8.65(9)
	9.142(82)	9.08(12)**	7.470(55)	9.81(17)
			8.422(84)	
T_2	4.578(11)	5.965(28)	6.957(41)	7.96(8)†
	6.579(30)	7.883(57)	7.93(11)	8.22(8)
	7.121(45)	8.45(14)†	8.63(7)$\star$	10.26(10)**
	7.122(76)			

Table 31. Continuum glueball masses in units of the string tension, in the limit $N \to \infty$. Fits are to $N \geq 2$ or $N \geq 3$ except for values labelled with a $\dagger$, and $\star$ indicates a poor fit, as explained in the text. Labels are R for the representations of the rotation symmetry of a cube, P for parity and C for charge conjugation.

continuum $J \sim$ cubic R		
J		cubic R
0	$\sim$	A_1
1	$\sim$	T_1
2	$\sim$	$E + T_2$
3	$\sim$	$A_2 + T_1 + T_2$
4	$\sim$	$A_1 + E + T_1 + T_2$
5	$\sim$	$E + 2T_1 + T_2$
6	$\sim$	$A_1 + A_2 + E + T_1 + 2T_2$
7	$\sim$	$A_2 + E + 2T_1 + 2T_2$
8	$\sim$	$A_1 + 2E + 2T_1 + 2T_2$

Table 32. Projection of continuum spin J states onto the cubic representations R.

continuum J^{PC} from cubic R		
J^{PC}		cubic R^{PC}
0^{++}gs	$\sim$	A_1^{++}gs
0^{++}ex1	$\sim$	A_1^{++}ex1
2^{++}gs	$\sim$	E^{++}gs $+ T_2^{++}$gs
2^{++}ex1	$\sim$	E^{++}ex1 $+ T_2^{++}$ex1
3^{++}gs	$\sim^*$	A_2^{++}gs $+ T_1^{++}$gs(ex1) $+ T_2^{++}$ex3(ex2)
4^{++}gs	$\sim^*$	A_1^{++}ex2 $+ E^{++}$ex2 $+T_1^{++}$ex1(gs) $+ T_2^{++}$ex2(ex3)
0^{-+}gs	$\sim$	A_1^{-+}gs
0^{-+}ex1	$\sim$	A_1^{-+}ex1
2^{-+}gs	$\sim$	E^{-+}gs $+ T_2^{-+}$gs
2^{-+}ex1	$\sim$	E^{-+}ex1 $+ T_2^{-+}$ex1
1^{-+}gs	$\sim$	T_1^{-+}gs
2^{+-}gs	$\sim$	E^{+-}gs $+ T_2^{+-}$ex2
1^{+-}gs	$\sim$	T_1^{+-}gs
1^{+-}ex1	$\sim$	T_1^{+-}ex2
3^{+-}gs	$\sim$	A_2^{+-}gs $+ T_1^{+-}$ex1 $+ T_2^{+-}$gs
2^{--}gs	$\sim$	E^{--}gs $+ T_2^{--}$gs
1^{--}gs	$\sim$	T_1^{--}gs

Table 33. Identification of continuum J^{PC} states from the results for the cubic representations in tables 23–31. Ground state denoted by *gs*, *i*'th excited state by *exi*. Where there is some ambiguity, a single star denotes 'likely' while two stars indicate 'significant uncertainty'.

$M(J^{PC})/\sqrt{\sigma}$ continuum limit				
J^{PC}	SU(2)	SU(3)	SU(4)	SU(5)
0^{++} gs	3.781(23)	3.405(21)	3.271(27)	3.156(31)
0^{++} ex1	6.126(38)	5.855(41)	5.827(62)	5.689(53)
2^{++} gs	5.349(20)	4.894(22)	4.742(15)	4.690(20)
2^{++} ex1	7.22(6)$^+$	6.788(40)	6.694(40)	6.607(45)
3^{++} gs	8.13(8)*	7.71(9)*		7.29(9)
4^{++} gs		7.60(12)*	7.36(9)*	7.41(10)
0^{-+} gs	6.017(61)	5.276(45)	5.020(46)	4.832(40)
0^{-+} ex1	8.00(15)	7.29(13)	7.33(11)	7.38(11)
2^{-+} gs	7.017(50)	6.32(9)	6.182(33)	6.187(50)
2^{-+} ex1	8.521(65)	8.18(8)	7.91(13)*	8.02(11)
1^{-+} gs	9.06(13)	8.48(12)	8.47(11)	8.29(13)
2^{+-} gs		8.91(15)	8.84(11)	8.49(15)
1^{+-} gs		6.065(40)	5.956(42)	5.915(45)
1^{+-} ex1		7.82(6)	7.51(8)	7.62(8)
3^{+-} gs		7.27(12)	7.03(7)	7.13(7)
2^{--} gs		8.08(15)	7.79(9)	7.97(6)
1^{--} gs		8.31(10)	7.60(9)	7.62(15)

Table 34. Continuum limit of glueball masses, in units of the string tension, for those J^{PC} representations we can identify. Ground state denoted by *gs*, *i*'th excited state by *exi*. Stars explained in text.

$M(J^{PC})/\sqrt{\sigma}$ continuum limit				
J^{PC}	SU(6)	SU(8)	SU(10)	SU(12)
0^{++} gs	3.102(32)	3.099(26)	3.102(37)	3.151(33)
0^{++} ex1	6.020(57)	5.87(7)	5.99(13)	5.914(82)
2^{++} gs	4.678(30)	4.660(20)	4.594(25)	4.646(30)
2^{++} ex1	6.54(7)	6.60(9)*	6.57(9)	6.71(6)
3^{++} gs	7.44(8)*	7.34(11)*	7.14(18)	
4^{++} gs		7.20(7)*	7.32(15)	
0^{-+} gs	4.967(43)	4.755(58)	4.835(60)	4.696(65)
0^{-+} ex1	7.14(13)	6.90(24)	7.03(14)	6.94(19)
2^{-+} gs	6.148(50)	6.043(55)	6.01(8)	6.05(7)
2^{-+} ex1	7.92(14)	8.10(11)	7.86(12)*	8.16(15)
1^{-+} gs	8.41(9)	8.24(15)	8.49(28)	8.59(12)
2^{+-} gs	8.83(9)	8.52(12)	8.62(12)	8.50(17)
1^{+-} gs	5.847(43)	5.801(38)	5.776(41)	5.741(60)
1^{+-} ex1	7.55(9)	7.43(9)*	7.79(13)	7.48(14)
3^{+-} gs	7.067(70)	6.999(70)	7.035(50)	6.89(10)
2^{--} gs	8.05(5)*	7.78(7)	7.74(15)	8.00(15)
1^{--} gs	7.41(13)	7.09(17)	7.27(17)	7.50(17)

Table 35. Continuum limit of glueball masses, in units of the string tension, for those J^{PC} representations we can identify. Ground state denoted by *gs*, *i*'th excited state by *exi*. Stars explained in text.

$M(J^{PC})/\sqrt{\sigma}$ lower bounds					
1^{++}	3^{-+}	0^{+-}	2^{+-}	0^{--}	3^{--}
≥ 9.0	≥ 9.7	≥ 9.2	≥ 8.6	≥ 10.0	≥ 8.6

Table 36. Lower bounds on masses of some of the low-J ground states not appearing in tables 34, 35.

$M_G\,GeV$ SU(3)				
J	P=+,C=+	P=-,C=+	P=+,C=-	P=-,C=-
0 gs	1.653(26)	2.561(40)	$\geq 4.52(15)$	$\geq 4.81(24)$
0 ex1	2.842(40)	3.54(8)		
2 gs	2.376(32)	3.07(6)	4.24(8)*	3.92(9)
2 ex1	3.30(5)	3.97(7)	$\geq 4.38(13)$	$\geq 4.55(11)$
1 gs	$\geq 4.52(6)$	4.12(8)	2.944(42)	4.03(7)
1 ex1		4.16(8)*	3.80(6)	$\geq 4.51(9)$
1 ex2		4.20(9)*		
3 gs	3.74(7)*	$\geq 4.75(13)$	3.53(8)	$\geq 4.35(9)$
4 gs	3.69(8)*	$\geq 4.45(14)$	4.38(8)**	$\geq 4.81(24)$

Table 37. Continuum limit of SU(3) glueball masses, in physical GeV units for those J^{PC} representations we can identify, with lower bounds in those cases where this is not possible. Ground state denoted by gs, first excited state by ex. Stars denote ambiguity.

$M_J/\sqrt{\sigma}$; SU(∞)				
J	P=+,C=+	P=-,C=+	P=+,C=-	P=-,C=-
0 gs	3.072(14)	4.711(26)	$\geq 9.26(16)$	$\geq 10.10(18)$
0 ex	5.845(50)	7.050(68)		
2 gs	4.599(14)	6.031(38)	8.566(76)	7.910(56)
2 ex	6.582(36)	7.936(54)	$\geq 9.14(15)$	$\geq 9.55(13)$
1 gs	$\geq 9.14(9)$	8.415(76)	5.760(25)	7.26(11)
1 ex			7.473(57)	$\geq 8.65(9)$
3 gs	7.263(56)	$\geq 9.73(12)$	6.988(41)	$\geq 8.61(13)$
4 gs	7.182(71)	$\geq 8.79(10)$	$\geq 9.26(16)$	$\geq 10.10(18)$

Table 38. Large N extrapolation of continuum glueball masses, in units of the string tension, for those J^{PC} representations we can identify, with lower bounds in those cases where this is not possible. Ground state denoted by gs, first excited state by ex.

$M/\sqrt{\sigma}$; continuum SU(3)							
paper	0^{++}	2^{++}	0^{-+}	2^{-+}	1^{+-}	3^{+-}	2^{--}
this work	3.405(21)	4.894(22)	5.276(45)	6.32(9)	6.065(40)	7.27(12)	8.08(15)
2005: ref. [9]	3.347(68)	4.891(65)	5.11(14)	6.32(11)	6.06(15)	7.43(20)	8.32(29)
2005: ref. [10]*	3.59(15)	5.03(11)	5.39(11)	6.40(14)	6.27(11)	7.58(12)	8.42(14)
2004: ref. [2]	3.55(7)	4.78(9)					
2001: ref. [1]	3.61(9)	5.13(22)					

Table 39. Some glueball masses in units of the string tension in the continuum limit of the SU(3) gauge theory: a comparison between this work and some earlier work. The starred calculation includes our tansformation of the units from the Sommer scale to the string tension.

$M/\sqrt{\sigma}$; continuum SU(8)							
paper	0^{++}	2^{++}	0^{-+}	2^{-+}	1^{+-}	3^{+-}	2^{--}
this work	3.099(26)	4.660(20)	4.755(58)	6.043(55)	5.801(38)	7.00(7)	7.78(7)
2005: ref. [9]	3.32(15)	4.65(19)	4.72(32)	5.67(40)	5.70(29)	7.74(79)	7.3(1.4)
2004: ref. [2]	3.55(12)	4.73(22)					

Table 40. Some glueball masses in units of the string tension in the continuum limit of the SU(8) gauge theory: a comparison between this work and some earlier work.

$Q_L(n_c)$: SU(8), $Q = 2$					
	$\beta = 45.50, 12^3 20$		$\beta = 46.70, 16^3 24$		$\beta = 47.75, 20^3 30$	
n_c	$\bar{Q}_L$	σ_{Q_L}	$\bar{Q}_L$	σ_{Q_L}	$\bar{Q}_L$	σ_{Q_L}
0	0.275(21)	0.836	0.333(23)	1.282	0.410(35)	1.956
1	1.199(6)	0.202	1.286(5)	0.265	1.345(7)	0.351
2	1.575(3)	0.070	1.631(2)	0.082	1.665(3)	0.103
3	1.699(2)	0.041	1.7465(7)	0.044	1.7743(9)	0.053
4	1.7576(7)	0.030	1.8005(6)	0.030	1.8254(6)	0.035
8	1.8437(3)	0.016	1.8781(3)	0.014	1.8970(2)	0.014
12	1.8744(3)	0.013	1.9046(2)	0.010	1.9212(1)	0.009
16	1.8912(3)	0.011	1.9186(2)	0.008	1.9339(1)	0.007
20	1.9021(3)	0.010	1.9275(1)	0.007	1.9418(1)	0.006

Table 41. Lattice topological charge Q_L as function of number of cooling sweeps, n_c, for fields which have $Q_L \simeq 2$ after 20 cooling sweeps: the average value, with error, and standard deviation. For small, intermediate and large β, in SU(8), all with similar volumes in physical units.

topology tunnelling time					
β	τ_Q	$\tilde{\tau}_Q$	β	τ_Q	$\tilde{\tau}_Q$
SU(3)			SU(4)		
6.235	100(2)	112(2)	11.20	499(9)	520(9)
6.338	247(6)	283(6)	11.40	2173(42)	2275(45)
6.50	1056(44)	1236(50)	11.60	12674(636)	13371(690)
6.60	3399(188)	3731(190)			
6.70	7973(674)	8973(744)			
SU(5)			SU(6)		
17.22	189(4)	196(4)	25.05	1158(31)	1177(31)
17.43	695(13)	721(13)	25.32	5992(262)	6105(272)
17.63	2686(90)	2749(93)	25.55	$23.6(1.8) \times 10^3$	$24.4(1.8) \times 10^3$
18.04	$35.7(3.7) \times 10^3$	$37.0(3.7) \times 10^3$	26.22	$1.43(99) \times 10^6$	$1.43(99) \times 10^6$
18.375	$40(17) \times 10^4$	$44(19) \times 10^4$			
SU(8)					
44.10	514(10)	528(10)			
44.85	$26.3(3.5) \times 10^3$	$26.3(3.5) \times 10^3$			
45.50	$7.1(3.5) \times 10^5$	$7.1(3.5) \times 10^5$			
45.50	$12.5(5.1) \times 10^5$	$12.5(5.1) \times 10^5$			
SU(10)			SU(12)		
69.20	4793(211)	4831(214)	99.86	$4.83(58) \times 10^4$	$4.83(58) \times 10^4$

Table 42. Average number of sweeps, τ_Q, between $\Delta Q = \pm 1$ changes normalised to a standard space-time volume of $(3/\sqrt{\sigma})^4$, with $\tilde{\tau}_Q$ including a correction for 'near-dislocations'.

$\ln\{\tau_Q\} = b - c(N)\ln\{a\sqrt{\sigma}\}$		
N	c	$11N/3 - 5$
3	6.82(7)	6.0
4	9.27(12)	$9.6\dot{6}$
5	11.13(20)	$13.3\dot{3}$
6	13.50(30)	17.0
8	17.58(43)	$24.3\dot{3}$

Table 43. Fitted values of $c(N)$ from figure 27 compared to the asymptotic dilute gas prediction in eq. (6.5).

SU(2) topology			
β	lattice	$\langle Q_L^2 \rangle$	$\langle Q_I^2 \rangle$
2.2986	$8^3 16$	2.266(9)	3.057(12)
	$12^3 16$	7.694(42)	9.600(49)
2.3714	$10^3 16$	2.705(9)	3.544(12)
	$14^3 16$	7.343(61)	9.220(77)
2.427	$12^3 16$	2.824(7)	3.551(8)
	16^4	6.635(56)	8.066(64)
	$20^3 16$	13.09(19)	15.41(22)
	$24^3 16$	22.56(20)	26.18(23)
2.509	$16^3 20$	3.411(13)	4.067(16)
	$22^3 20$	8.822(58)	10.137(65)
2.60	$22^3 30$	4.491(31)	5.109(33)
	30^4	11.48(10)	12.65(12)
2.65	$26^3 34$	4.702(41)	5.268(45)
2.70	$28^3 40$	3.786(36)	4.181(39)
	40^4	11.07(14)	12.09(14)
2.75	$34^3 46$	4.328(88)	4.711(94)
2.80	$40^3 54$	4.43(12)	4.76(12)

Table 44. Average values of Q_L^2, after 20 cooling sweeps, in SU(2) for various values of β and lattice sizes. Q_I is the projection of Q_L to an integer value.

SU(3) topology				SU(4) topology			
β	lattice	$\langle Q_L^2 \rangle$	$\langle Q_I^2 \rangle$	β	lattice	$\langle Q_L^2 \rangle$	$\langle Q_I^2 \rangle$
5.6924	$8^3 16$	4.034(21)	5.452(29)	10.70	$12^3 16$	5.813(37)	7.084(48)
5.80	$10^3 16$	4.021(13)	5.111(16)	10.85	$14^3 20$	5.718(45)	6.674(53)
5.8941	$12^3 16$	3.570(35)	4.352(43)	11.02	$18^3 20$	6.010(95)	6.78(11)
5.99	$14^3 20$	3.790(48)	4.428(56)	11.20	22^4	5.97(33)	6.57(36)
6.0625	$14^3 20$	2.312(22)	2.649(26)	11.40	26^4	6.19(67)	6.68(73)
6.235	$18^3 26$	2.32(12)	2.55(13)	11.60	30^4	5.52(73)	5.80(78)
6.3380	$22^3 30$	2.72(13)	2.94(14)				
6.50	$26^3 38$	2.09(20)	2.23(21)				
6.60	$32^3 40$	2.60(35)	2.74(37)				
6.70	$36^3 44$	1.54(30)	1.61(31)				

Table 45. Average values of Q_L^2, after 20 cooling sweeps, in SU(3) and in SU(4) for the values of β and lattices shown. Q_I is the projection of Q_L to an integer value.

SU(5) topology				SU(6) topology			
β	lattice	$\langle Q_L^2 \rangle$	$\langle Q_I^2 \rangle$	β	lattice	$\langle Q_L^2 \rangle$	$\langle Q_I^2 \rangle$
16.98	$10^3 16$	3.273(25)	3.906(30)	24.67	$10^3 16$	3.178(45)	3.747(53)
17.22	$12^3 16$	2.682((60)	3.073(68)	25.05	$12^3 16$	2.50(13)	2.83(15)
17.43	$14^3 20$	2.95(13)	3.30(14)	25.32	$14^3 20$	2.76(32)	3.07(35)
17.63	$16^3 20$	2.86(31)	3.15(35)	25.35	$14^3 20$	2.91(60)	3.24(67)
18.04	$20^3 24$	3.44(1.27)	3.71(1.36)	25.35	$18^3 18$	5.83(78)	6.48(87)
18.375	$24^3 30$	2.21(86)	2.35(92)				

Table 46. Average values of Q_L^2, after 20 cooling sweeps, in SU(5) and in SU(6) for the values of β and lattices shown. Q_I is the projection of Q_L to an integer value.

continuum topological susceptibility						
group	$\chi_L^{1/4}/\sqrt{\sigma}$	$\beta \in$	χ^2/n_{df}	$\chi_I^{1/4}/\sqrt{\sigma}$	$\beta \in$	χ^2/n_{df}
SU(2)	0.4773(14)	[2.509,2.75]	0.46	0.4857(14)	[2.509,2.75]	0.55
SU(3)	0.4196(35)	[5.8941,6.60]	0.85	0.4246(36)	[5.8941,6.60]	0.89
SU(4)	0.3925(25)	[10.70,11.60]	0.19	0.3964(27)	[10.70,11.60]	0.26
SU(5)	0.3786(59)	[16.98,18.375]	0.44	0.3818(60)	[16.98,18.375]	0.45
SU(6)	0.386(13)	[24.67,25.35]	0.29	0.390(12)	[24.67,25.35]	0.30
SU(∞)	0.3655(27)		0.92	0.3681(28)		0.93

Table 47. Continuum limit of the topological susceptibility in units of the string tension for the gauge groups shown; χ_L is from Q_L^2 and χ_I is from Q_I^2. Fitted range of β also shown, as is the chi-squared per degree of freedom, χ^2/n_{df}.

$\langle Q_{\text{hot}} \rangle_{Q=Q_I} = Z_Q(\beta) Q_I$							
SU(2)		SU(3)		SU(4)		SU(5)	
β	$Z_Q(\beta)$	β	$Z_Q(\beta)$	β	$Z_Q(\beta)$	β	$Z_Q(\beta)$
2.452	0.1386(23)	5.6924	0.0646(9)	10.70	0.0948(14)	16.98	0.0992(15)
2.65	0.233(12)	5.80	0.0877(10)	10.85	0.1146(20)	17.22	0.1137(20)
2.70	0.239(17)	5.99	0.1306(26)	11.02	0.1347(35)	17.43	0.1348(26)
2.75	0.258(18)	6.0625	0.1462(31)	11.02	0.1397(29)	17.63	0.1476(31)
2.80	0.239(22)	6.235	0.1808(54)	11.20	0.1524(46)	18.04	0.1587(48)
		6.338	0.2044(65)	11.40	0.1710(66)	18.375	0.190(11)
		6.50	0.231(10)	11.60	0.184(10)		
		6.60	0.232(19)				
		6.70	0.241(28)				

Table 48. Multiplicative renormalisation factor, $Z_Q(\beta)$, relating the average lattice topological charge, Q_{hot}, calculated on the rough Monte Carlo fields, and the integer valued topological charge Q_I calculated after 20 'cooling' sweeps of those fields. For the gauge groups and β shown.

$\langle Q_{\text{hot}} \rangle_{Q=Q_I} = Z_Q(\beta) Q_I$							
SU(6)		SU(8)		SU(10)		SU(12)	
β	$Z_Q(\beta)$	β	$Z_Q(\beta)$	β	$Z_Q(\beta)$	β	$Z_Q(\beta)$
24.67	0.0976(20)	44.10	0.0912(19)	69.20	0.0930(19)	99.86	0.0899(17)
25.05	0.1132(29)	44.85	0.1194(31)	70.38	0.1165(27)	101.55	0.1129(26)
25.32	0.1316(40)	45.50	0.1254(35)	71.38	0.1283(37)	103.03	0.1292(33)
25.55	0.1444(56)	46.10	0.1491(50)	72.40	0.1525(41)	104.55	0.1566(46)
26.22	0.1716(75)	46.70	0.1617(54)	73.35	0.1731(52)	105.95	0.1561(66)
26.71	0.170(12)	47.75	0.1866(88)				

Table 49. Multiplicative renormalisation factor, $Z_Q(\beta)$, relating the average lattice topological charge, Q_{hot}, calculated on the rough Monte Carlo fields, and the integer valued topological charge Q_I calculated after 20 'cooling' sweeps of those fields. For the gauge groups and β shown.

$Z_Q^{\text{int}} = 1 - z_0 g^2 N - z_1 (g^2 N)^2$			
N	z_0	z_1	χ^2/n_{df}
2	0.190(30)	0.023(9)	1.17
3	0.162(10)	0.0425(31)	0.62
4	0.156(20)	0.047(7)	1.32
5	0.203(21)	0.035(7)	2.76
6	0.205(30)	0.036(11)	1.37
8	0.187(24)	0.043(9)	1.71
10	0.141(44)	0.060(16)	1.05
12	0.182(24)	0.071(22)	2.22

Table 50. Interpolating funtions for the multiplicative renormalisation factor, $Z_Q(\beta)$, for our SU(N) calculations, with $g^2 N = 2N^2/\beta$.
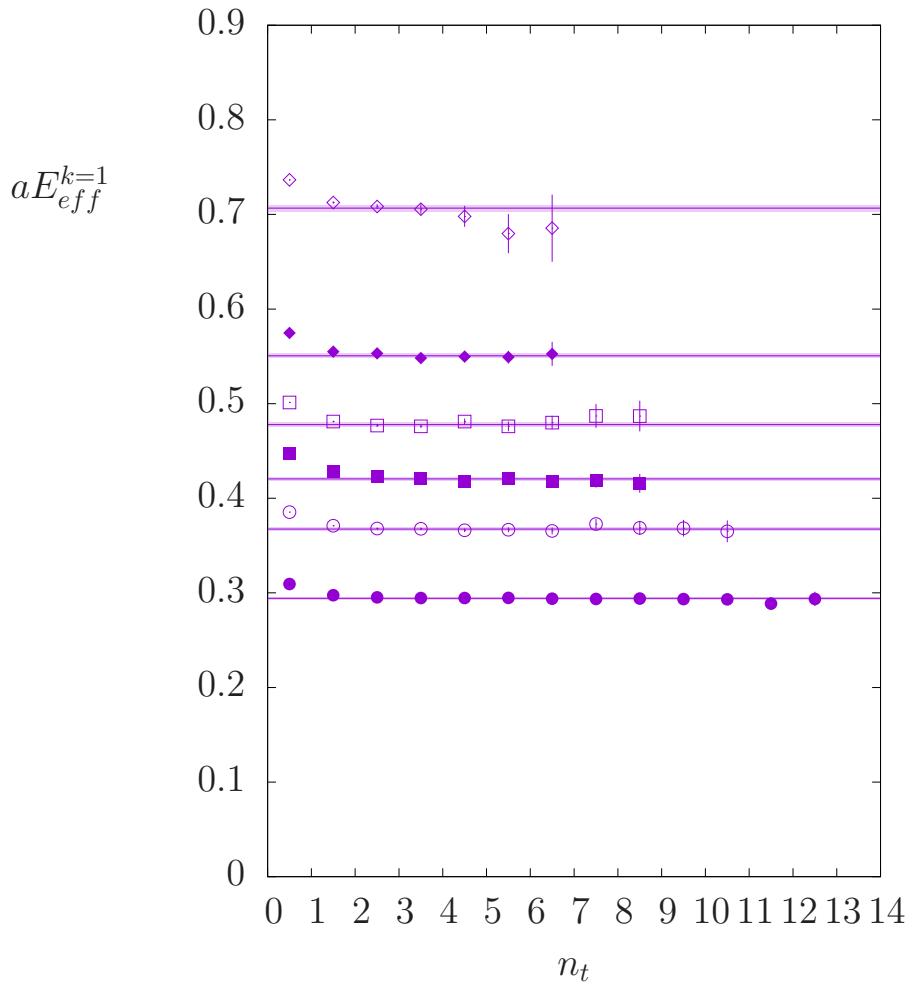
Figure 1. Effective energies of the ground state of a fundamental $k = 1$ flux tube winding around a spatial torus, extracted from the best correlator $C(t)$ between $t = an_t$ and $t = a(n_t + 1)$. For SU(8) and at $\beta = 44.10, 44.85, 45.50, 46.10, 46.70, 47.75$ in descending order. Lines are our estimates of the $t \to \infty$ asymptotic energies. The nearly invisible bands around those lines denote the errors on those estimates.
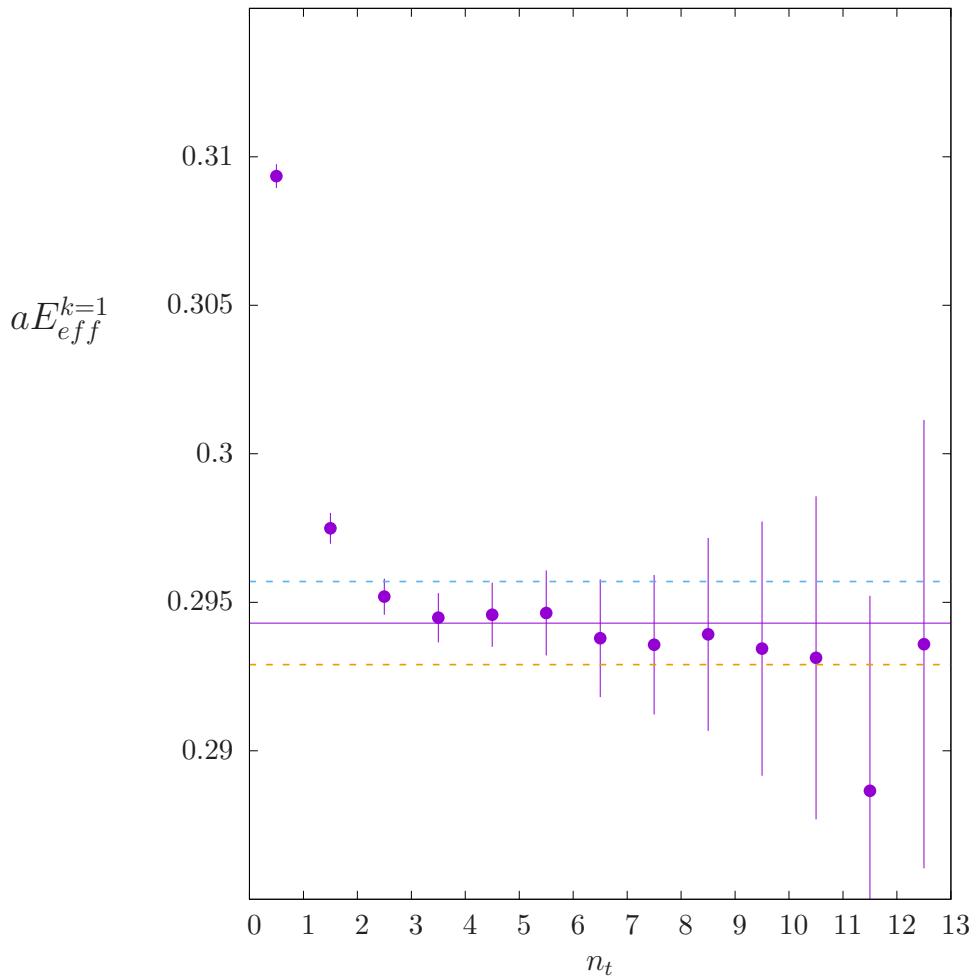
Figure 2. Effective energy of the ground state of a fundamental $k = 1$ flux tube winding around a spatial torus, as in figure 1, for $\beta = 47.75$ in SU(8), with a rescaling sufficient to expose the errors. The solid line is the best estimate from a fit to the correlation function, and the dashed lines show the ± 1 standard deviation fits.
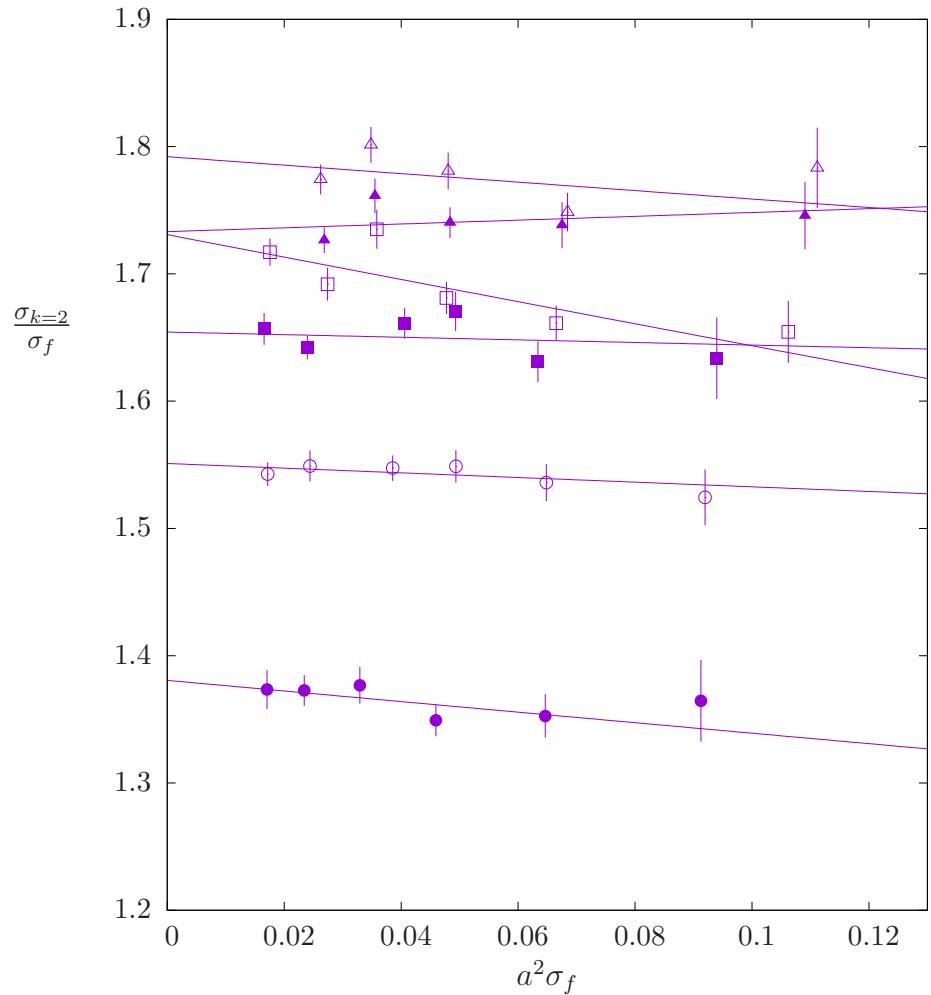
Figure 3. $k = 2$ string tensions, σ_k, in SU(N) gauge theories for $N = 4, 5, 6, 8, 10, 12$ in ascending order, in units of the $k = 1$ fundamental string tension, σ_f. Lines are extrapolations to the continuum limits.
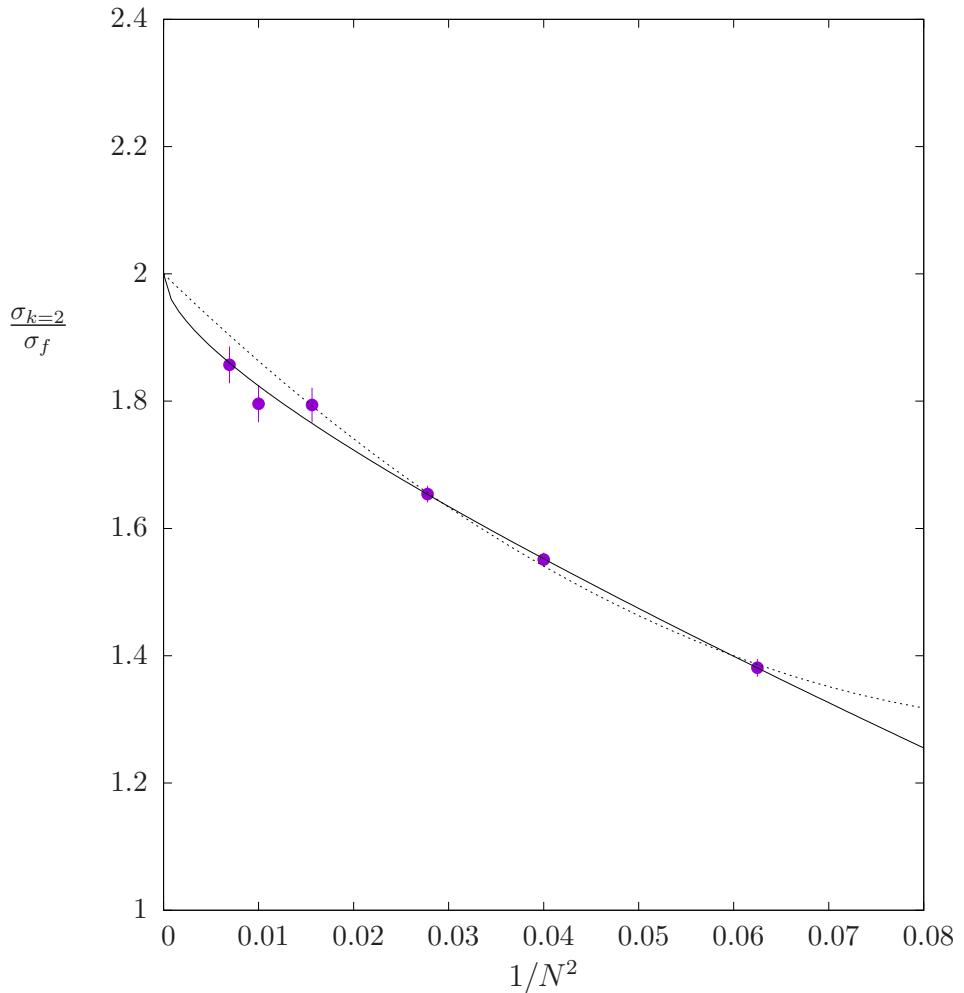
Figure 4. Continuum limit of $k = 2$ string tension, σ_k, in units of the $k = 1$ fundamental string tension, σ_f, for our SU(N) gauge theories. Solid line is the best fit in powers of $1/N$ and dashed line is the best fit in powers of $1/N^2$, with the constraint that the ratio is 2 at $N = \infty$.
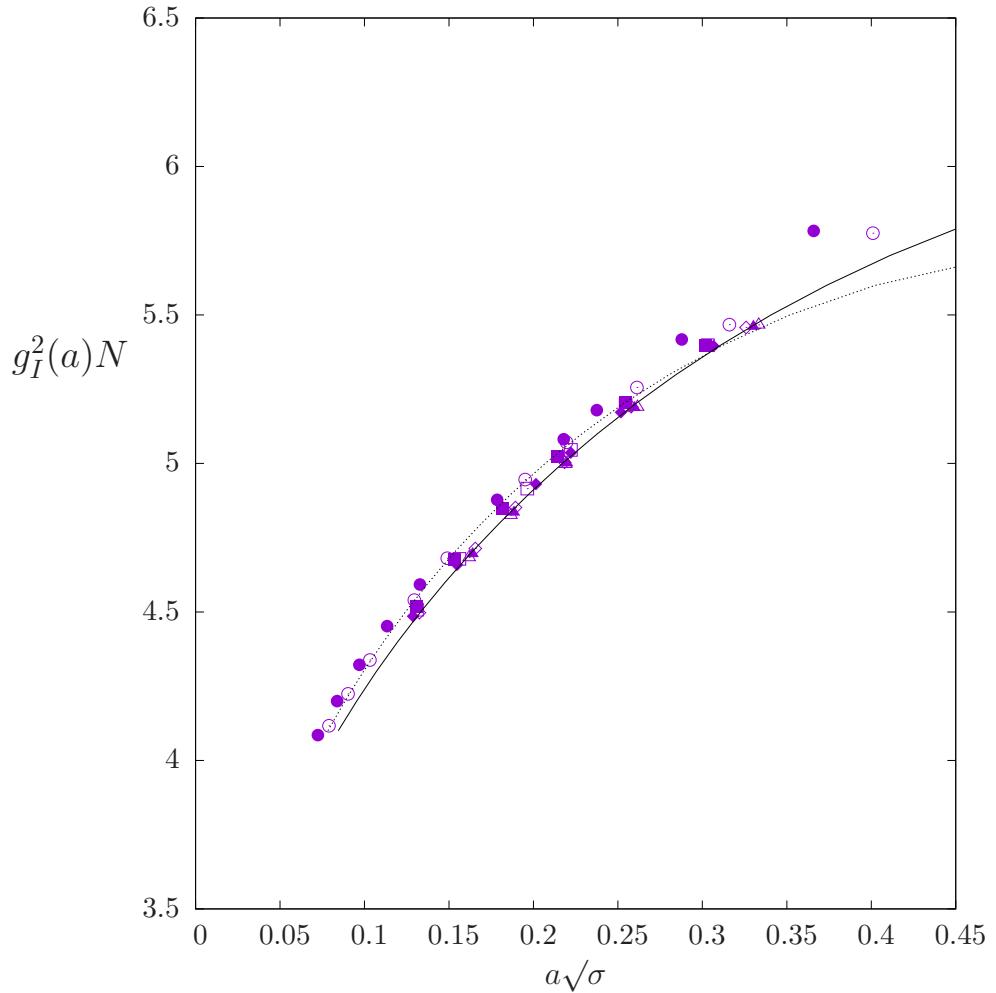
Figure 5. Running (mean-field improved) 't Hooft coupling on the lattice scale a, expressed in units of the string tension, for SU(2), •, SU(3), ∘, SU(4), ■, SU(5), □, SU(6), ♦, SU(8), ◊, SU(10), ▲, SU(12), △. Solid and dashed lines are (improved) perturbative fits to SU(8) and SU(3) respectively.
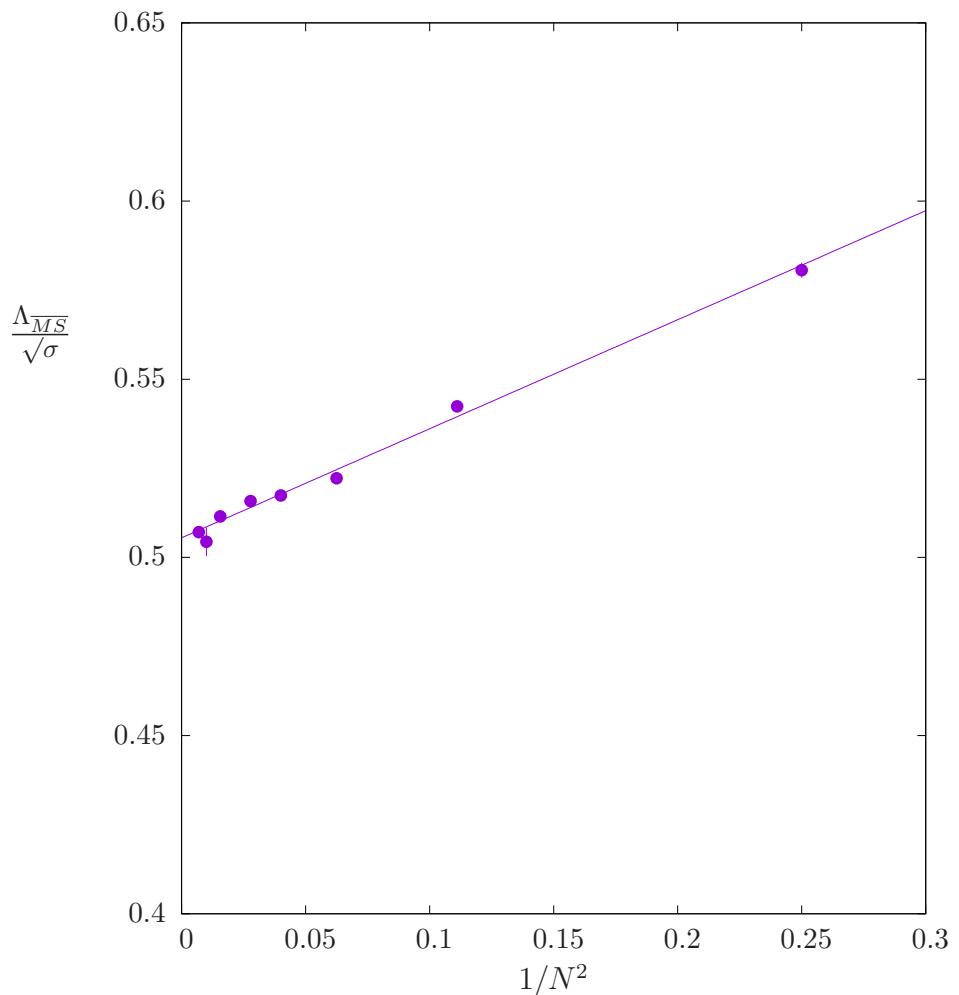
Figure 6. Values of the scale parameter $\Lambda_{\overline{MS}}$ in units of the string tension in our $\mathrm{SU}(N)$ gauge theories.
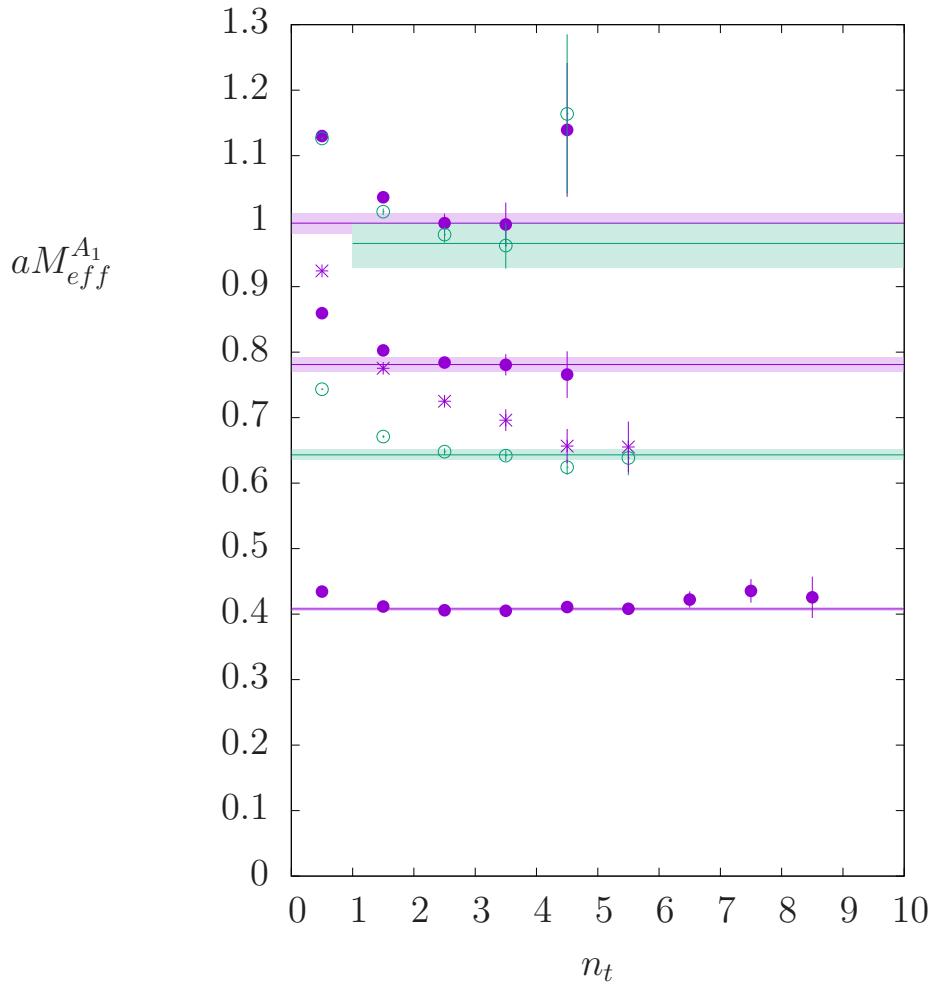
Figure 7. Effective masses for the lightest three A_1^{++} ($\bullet$) and the lightest two A_1^{-+} ($\circ$) glueball states, as well as the main A_1^{++} ditorelon state ($*$). Lines are our best glueball mass estimates, with bands corresponding to ± 1 standard deviations. All on a $20^3 30$ lattice at $\beta = 47.75$ in SU(8). In the continuum limit the lightest two glueball states in each sector become the lightest two $J^{PC} = 0^{++}$ and $J^{PC} = 0^{-+}$ glueballs. The ditorelon disappears in the thermodynamic limit.
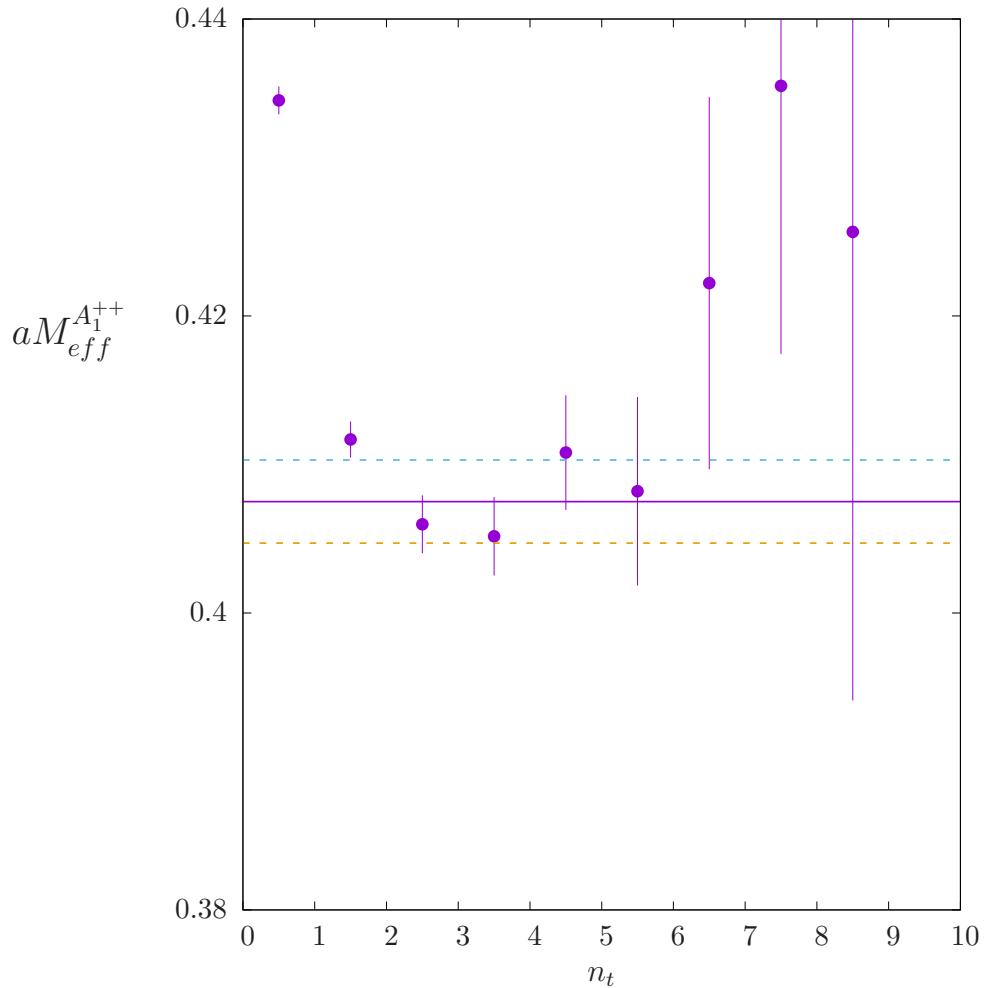
Figure 8. Effective mass plot for the ground state A_1^{++} ($\bullet$) on a $20^3 30$ lattice at $\beta = 47.75$ in SU(8), as in figure 7, but rescaled so as to expose the errors on the effective masses. The straight line is the best estimate for the mass obtained by fitting the correlation function, and the two dashed lines bound the ± 1 standard deviation error band on this mass.
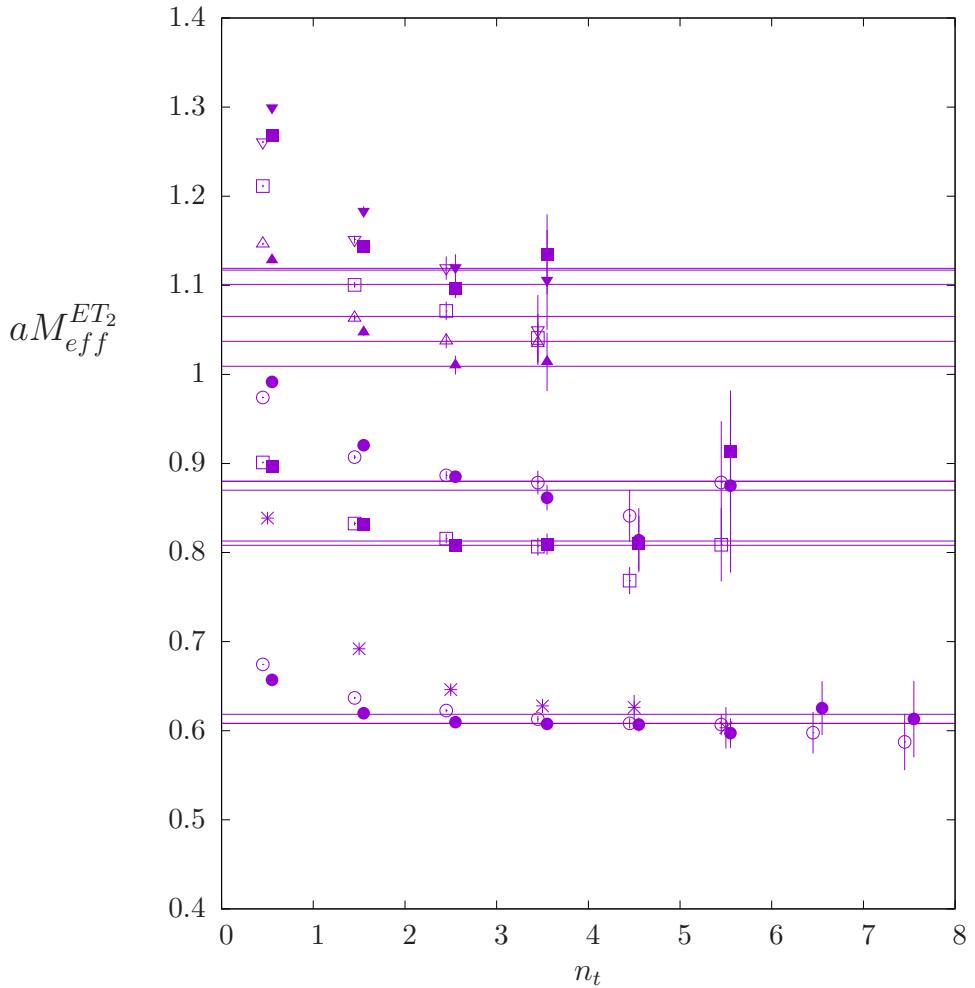
Figure 9. Effective masses for the lightest two E^{++} ($\bullet$) and T_2^{++} ($\circ$) glueballs; the lightest two E^{-+} ($\blacksquare$) and T_2^{-+} ($\square$) glueballs; the lightest E^{+-} ($\blacktriangledown$) and T_2^{+-} ($\triangledown$) glueballs; and the lightest E^{--} ($\blacktriangle$) and T_2^{--} ($\triangle$) glueballs. The state labelled by $*$ is, mainly, the E^{++} ditorelon. Lines are mass estimates. All on a $20^3 30$ lattice at $\beta = 47.75$ in SU(8). In the continuum limit each of the E doublets and corresponding T_2 triplets will pair up to give the five states of a $J = 2$ glueball.
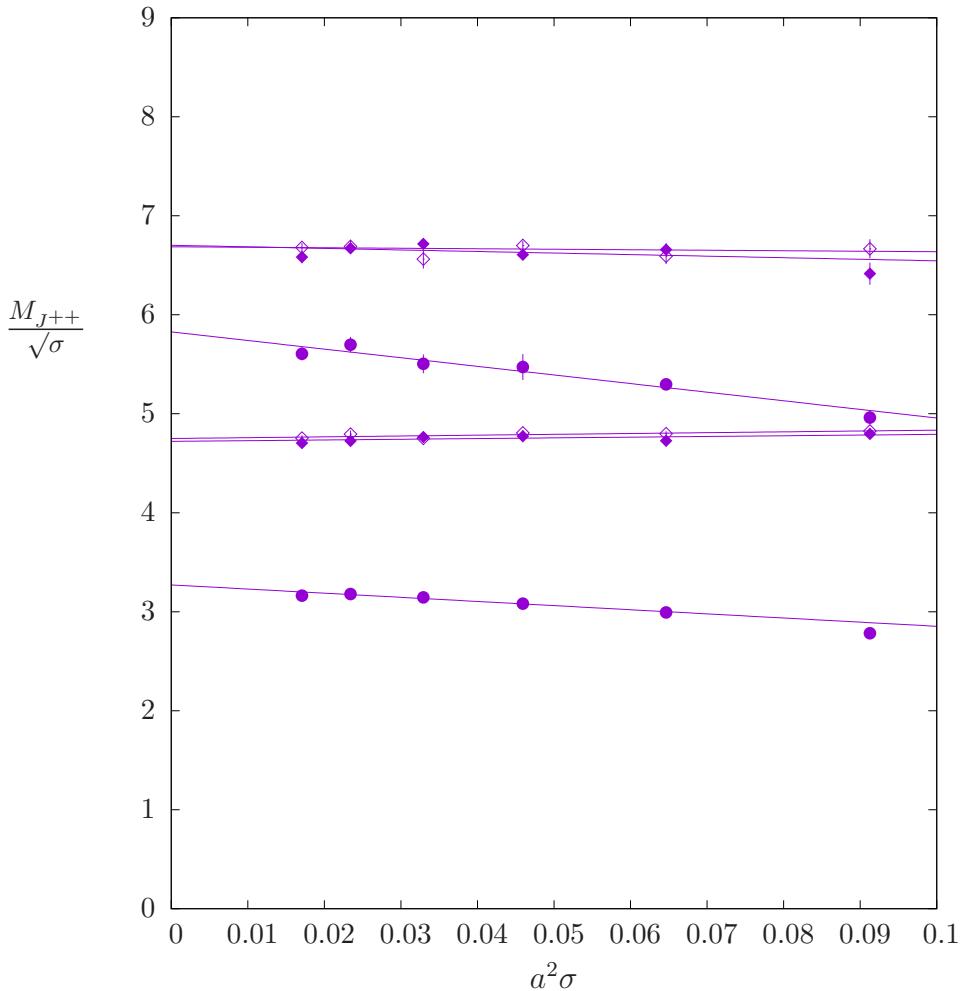
Figure 10. Lightest two glueball masses in the A_1^{++} (●), E^{++} (♦) and T_2^{++} (◇) sectors, in units of the string tension. Lines are linear extrapolations to the continuum limit. In that limit the A_1^{++} states become the lightest two $J^{PC} = 0^{++}$ scalar glueballs while the doublet E^{++} and triplet T_2^{++} pair up to give the five components of each of the lightest two $J^{PC} = 2^{++}$ glueballs. All in SU(4).
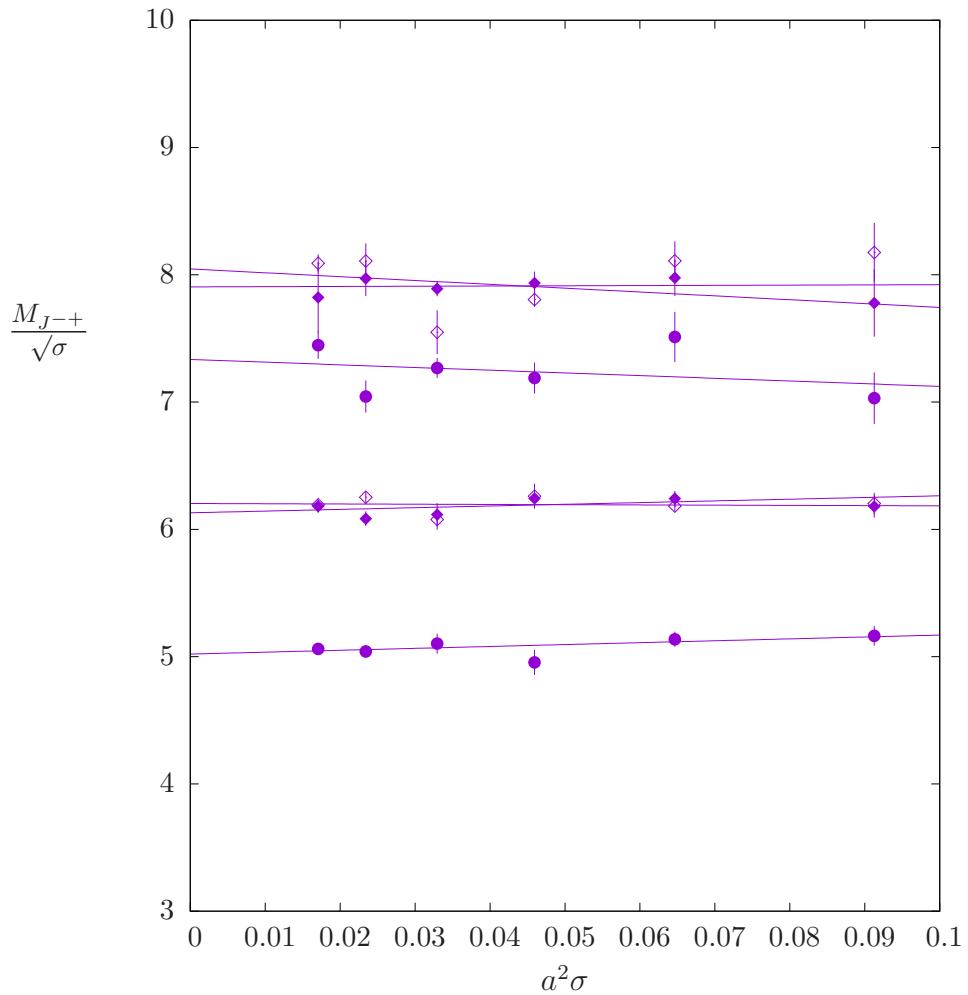
Figure 11. Lightest two glueball masses in the A_1^{-+} (•), E^{-+} (♦) and T_2^{-+} (◊) sectors, in units of the string tension. Lines are linear extrapolations to the continuum limit. In that limit the A_1^{-+} states become the lightest two $J^{PC} = 0^{-+}$ pseudoscalar glueballs while the doublet E^{--+} and triplet T_2^{-+} pair up to give the five components of each of the lightest two $J^{PC} = 2^{-+}$ glueballs. All in SU(4).
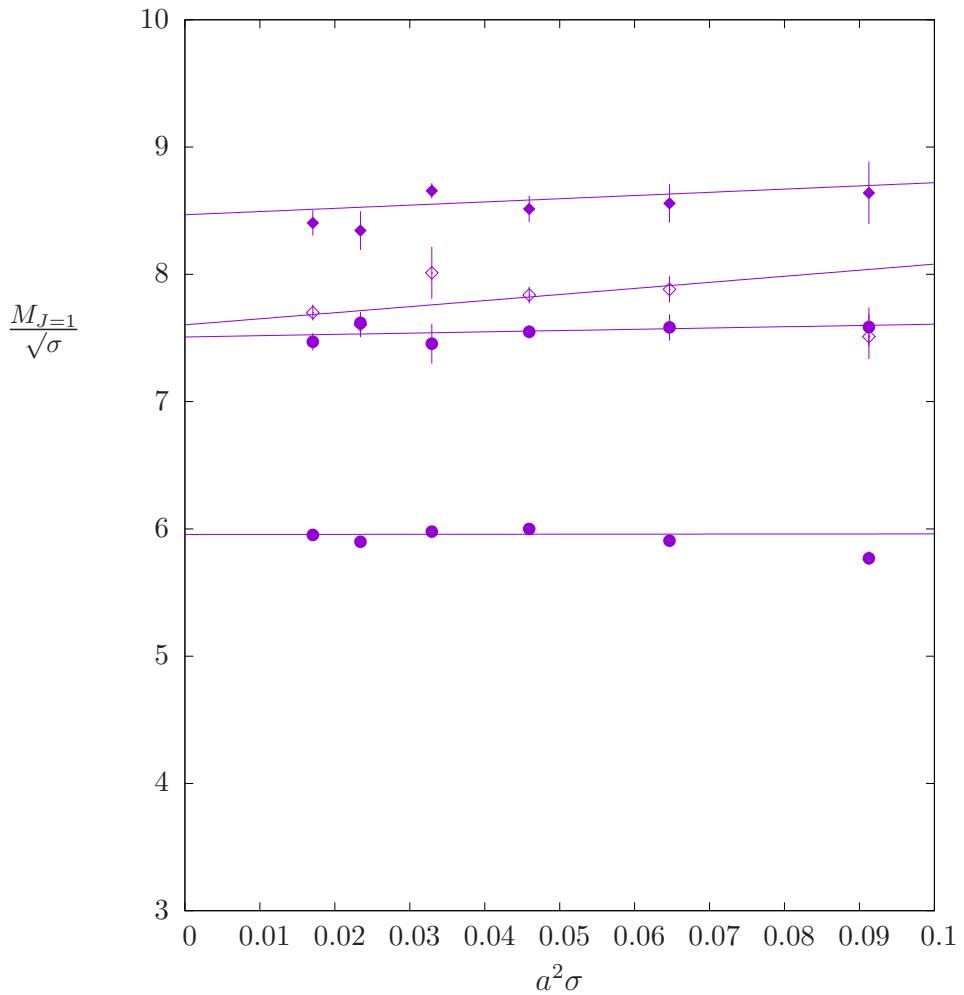
Figure 12. Lightest two glueball masses in the T_1^{+-} ($\bullet$) representation and the lightest ones in the T_1^{-+} ($\blacklozenge$) and T_1^{--} ($\lozenge$) representations, in units of the string tension. Lines are linear extrapolations to the continuum limit. In that limit the T_1^{+-} states become the lightest two $J^{PC} = 1^{+-}$ glueballs while the other two becomes the 1^{-+} and 1^{--} ground state glueballs. All in SU(4).
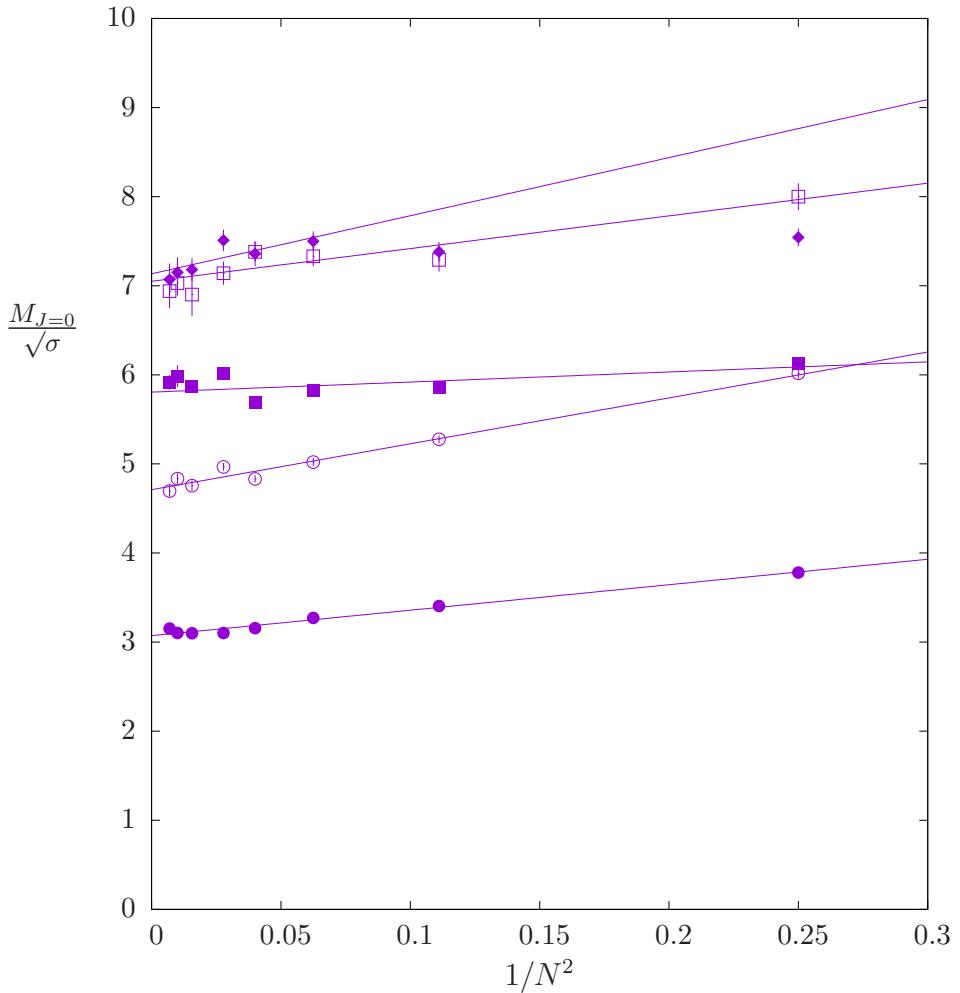
Figure 13. Continuum masses of the lightest ($\bullet$) and first excited ($\blacksquare$) $J^{PC} = 0^{++}$ scalars and of the lightest ($\circ$) and first excited ($\square$) 0^{-+} pseudoscalars, in units of the string tension. The state denoted by $\blacklozenge$ is either the 4^{++} ground state or the second excited 0^{++}. With extrapolations from values in the range $N \in [2, 12]$ to $N = \infty$.
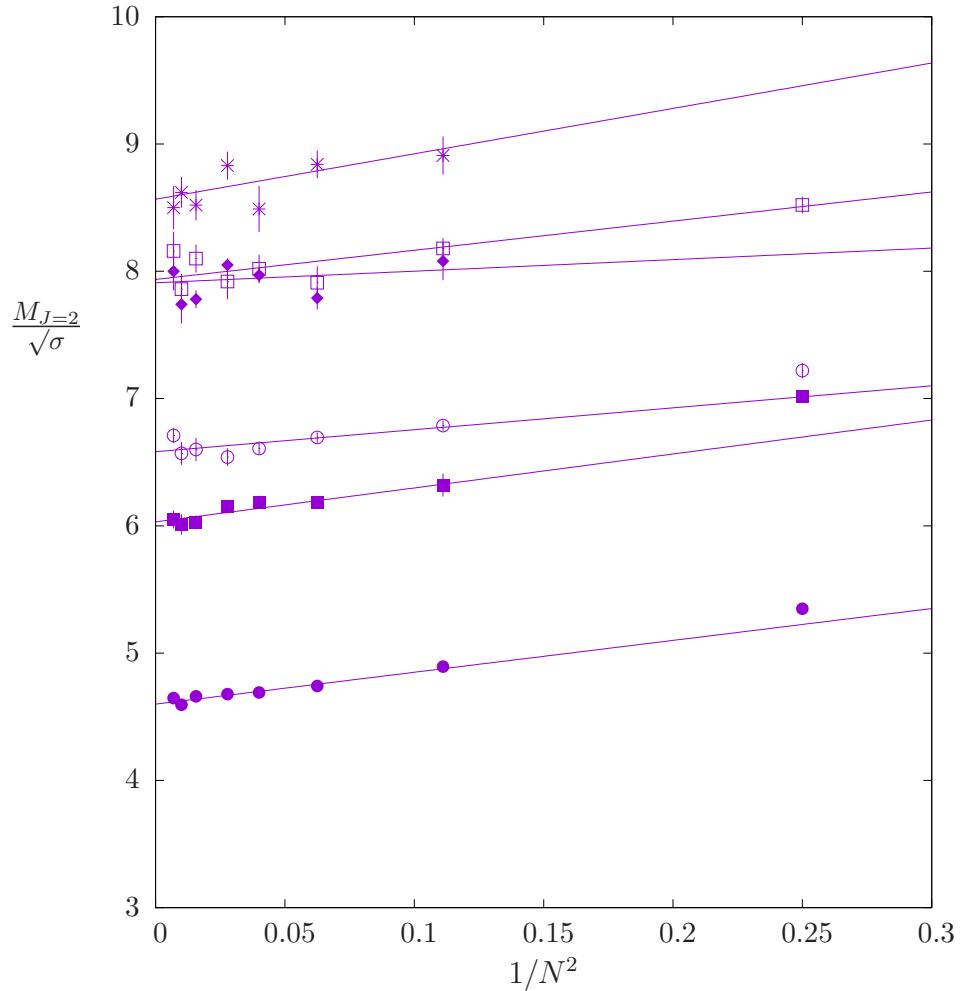
Figure 14. Continuum masses of the lightest ($\bullet$) and first excited ($\circ$) $J^{PC} = 2^{++}$ tensors, the lightest ($\blacksquare$) and first excited ($\square$) 2^{-+} pseudotensors, the lightest 2^{+-} ($*$), and the lightest 2^{--} ($\blacklozenge$), all in units of the string tension. With extrapolations to $N = \infty$ from $N \leq 12$.
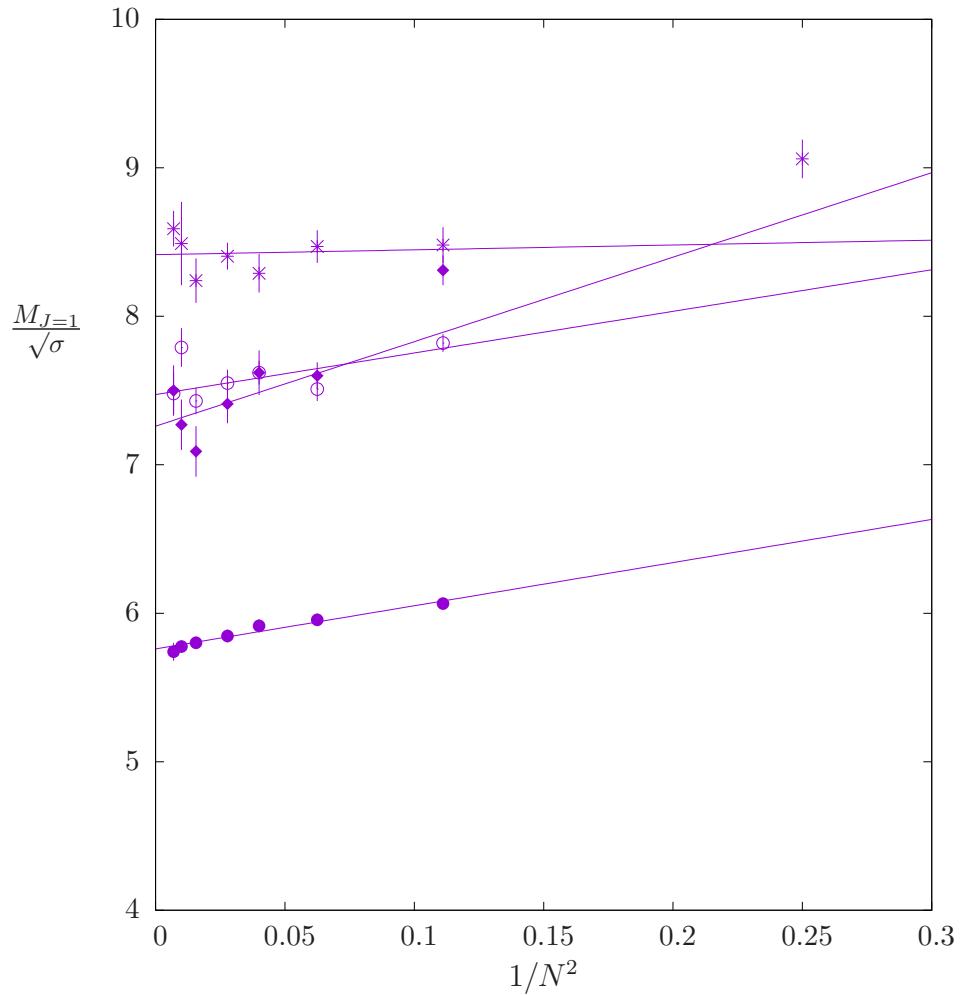
Figure 15. Continuum masses of the lightest (●) and first excited (○) $J^{PC} = 1^{+-}$ glueballs, as well as the lightest 1^{-+} (∗) and 1^{--} (♦) glueballs. in units of the string tension, with extrapolations to $N = \infty$.
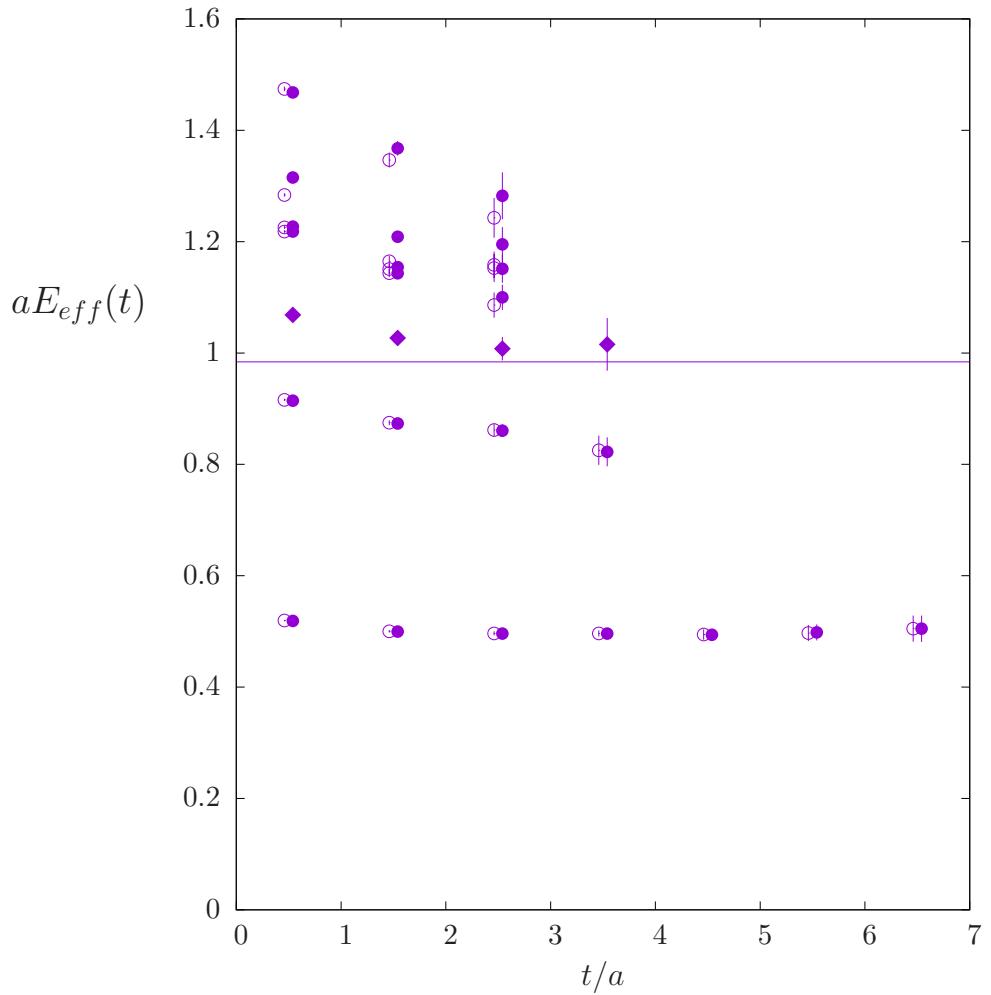
Figure 16. Effective masses for the lightest few glueballs in the 'scalar' A_1^{++} representation, for the single trace operators (○) and for the same set augmented with double trace operators (filled points), with points shifted for clarity. The extra 'scattering' state amongst the latter is shown as ◆. Horizontal line indicates twice the mass of the lightest glueball. On the $26^3 26$ lattice at $\beta = 6.235$ in SU(3).
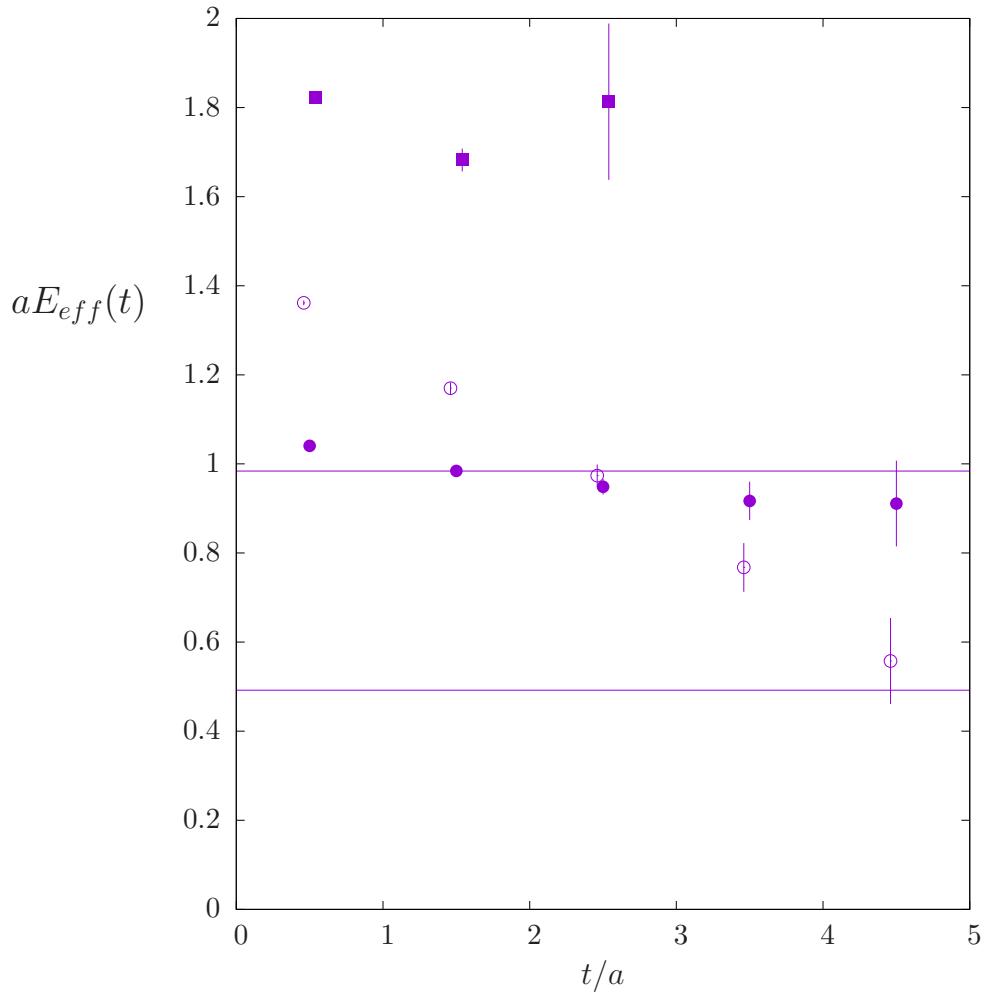
Figure 17. Effective masses for the lightest three states in the 'scalar' A_1^{++} representation, for the double trace operators. Lower horizontal line indicates the mass of the lightest glueball, and upper horizontal line indicates twice the mass of the lightest glueball. On the $26^3 26$ lattice at $\beta = 6.235$ in SU(3).
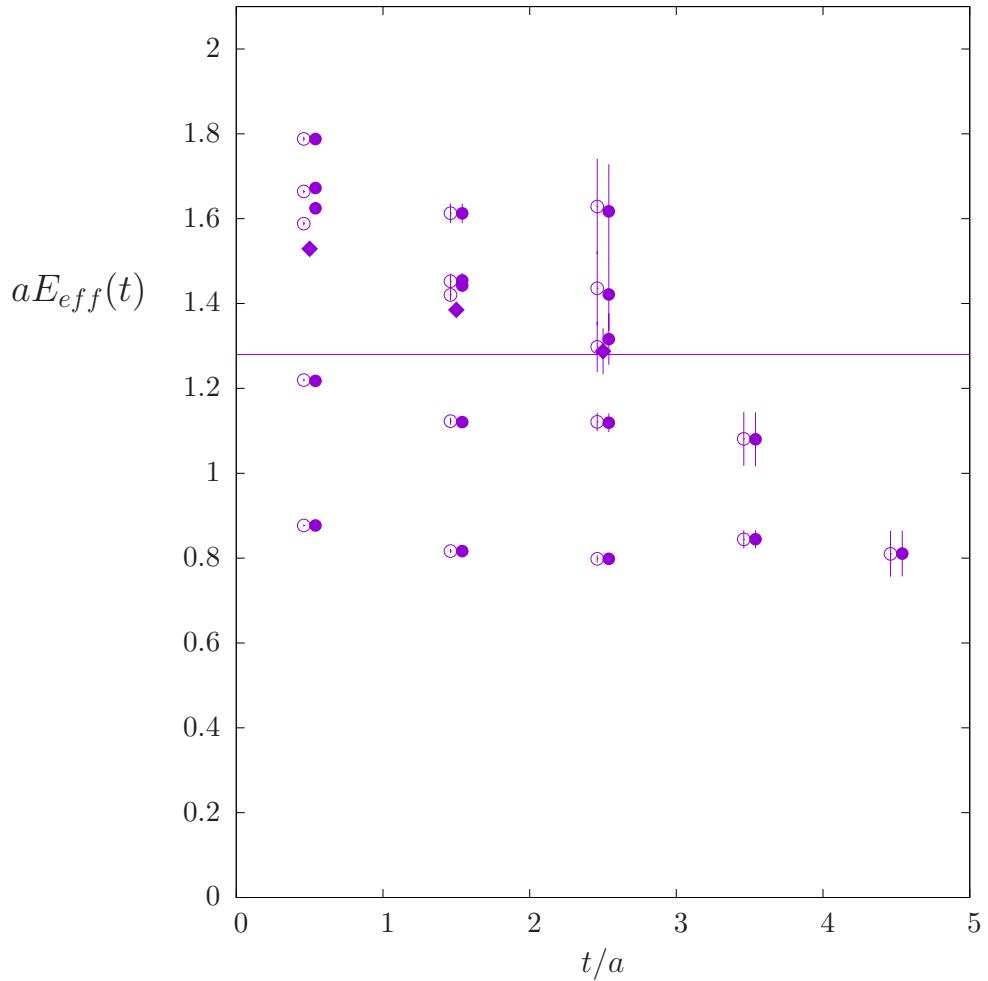
Figure 18. Effective masses for the lightest few glueballs in the 'pseudoscalar' A_1^{-+} representation, for the single trace operators (∘) and for the same set augmented with double trace operators (filled points), with points shifted for clarity. The likely extra 'scattering' state amongst the latter is shown as ♦. Horizontal line indicates the sum of the lightest A_1^{++} and A_1^{-+} glueball masses. On the $26^3 26$ lattice at $\beta = 6.235$ in SU(3).
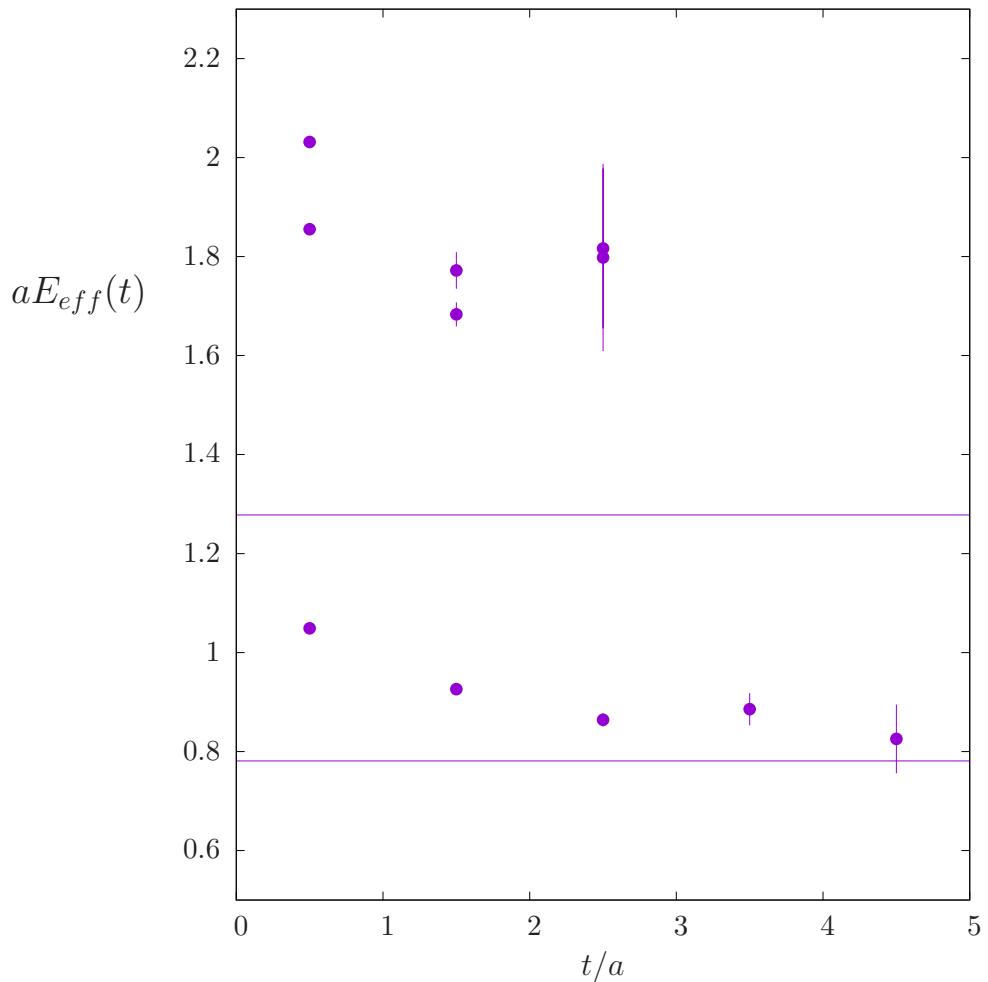
Figure 19. Effective masses for the lightest three states in the 'pseudoscalar' A_1^{-+} representation, for the double trace operators. Lower horizontal line indicates the mass of the lightest A_1^{-+} glueball, and upper horizontal line indicates the sum of the masses of the lightest A_1^{++} and A_1^{-+} glueballs. On the $26^3 26$ lattice at $\beta = 6.235$ in SU(3).
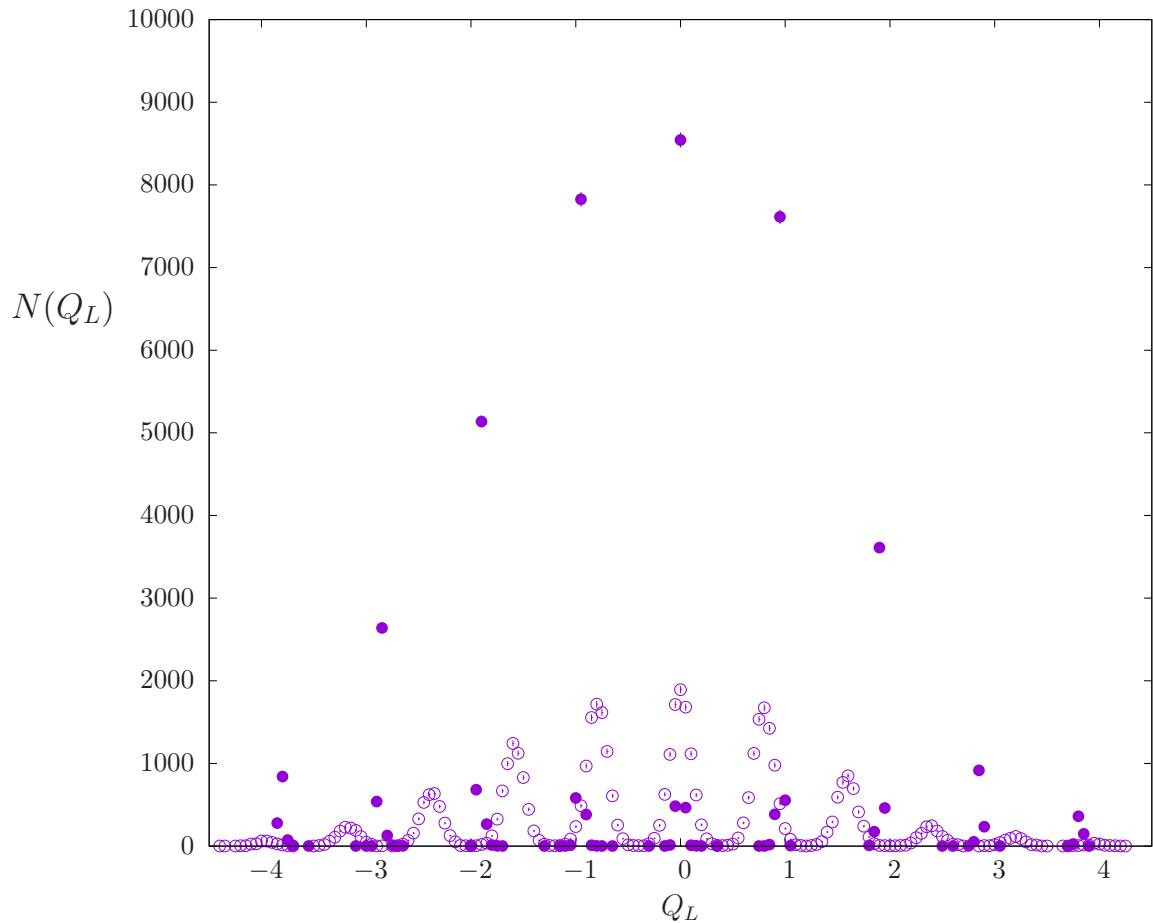
Figure 20. The number of lattice fields with topological charge Q_L after 2 ($\circ$) and after 20 ($\bullet$) cooling sweeps, from sequences of SU(5) fields generated at $\beta = 17.63$. $N(Q_L) = 0$ points suppressed.
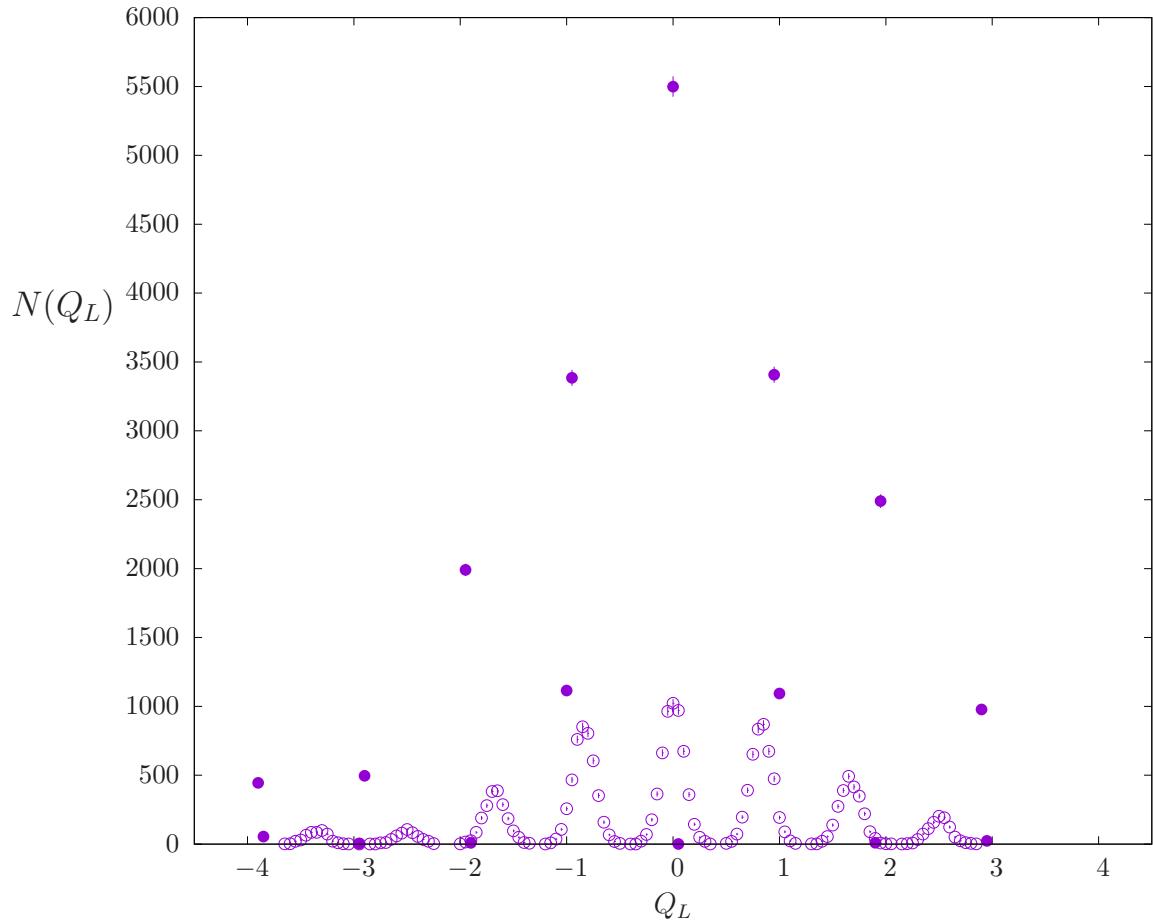
Figure 21. The number of lattice fields with topological charge Q_L after 2 (○) and after 20 (●) cooling sweeps, from sequences of SU(8) fields generated at $\beta = 47.75$. $N(Q_L) = 0$ points suppressed.
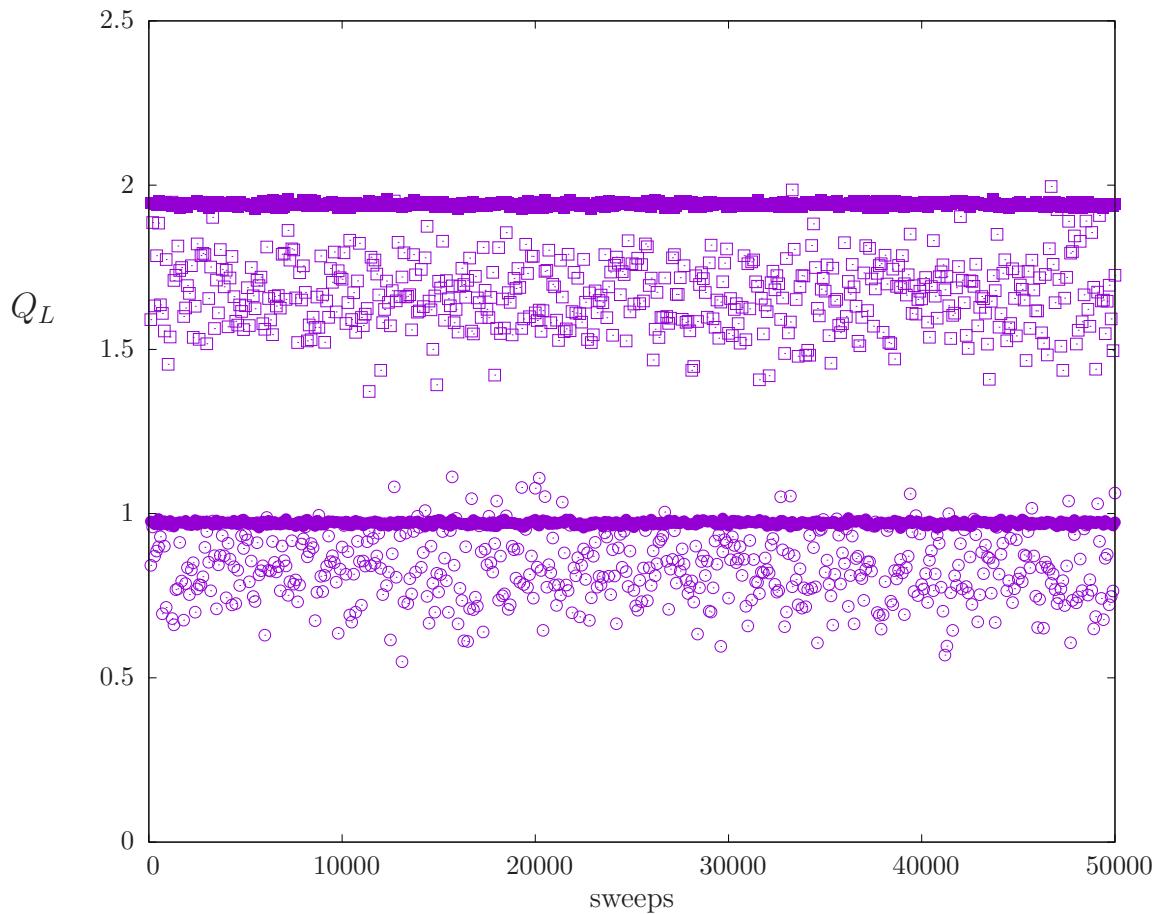
Figure 22. The lattice topological charge Q_L for two sequences of SU(8) lattice fields, calculated after 2 ($\circ$, $\square$) and 20 ($\bullet$, $\blacksquare$) cooling sweeps. Calculations of Q_L made every 100 Monte Carlo sweeps for each sequence of 50000 sweeps, at $\beta = 47.75$ on a $20^3 30$ lattice.
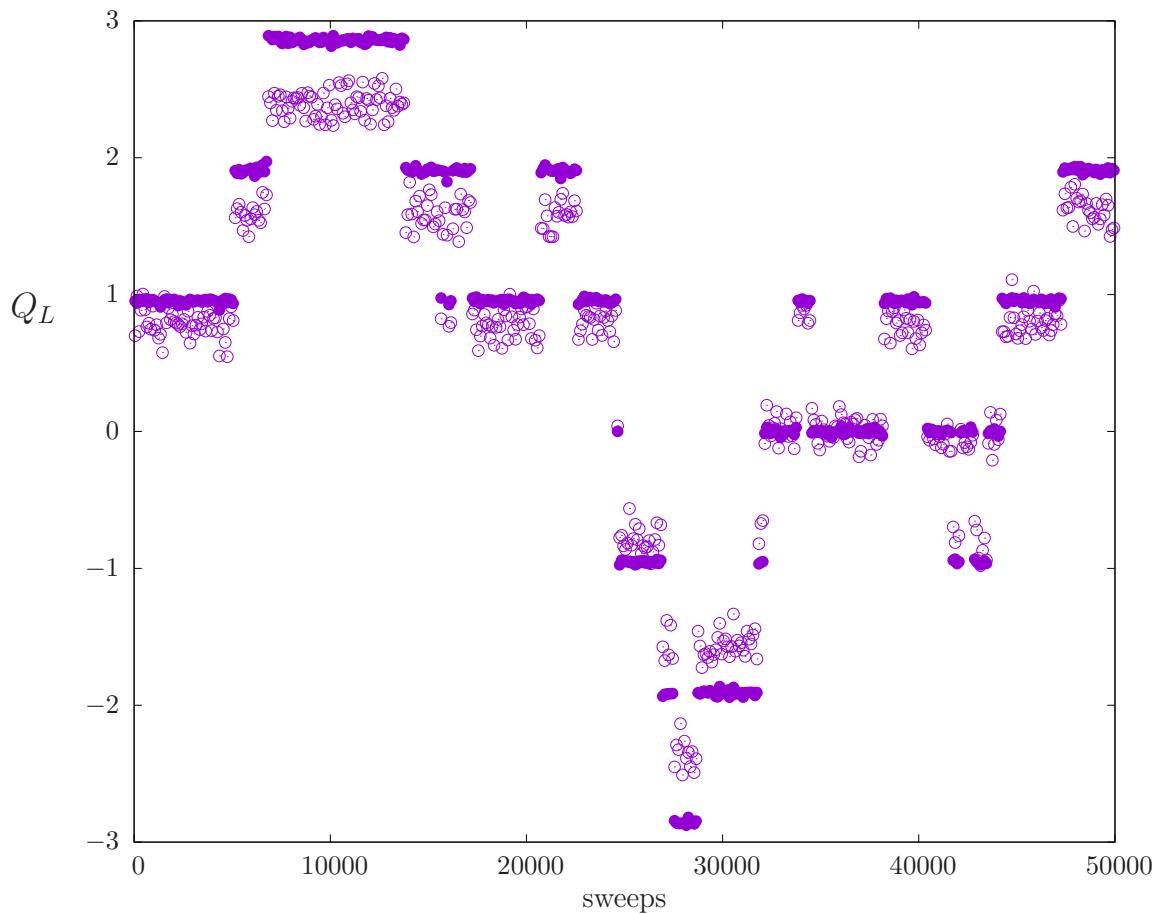
Figure 23. The lattice topological charge Q_L for a sequence of SU(5) lattice fields after 2 (○) and 20 (●) cooling sweeps. Calculations of Q_L every 100 Monte Carlo sweeps over a sequence of 50000 sweeps, at $\beta = 17.63$ on a $16^3 20$ lattice.
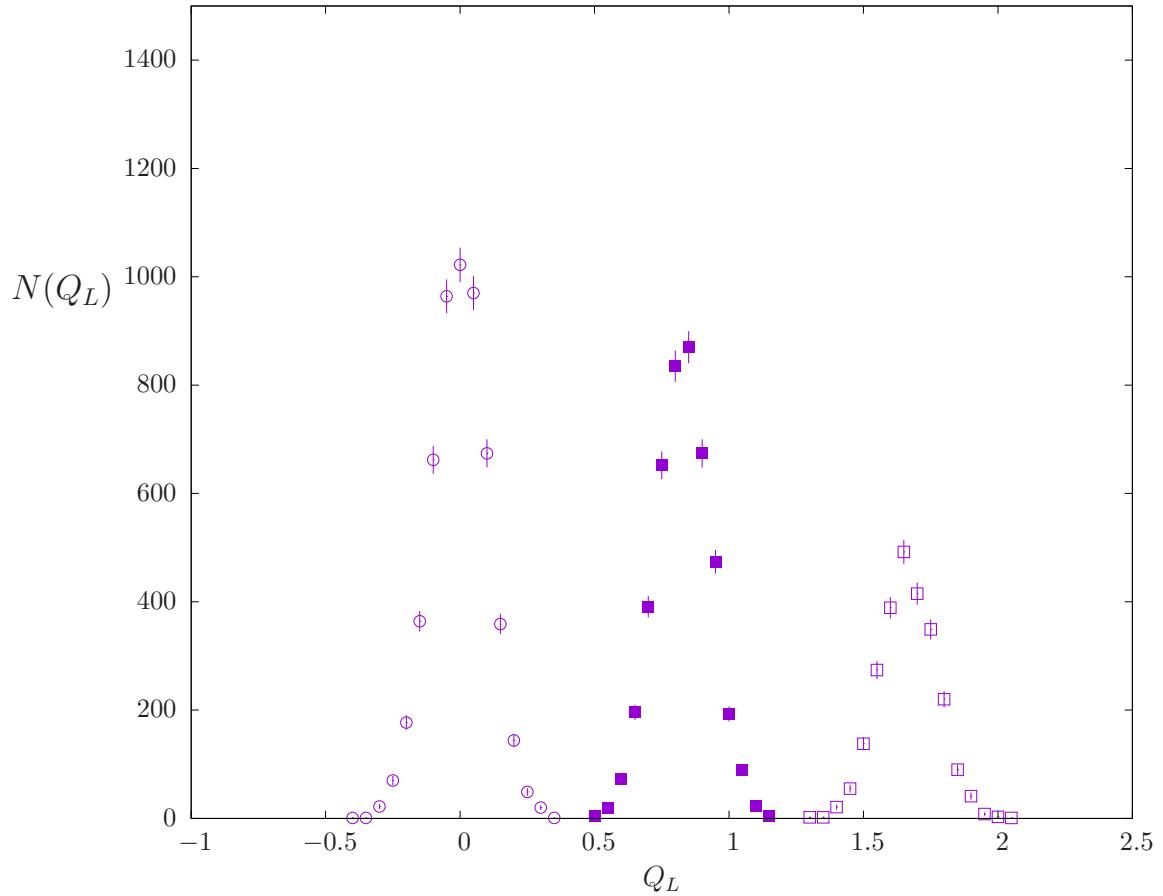
Figure 24. The distribution in the topological charge Q_L as obtained after 2 cooling sweeps, for fields that after 20 cooling sweeps have topological charges $Q = 0$ (○), $Q = 1$ (■) and $Q = 2$ (□). $N(Q_L) = 0$ points suppressed. From the same sequences of SU(8) fields generated at $\beta = 47.75$ plotted in figure 21.
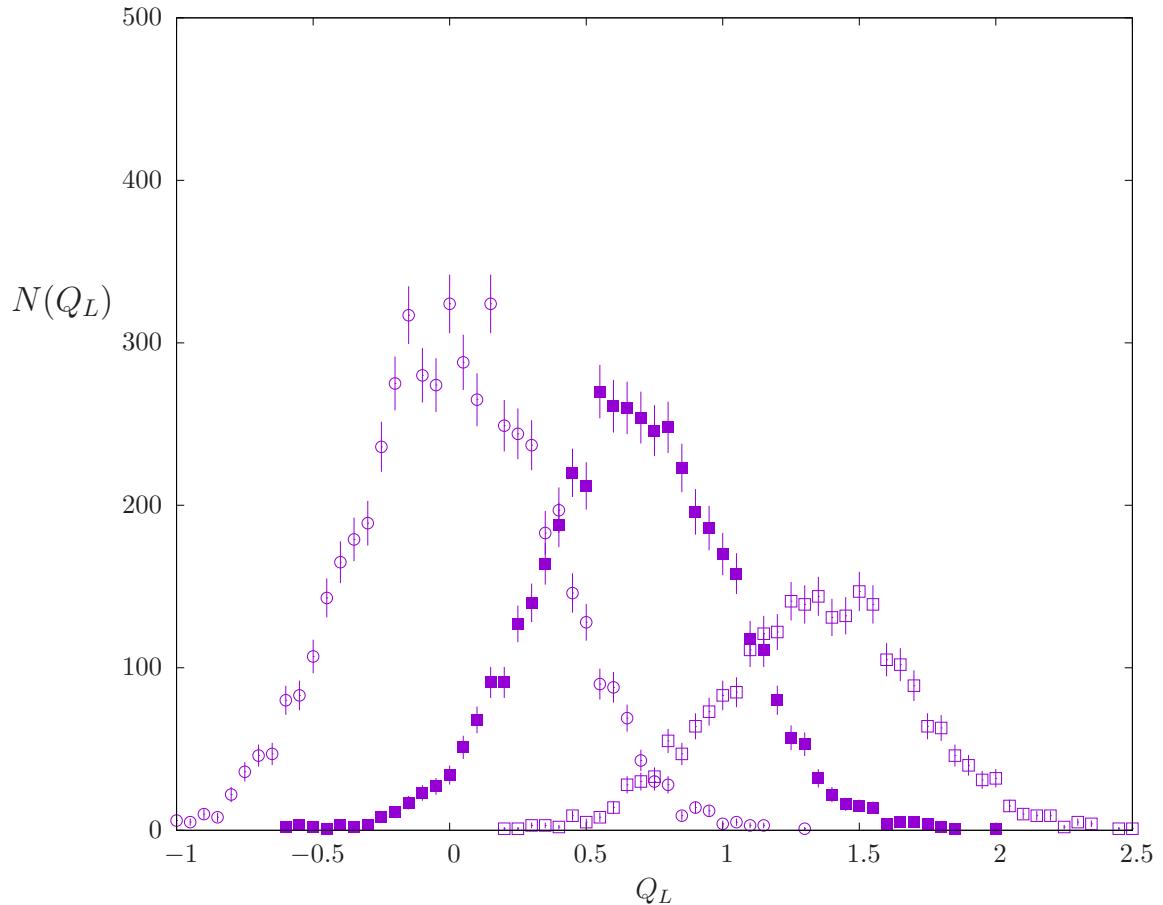
Figure 25. The distribution in the topological charge Q_L as obtained after only 1 cooling sweep, for fields that after 20 cooling sweeps have topological charges $Q = 0$ (○), $Q = 1$ (■) and $Q = 2$ (□). $N(Q_L) = 0$ points suppressed. From the same sequence of SU(8) fields generated at $\beta = 47.75$ plotted in figure 21.
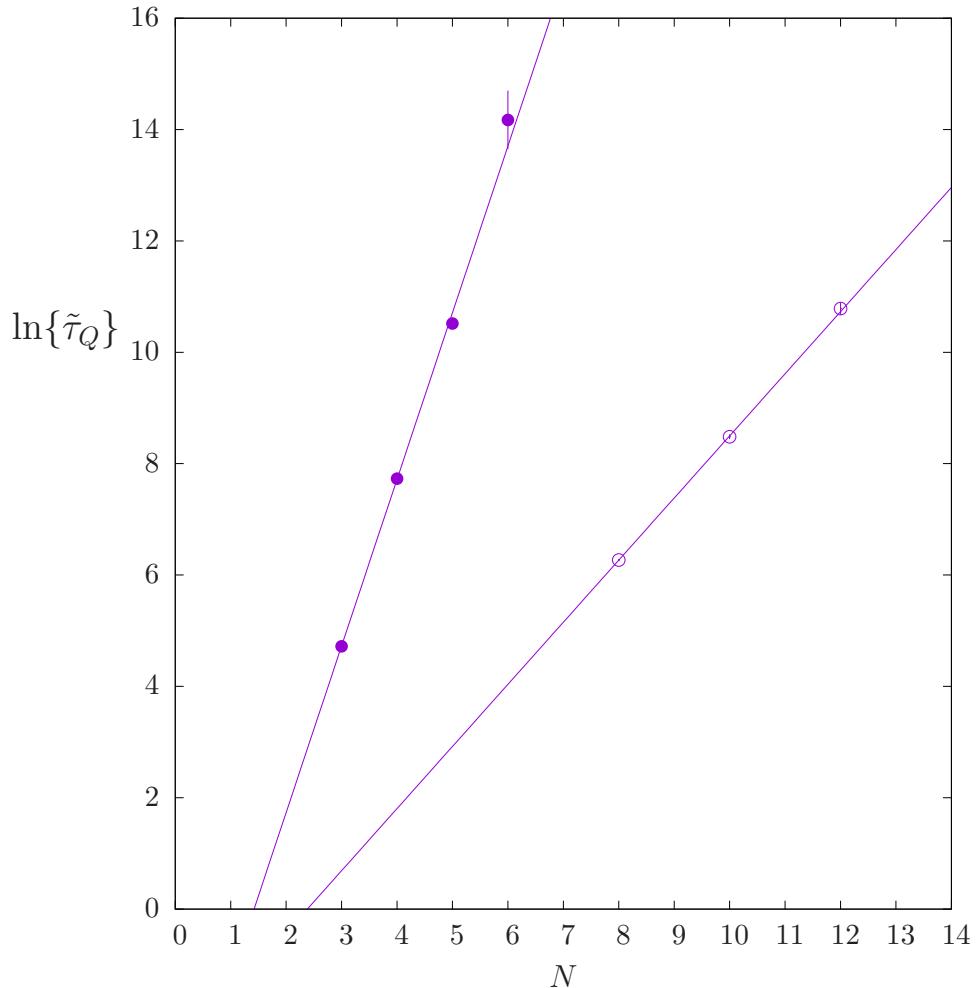
Figure 26. Correlation length $\tilde{\tau}_Q$, the average number of sweeps between changes of Q by ± 1, measured for the SU(N) lattice topological charge for $a\sqrt{\sigma} \sim 0.15$ (•) and for $a\sqrt{\sigma} \sim 0.33$ (∘). Lines are fits $\tilde{\tau}_Q = b \exp\{cN\}$.
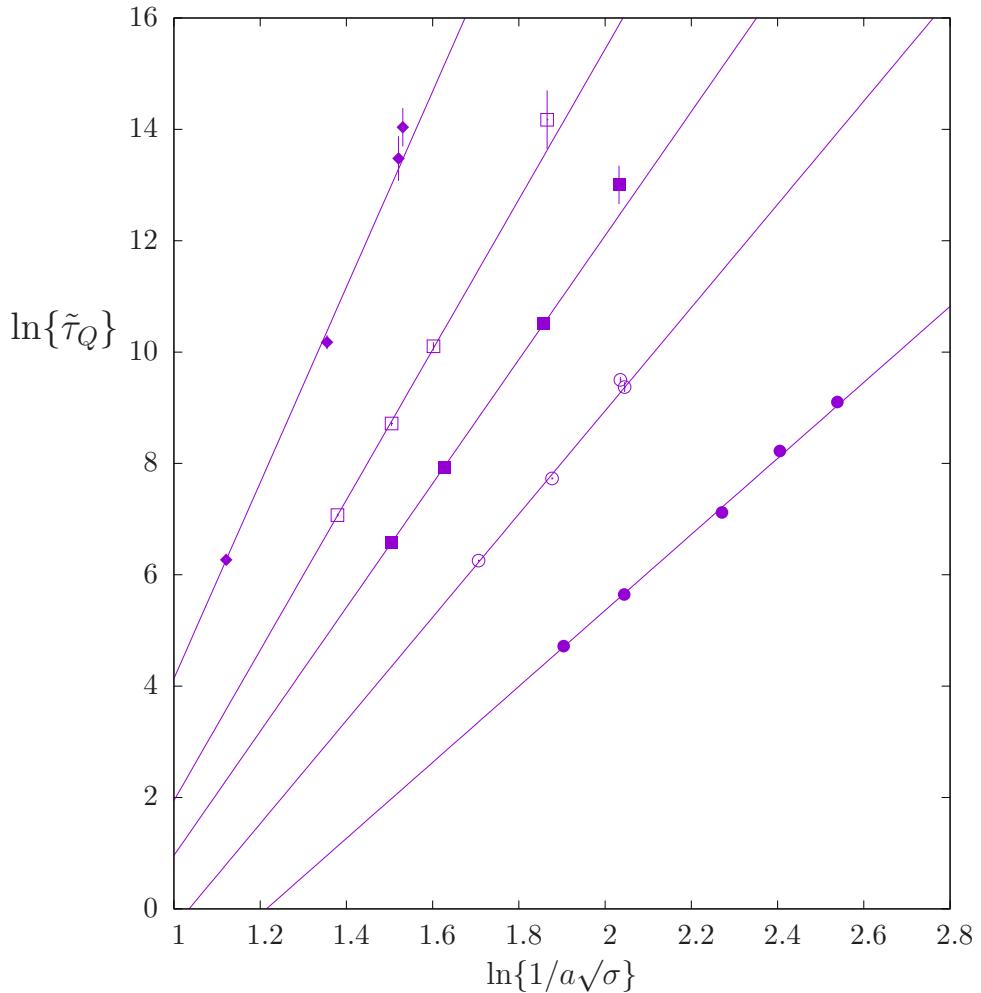
Figure 27. Variation of $\tilde{\tau}_Q$, the average number of sweeps between changes of Q by ± 1, against the lattice spacing and normalised to our standard space-time volume $V = (3/\sqrt{\sigma})^4$. For SU(3) ($\bullet$), SU(4) ($\circ$), SU(5) ($\blacksquare$), SU(6) ($\square$), SU(8) ($\blacklozenge$). The two pairs of points nearly overlapping are obtained at same a but from different volumes. Lines are fits $\tilde{\tau}_Q = b\{1/a\sqrt{\sigma}\}^c$.
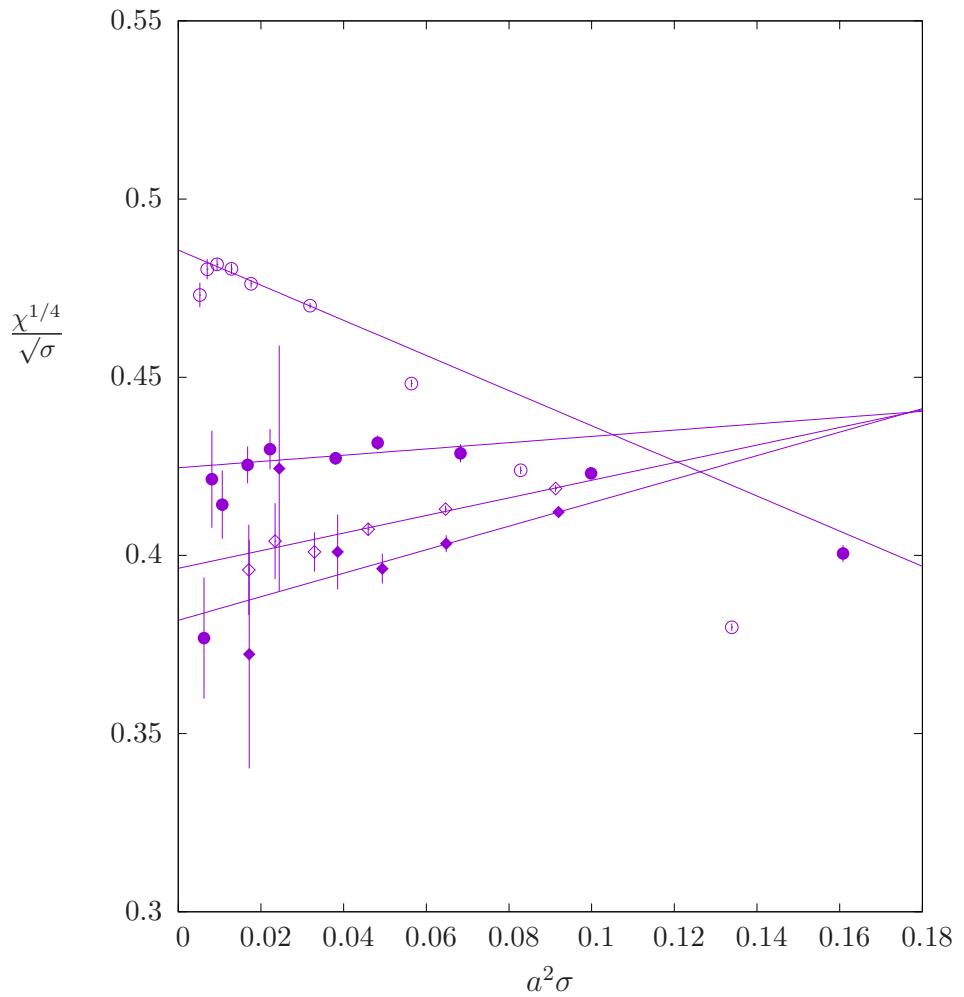
Figure 28. Continuum extrapolations of the topological susceptibility in units of the string tension for continuum SU(2), ∘, SU(3), •, SU(4), ◊, and SU(5), ◆, gauge theories.
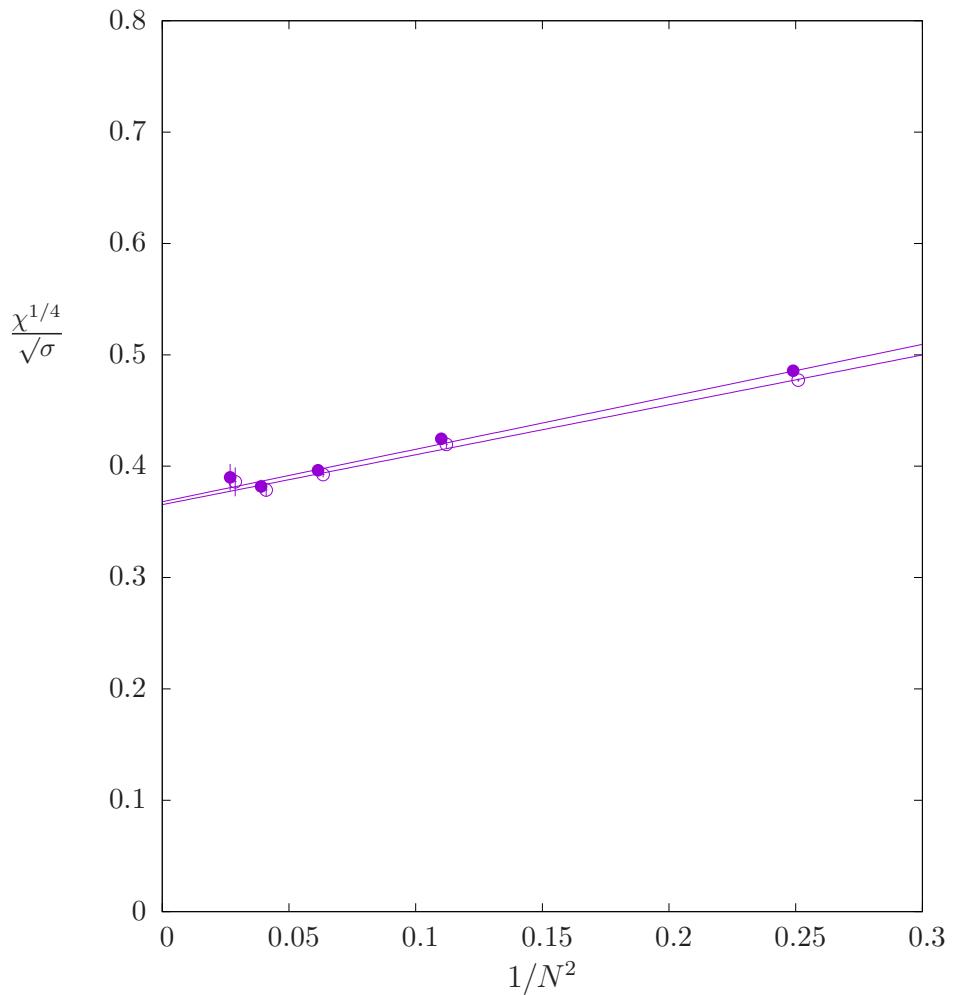
Figure 29. Topological susceptibility in units of the string tension for continuum SU(N) gauge theories with $N = 2, 3, 4, 5, 6$. For integer valued charge, •, and for non-integer lattice charge, ○. Points shifted slightly for clarity. Lines are extrapolations to $N = \infty$.
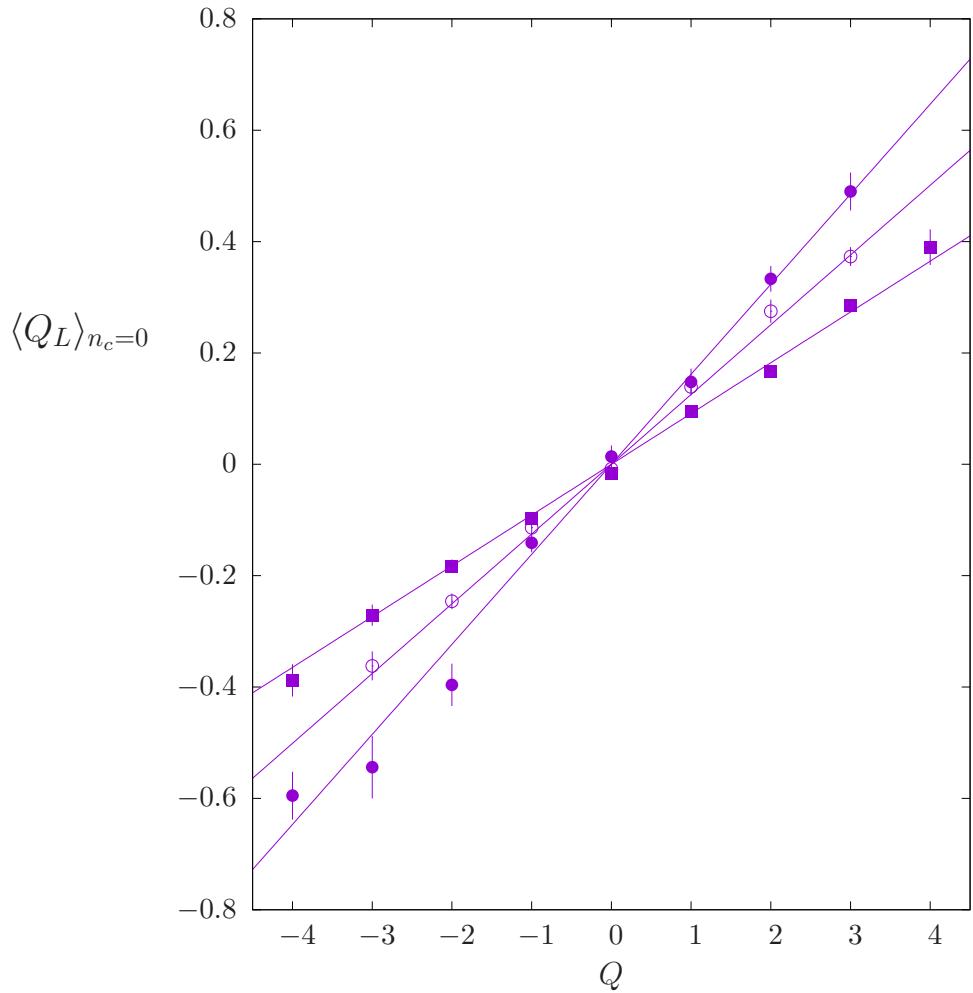
Figure 30. Average value of topological charge on lattice fields that have charge Q after 20 cooling sweeps. In SU(8) at $\beta = 44.10$, ■, $\beta = 45.50$, ○, and $\beta = 46.70$, ●. Slope of fits gives the renormalisation factor $Z_Q(\beta)$.

References

[1] B. Lucini and M. Teper, SU(*N*) *gauge theories in four-dimensions: Exploring the approach to* $N = \infty$, *JHEP* **06** (2001) 050 [`hep-lat/0103027`] [ɪɴSPIRE].

[2] B. Lucini, M. Teper and U. Wenger, *Glueballs and k-strings in* SU(*N*) *gauge theories: Calculations with improved operators*, *JHEP* **06** (2004) 012 [`hep-lat/0404008`] [ɪɴSPIRE].

[3] B. Lucini, A. Rago and E. Rinaldi, *Glueball masses in the large N limit*, *JHEP* **08** (2010) 119 [`arXiv:1007.3879`] [ɪɴSPIRE].

[4] E. Bennett et al., *Glueballs and strings in* Sp(2*N*) *Yang-Mills theories*, *Phys. Rev. D* **103** (2021) 054509 [`arXiv:2010.15781`] [ɪɴSPIRE].

[5] C. Michael and M. Teper, *The Glueball Spectrum in* SU(3), *Nucl. Phys. B* **314** (1989) 347 [ɪɴSPIRE].

[6] UKQCD collaboration, *A Comprehensive lattice study of* SU(3) *glueballs*, *Phys. Lett. B* **309** (1993) 378 [`hep-lat/9304012`] [ɪɴSPIRE].

[7] C.J. Morningstar and M.J. Peardon, *The Glueball spectrum from an anisotropic lattice study*, *Phys. Rev. D* **60** (1999) 034509 [`hep-lat/9901004`] [ɪɴSPIRE].

[8] H.B. Meyer and M.J. Teper, *Glueball Regge trajectories and the Pomeron: A Lattice study*, *Phys. Lett. B* **605** (2005) 344 [`hep-ph/0409183`] [ɪɴSPIRE].

[9] H.B. Meyer, *Glueball Regge trajectories*, other thesis, 2004 [`hep-lat/0508002`] [ɪɴSPIRE].

[10] Y. Chen et al., *Glueball spectrum and matrix elements on anisotropic lattices*, *Phys. Rev. D* **73** (2006) 014516 [`hep-lat/0510074`] [ɪɴSPIRE].

[11] A. Athenodorou and M. Teper, *The glueball spectrum of* SU(3) *gauge theory in* $3 + 1$ *dimensions*, *JHEP* **11** (2020) 172 [`arXiv:2007.06422`] [ɪɴSPIRE].

[12] M.G. Pérez, A. González-Arroyo and M. Okawa, *Meson spectrum in the large N limit*, *JHEP* **04** (2021) 230 [`arXiv:2011.13061`] [ɪɴSPIRE].

[13] M. García Pérez, A. González-Arroyo, M. Koren and M. Okawa, *The spectrum of* $2 + 1$ *dimensional Yang-Mills theory on a twisted spatial torus*, *JHEP* **07** (2018) 169 [`arXiv:1807.03481`] [ɪɴSPIRE].

[14] B. Lucini, M. Teper and U. Wenger, *The High temperature phase transition in* SU(*N*) *gauge theories*, *JHEP* **01** (2004) 061 [`hep-lat/0307017`] [ɪɴSPIRE].

[15] B. Lucini, M. Teper and U. Wenger, *Properties of the deconfining phase transition in* SU(*N*) *gauge theories*, *JHEP* **02** (2005) 033 [`hep-lat/0502003`] [ɪɴSPIRE].

[16] N. Husung, P. Marquard and R. Sommer, *Asymptotic behavior of cutoff effects in Yang-Mills theory and in Wilson's lattice QCD*, *Eur. Phys. J. C* **80** (2020) 200 [`arXiv:1912.08498`] [ɪɴSPIRE].

[17] M. Teper, *An Improved Method for Lattice Glueball Calculations*, *Phys. Lett. B* **183** (1987) 345 [ɪɴSPIRE].

[18] M. Teper, *The Scalar and Tensor Glueball Masses in Lattice Gauge Theory*, *Phys. Lett. B* **185** (1987) 121 [ɪɴSPIRE].

[19] M. Lüscher, *Volume Dependence of the Energy Spectrum in Massive Quantum Field Theories. 1. Stable Particle States*, *Commun. Math. Phys.* **104** (1986) 177 [ɪɴSPIRE].

[20] G. 't Hooft, *Computation of the Quantum Effects Due to a Four-Dimensional Pseudoparticle*, *Phys. Rev. D* **14** (1976) 3432 [*Erratum ibid.* **18** (1978) 2199] [ɪɴSPIRE].

[21] S. Coleman, *The uses of instantons*, in *Aspects of Symmetry. Selected Erice Lectures*, chapter 7, pp. 265–350, Cambridge University Press (1985) [DOI].

[22] G. 't Hooft, *A Planar Diagram Theory for Strong Interactions*, *Nucl. Phys. B* **72** (1974) 461 [ɪɴSPIRE].

[23] S. Coleman, *1/N*, in *Aspects of Symmetry. Selected Erice Lectures*, chapter 8, pp. 351–402, Cambridge University Press (1985) [DOI].

[24] E. Witten, *Baryons in the 1/n Expansion*, *Nucl. Phys. B* **160** (1979) 57 [ɪɴSPIRE].

[25] E. Witten, *Instantons, the Quark Model, and the 1/n Expansion*, *Nucl. Phys. B* **149** (1979) 285 [ɪɴSPIRE].

[26] M.J. Teper, *Instantons and the 1/N Expansion*, *Z. Phys. C* **5** (1980) 233 [ɪɴSPIRE].

[27] L. Del Debbio, H. Panagopoulos, P. Rossi and E. Vicari, *k string tensions in* SU(N) *gauge theories*, *Phys. Rev. D* **65** (2002) 021501 [hep-th/0106185] [ɪɴSPIRE].

[28] E. Witten, *Theta dependence in the large N limit of four-dimensional gauge theories*, *Phys. Rev. Lett.* **81** (1998) 2862 [hep-th/9807109] [ɪɴSPIRE].

[29] L. Del Debbio, H. Panagopoulos and E. Vicari, *θ dependence of* SU(N) *gauge theories*, *JHEP* **08** (2002) 044 [hep-th/0204125] [ɪɴSPIRE].

[30] S. Aoki, H. Fukaya, S. Hashimoto and T. Onogi, *Finite volume QCD at fixed topological charge*, *Phys. Rev. D* **76** (2007) 054508 [arXiv:0707.0396] [ɪɴSPIRE].

[31] O. Aharony and Z. Komargodski, *The Effective Theory of Long Strings*, *JHEP* **05** (2013) 118 [arXiv:1302.6257] [ɪɴSPIRE].

[32] S. Dubovsky, R. Flauger and V. Gorbenko, *Flux Tube Spectra from Approximate Integrability at Low Energies*, *J. Exp. Theor. Phys.* **120** (2015) 399 [arXiv:1404.0037] [ɪɴSPIRE].

[33] M. Lüscher and P. Weisz, *String excitation energies in* SU(N) *gauge theories beyond the free-string approximation*, *JHEP* **07** (2004) 014 [hep-th/0406205] [ɪɴSPIRE].

[34] J.M. Drummond, *Universal subleading spectrum of effective string theory*, hep-th/0411017 [ɪɴSPIRE].

[35] A. Athenodorou, B. Bringoltz and M. Teper, *Closed flux tubes and their string description in D = 3 + 1* SU(N) *gauge theories*, *JHEP* **02** (2011) 030 [arXiv:1007.4720] [ɪɴSPIRE].

[36] B. Lucini and M. Teper, *Confining strings in* SU(N) *gauge theories*, *Phys. Rev. D* **64** (2001) 105019 [hep-lat/0107007] [ɪɴSPIRE].

[37] A. Hasenfratz and P. Hasenfratz, *The Connection Between the Lambda Parameters of Lattice and Continuum QCD*, *Phys. Lett. B* **93** (1980) 165 [ɪɴSPIRE].

[38] R.F. Dashen and D.J. Gross, *The Relationship Between Lattice and Continuum Definitions of the Gauge Theory Coupling*, *Phys. Rev. D* **23** (1981) 2340 [ɪɴSPIRE].

[39] J. Ambjørn, P. Olesen and C. Peterson, *Stochastic Confinement and Dimensional Reduction. 1. Four-Dimensional* SU(2) *Lattice Gauge Theory*, *Nucl. Phys. B* **240** (1984) 189 [INSPIRE].

[40] G.P. Lepage, *Redesigning lattice QCD*, *Lect. Notes Phys.* **479** (1997) 1 [hep-lat/9607076] [INSPIRE].

[41] G. Parisi, *Recent Progresses in Gauge Theories*, *AIP Conf. Proc.* **68** (1980) 1531 [INSPIRE].

[42] C. Allton, M. Teper and A. Trivini, *On the running of the bare coupling in* SU(N) *lattice gauge theories*, *JHEP* **07** (2008) 021 [arXiv:0803.1092] [INSPIRE].

[43] M. Lüscher, R. Sommer, P. Weisz and U. Wolff, *A Precise determination of the running coupling in the* SU(3) *Yang-Mills theory*, *Nucl. Phys. B* **413** (1994) 481 [hep-lat/9309005] [INSPIRE].

[44] S. Capitani, M. Lüscher, R. Sommer and H. Wittig, *Non-perturbative quark mass renormalization in quenched lattice QCD*, *Nucl. Phys. B* **544** (1999) 669 [*Erratum ibid.* **582** (2000) 762] [hep-lat/9810063] [INSPIRE].

[45] C.R. Allton, *Lattice Monte Carlo data versus perturbation theory*, hep-lat/9610016 [INSPIRE].

[46] R. Sommer, *A New way to set the energy scale in lattice gauge theories and its applications to the static force and* α_s *in* SU(2) *Yang-Mills theory*, *Nucl. Phys. B* **411** (1994) 839 [hep-lat/9310022] [INSPIRE].

[47] R. Sommer, *Scale setting in lattice QCD*, *PoS* **LATTICE2013** (2014) 015 [arXiv:1401.3270] [INSPIRE].

[48] K.-I. Ishikawa, I. Kanamori, Y. Murakami, A. Nakamura, M. Okawa and R. Ueno, *Non-perturbative determination of the* Λ*-parameter in the pure* SU(3) *gauge theory from the twisted gradient flow coupling*, *JHEP* **12** (2017) 067 [arXiv:1702.06289] [INSPIRE].

[49] N. Husung, M. Koren, P. Krah and R. Sommer, SU(3) *Yang-Mills theory at small distances and fine lattices*, *EPJ Web Conf.* **175** (2018) 14024 [arXiv:1711.01860] [INSPIRE].

[50] K. Ishikawa, G. Schierholz and M. Teper, *Calculation of the Glueball Mass Spectrum of* SU(2) *and* SU(3) *Nonabelian Lattice Gauge Theories I: Introduction and* SU(2), *Z. Phys. C* **19** (1983) 327 [INSPIRE].

[51] K. Ishikawa, A. Sato, G. Schierholz and M. Teper, *Calculation of the Glueball Mass Spectrum of* SU(2) *and* SU(3) *Nonabelian Lattice Gauge Theories II:* SU(3), *Z. Phys. C* **21** (1983) 167 [INSPIRE].

[52] U.M. Heller, SU(3) *lattice gauge theory in the fundamental adjoint plane and scaling along the Wilson axis*, *Phys. Lett. B* **362** (1995) 123 [hep-lat/9508009] [INSPIRE].

[53] P. Weisz, *Renormalization and lattice artifacts*, in *Les Houches Summer School: Session 93: Modern perspectives in lattice QCD: Quantum field theory and high performance computing*, pp. 93–160 (2010) [arXiv:1004.3462] [INSPIRE].

[54] P. Conkey, S. Dubovsky and M. Teper, *Glueball spins in* D = 3 *Yang-Mills*, *JHEP* **10** (2019) 175 [arXiv:1909.07430] [INSPIRE].

[55] P. Di Vecchia, K. Fabricius, G.C. Rossi and G. Veneziano, *Preliminary Evidence for* $U_A(1)$ *Breaking in QCD from Lattice Calculations*, *Nucl. Phys. B* **192** (1981) 392 [INSPIRE].

[56] M. Campostrini, A. Di Giacomo and H. Panagopoulos, *The Topological Susceptibility on the Lattice*, *Phys. Lett. B* **212** (1988) 206 [INSPIRE].

[57] M. Teper, *Instantons in the Quantized* SU(2) *Vacuum: A Lattice Monte Carlo Investigation*, *Phys. Lett. B* **162** (1985) 357 [ɪɴSPIRE].

[58] UKQCD collaboration, *Topological structure of the* SU(3) *vacuum*, *Phys. Rev. D* **58** (1998) 014505 [hep-lat/9801008] [ɪɴSPIRE].

[59] M. Lüscher, *Properties and uses of the Wilson flow in lattice QCD*, *JHEP* **08** (2010) 071 [*Erratum ibid.* **03** (2014) 092] [arXiv:1006.4518] [ɪɴSPIRE].

[60] M. Lüscher and P. Weisz, *Perturbative analysis of the gradient flow in non-abelian gauge theories*, *JHEP* **02** (2011) 051 [arXiv:1101.0963] [ɪɴSPIRE].

[61] M. Lüscher, *Future applications of the Yang-Mills gradient flow in lattice QCD*, *PoS* **LATTICE2013** (2014) 016 [arXiv:1308.5598] [ɪɴSPIRE].

[62] C. Bonati and M. D'Elia, *Comparison of the gradient flow with cooling in* SU(3) *pure gauge theory*, *Phys. Rev. D* **89** (2014) 105005 [arXiv:1401.2441] [ɪɴSPIRE].

[63] C. Alexandrou, A. Athenodorou and K. Jansen, *Topological charge using cooling and the gradient flow*, *Phys. Rev. D* **92** (2015) 125014 [arXiv:1509.04259] [ɪɴSPIRE].

[64] C. Alexandrou et al., *Comparison of topological charge definitions in Lattice QCD*, *Eur. Phys. J. C* **80** (2020) 424 [arXiv:1708.00696] [ɪɴSPIRE].

[65] G. Cossu, D. Lancastera, B. Lucini, R. Pellegrini and A. Rago, *Ergodic sampling of the topological charge using the density of states*, *Eur. Phys. J. C* **81** (2021) 375 [arXiv:2102.03630] [ɪɴSPIRE].

[66] G. Veneziano, U(1) *Without Instantons*, *Nucl. Phys. B* **159** (1979) 213 [ɪɴSPIRE].

[67] E. Witten, *Current Algebra Theorems for the* U(1) *Goldstone Boson*, *Nucl. Phys. B* **156** (1979) 269 [ɪɴSPIRE].

[68] C. Bonanno, C. Bonati and M. D'Elia, *Large-N* SU(N) *Yang-Mills theories with milder topological freezing*, *JHEP* **03** (2021) 111 [arXiv:2012.14000] [ɪɴSPIRE].

[69] M. Hasenbusch, *Fighting topological freezing in the two-dimensional CPN-1 model*, *Phys. Rev. D* **96** (2017) 054504 [arXiv:1706.04443] [ɪɴSPIRE].

[70] M. Lüscher and F. Palombi, *Universality of the topological susceptibility in the* SU(3) *gauge theory*, *JHEP* **09** (2010) 110 [arXiv:1008.0732] [ɪɴSPIRE].

[71] C. Bonati, M. D'Elia, P. Rossi and E. Vicari, θ *dependence of* 4D SU(N) *gauge theories in the large-N limit*, *Phys. Rev. D* **94** (2016) 085017 [arXiv:1607.06360] [ɪɴSPIRE].

[72] T. van Ritbergen, J.A.M. Vermaseren and S.A. Larin, *The Four loop β-function in quantum chromodynamics*, *Phys. Lett. B* **400** (1997) 379 [hep-ph/9701390] [ɪɴSPIRE].

[73] C. Christou, A. Feo, H. Panagopoulos and E. Vicari, *The three loop β-function of* SU(N) *lattice gauge theories with Wilson fermions*, *Nucl. Phys. B* **525** (1998) 387 [*Erratum ibid.* **608** (2001) 479] [hep-lat/9801007] [ɪɴSPIRE].

[74] B. Alles, A. Feo and H. Panagopoulos, *Asymptotic scaling corrections in QCD with Wilson fermions from the three loop average plaquette*, *Phys. Lett. B* **426** (1998) 361 [*Erratum ibid.* **553** (2003) 337] [hep-lat/9801003] [ɪɴSPIRE].